UNIVERSITÉ DE SHERBROOKE
Faculté de génie
Département de génie chimique et de génie biotechnologique

SUIVI DE L'OPÉRATION D'ENROBAGE POUR LE DÉVELOPPEMENT D'UNE FORME POSOLOGIQUE FACILE À AVALER POUR DES FINS PÉDIATRIQUES : ÉTUDE DU PROCÉDÉ ET DÉVELOPPEMENT D'OUTILS POUR UN SUIVI EN TEMPS RÉEL

Monitoring the coating operation for the development of an easy-to-swallow dosage form for pediatric use: building process understanding and tool development for real-time monitoring

Thèse de doctorat

Spécialité : génie chimique

Bárbara SANTOS SILVA

Sherbrooke (Québec) Canada

Février 2018

JURY MEMBERS

Ryan GOSSELIN

Supervisor

Nicolas ABATZOGLOU

Examiner

Pierre-Philippe LAPOINTE-GARANT

Examiner

Jukka RANTANEN

External examiner

RÉSUMÉ

Malgré les mesures récentes des organismes de réglementation, il y a encore des lacunes dans la mise en œuvre de formulations adaptées à l'âge à l'intention de la population pédiatrique. Les différences au sein de cette population, conjuguées à la non-adhésion thérapeutique due au mauvais goût des médicaments, présentent de grands défis pour la formulation de médicaments pris par voie orale. Des formulations orales solides souples, comme les microsphères, ont été proposées comme solutions de rechange aux formulations déjà commercialisées, comme les comprimés ou les formes posologiques orales liquides. Les microsphères sont des systèmes matriciels dans lesquels le principe actif (PA) est dispersé. Le PA est donc subdivisé en plusieurs petites unités posologiques. De plus, les microsphères peuvent être enrobées afin de masquer le goût. La stratégie consiste à appliquer une barrière protectrice à la microsphère qui empêchera la libération du médicament dans la cavité buccale, tout en maintenant une libération immédiate dès que le produit médicamenteux atteint le site d'absorption, pour ainsi obtenir un profil neutre sur le plan du goût sans affecter la biodisponibilité du PA. Les lits d'air fluidisé avec : Wurster sont utilisés depuis plusieurs années dans l'industrie pharmaceutique pour enrober les petites particules, car ils produisent des particules uniformément enrobés.

La nécessité d'acquérir une meilleure compréhension des procédés conventionnels utilisés dans l'industrie pharmaceutique est connue. Les organismes de réglementation favorisent l'utilisation des principes de qualité par la conception, ainsi que des nouvelles technologies, comme les outils de la technologie d'analyse des procédés (PAT), dans le but d'élaborer une stratégie pour transformer un procédé de fabrication qui se rapproche davantage d'une forme d'art en procédé basé sur des données scientifiques. La présente thèse porte spécifiquement sur cette question et plus particulièrement sur une meilleure compréhension de la relation entre la formulation de la solution d'enrobage et le procédé d'enrobage pour la dissolution du PA.

Dans le cadre de ces travaux, un plan d'expérience D-optimal couplé à la mise en œuvre de trois outils PAT en ligne a permis d'identifier les paramètres critiques du procédé et les attributs critiques du matériau (formulation de la solution d'enrobage) qui influencent la libération *in-vitro* du PA au pH buccal. Le niveau de l'enrobage, le niveau de plastifiant, le débit, la température du lit et le durcissement sont les paramètres critiques identifiés pour une formation complète du film. La criticité de la morphologie de l'enrobage sur la dissolution dans la salive simulée est également démontrée. La performance en ligne de la spectroscopie Raman, de la spectroscopie proche infrarouge et de la mesure de la réflectance du faisceau focalisé, ainsi que les données du procédé et les attributs des matières premières sont évalués et comparés pour faire le suivi du procédé d'enrobage des microsphères. En recourant à une analyse *multiblock partial least squares*, il est démontré que la spectroscopie Raman a une performance supérieure pour assurer le suivi du procédé et obtenir ainsi un enrobage constant pour la membrane barrière à couche mince, essentielle à l'observance du patient.

Mots clefs : enrobage, lit d'air fluidisé avec Wurster, masquage du goût, microsphères, technologie d'analyse des procédés

ABSTRACT

Despite recent incentives provided by regulatory agencies there is still a gap in the implementation of age-appropriate formulations for the pediatric population. The differences within this population, coupled with the non-compliance due to poor taste, present great challenges for oral drug formulation. Flexible solid oral formulations, such as microspheres, have been proposed as alternatives to existing marketed formulations such as tablets or liquid oral dosage forms. Microspheres are matrix systems where the Active Pharmaceutical Ingredient (API) is dispersed. The API is thus subdivided into a plurality of small dosage units. Additionally, microspheres can be coated as a strategy to achieve taste masking. It consists in applying a protective barrier to the microsphere that will prevent the release of drug in the oral cavity, while maintaining an immediate release once the drug product reaches the absorption site, thereby achieving a taste neutral profile without adversely affect the bioavailabity of the API. To coat small particles Wurster fluid bed coaters have been used for many years in the pharmaceutical industry, as they produce uniformly coated particles.

There is a recognized need to better understand conventional processes used within the pharmaceutical industry. The regulatory agencies have encouraged the employment of quality by design principles, together with new technologies, such as Process Analytical Technology (PAT) tools, with the aim of developing a strategy to transform, what is generally considered an art form, into sound science based processes. This thesis specifically concerns this issue by focusing on better understanding the relation between both coating formulation and coating process to dissolution of the API.

In this work, a D-optimal design coupled with the implementation of three in-line PAT tools helped identify the critical process parameters and critical material attributes (coating formulation) influencing *in-vitro* API release at mouth pH. Coating level, plasticizer level, spray rate and product bed temperature and curing are the identified critical parameters for a complete film formation. The criticality of coating morphology on the dissolution in simulated saliva is also demonstrated. The in-line performance of Raman spectroscopy, near infrared spectroscopy and focused beam reflectance measurement, together with process data and raw material attribute is evaluated and compared to monitor the microsphere coating process. By resorting to multiblock partial least squares it is shown that Raman has superior performance to ensure consistent coating performance for thin film barrier membrane, essential to patient compliance.

Key words: Coating, fluid bed with Wurster insert, taste masking, microspheres, process analytical technology

ACKNOWLEDGEMENTS

In Portugal there is a book called *O livro dos porquês*, which loosely translates to: the book of why(s). I was always promised this book (especially during car rides), but sadly I never got it. Naturally I had to find other books that helped me answer some of my whys. With this document I was not able to summarize all the "because" I found during my doctoral studies (especially the personal lessons), but we have to start somewhere…

From the very beginning: Professor Ryan Gosselin. Ryan, I am truly grateful you have taken me under your wing and accepted to be my supervisor. It was a pleasure to learn from someone that is as passionate about teaching as you are. Thank you for sharing your scientific insight, enthusiasm, support and for always challenging me. You always keep an open door and I cannot thank you enough for your guidance throughout the project.

I would like to leave a very special word to Pierre-Philippe Lapointe-Garant for sharing his expertise, problem-solving attitude and positive thinking. Thank you for always pushing me to think outside the box to find a solution. I am deeply indebted to Jeremy Bartlett and Matthew Santangelo for having me welcomed in Groton. Jeremy, thank you for bringing things into broader perspective, your passion and enthusiasm are contagious. Matt, whenever there was something I wanted to try, you always knew how to make it happen. Thank you for all the discussions and unconditional support. I would also like to thank all other colleagues from Pfizer, especially those from MPAC and DPD. Steve Hammond and Jean-Sébastien Simard your eagerness for science made this all possible.

I would like to recognize Professor Nicolas Abatzoglou for always finding time to share his broad knowledge base and passion for science. Thank you as well to all my graduate colleagues, but specially Marie-Josée, Clémence, Pedro, Pierre-Luc and Emmanuel: thank you for the teachings, discussions and friendship.

Thank you to all my friends (from the old continent and the new). Charlotte, Jean-Paul, Jacqueline, Joëlle, Violaine and Candice, you welcomed me with open arms into your homes. Your kindness and warmth always made me forget the -40°C outside. *Vous les copains, je ne vous oublierais jamais*. Keya and Mini, thank you for being so positive and for all the delicious Indian delicacies you fed me after hours. Martina, Nanna, Iris, Britta and Jess thank you for making it all the way across the "pond(s)", it was wonderful to share my new home with you. André, Catarina(s), Sara(s), Maria, Leonor and Joana thank you for making me feel like Portugal was just a phone call away.

I am grateful to my family for giving me the encouragement I needed when I was so far away from them. I would never have managed without you. To my dad and my mom thank you for always making me feel loved, encouraging me to pursue my education and being role models of hard work and endurance. Words cannot describe how thankful I am for all you have given me. To my grandmother, thank you for being an example of kindness and strong character. To my *querido avô* José Carlos, who will never stop fighting for what he believes, I am so proud of being your granddaughter. Pia and Peter, thank you for being strong and teaching me about *lagom är bäst* (it really is!). Tobias, you were with me every step of the way (even when we were continents apart), this is as much mine as it is yours, thank you for being my best friend and bringing music and structure(s) into my life.

During these last four (something) years many were the people that contributed to help make this work possible, I will forever be in your debt.

Um enorme obrigada a todos / thank you all / *merci à vous tous* / *tack så mycket*!

TABLE OF CONTENTS

LIST OF FIGURES

LIST OF TABLES

CHAPTER 1 INTRODUCTION

1.1 Context and motivation

There are different challenges concerning the development of pediatric drug formulations, for example, an important factor (that is often overlooked), is the heterogeneity within the pediatric population[1] — it includes well defined sub-populations (pre-term newborns, newborns, infants and toddlers, children and adolescence) that will exhibit different responses not only for the active substance but also to the excipients added[2]. The Safety and Toxicity of Excipients for Pediatrics (STEP) database has been created to address the need to capture, manage and maintain valid safety, tolerability and toxicity of excipients used world-wide for pediatric drug formulation[3].

Nonetheless, it is frequent for physicians to prescribe medication that has not been approved for use in pediatric patients[4]. Pediatric labeling is a relatively small market (less than 10% of the pharmaceutical market[4]), research is expensive and complicated, and there are numerous practical and moral issues associated with clinical trials for pediatric studies. As a consequence, most of the time, medication is prescribed for pediatric use without taking into consideration neither the differences in pharmacokinetics and pharmacodynamics between pediatric patients and adults, nor disease states[5].

The adopted strategy has been to encourage pediatric drug studies through regulatory requirements and financial incentives. In order to promote the required synergy for the development and availability of age appropriate medicines for children, pediatric regulatory environment have been created all over the world. In the United States of America, the Best Pharmaceuticals for Children Act and the Pediatric Research Equity Act were created. The Pediatric Research Equity Act can make it mandatory to perform safety testing in all relevant pediatric subpopulations for a drug submitted in a new drug or, new biologics applications for adult indication if the Food and Drug Administration (FDA) so requires[6]. The *Best Pharmaceuticals for Children Act* grants new products, that complete pediatric testing, a 6-month patent extension (regardless of the approval for pediatric patients)[6]. Companies that test orphaned drugs are granted a two-year extension of the standard ten-year market exclusivity and furthermore, there is a new authorization category, the Pediatric Use Marketing Authorization, encouraging pediatric testing of drugs whose patent exclusivity has expired. Such testing may result in an additional ten-year market exclusivity.[7] In the European Union, it is the Pediatric Regulation stimulating the new trials and formulations[8]. A list of high priority medicines

has been released in an attempt to guide the research where it is needed, focusing on off-label drugs and gaps in pediatric data [9].

Within the currently prescribed medication, lack of adherence by the pediatric population has long been acknowledged as a problem[10]. DiMatteo[11] estimated that the yearly cost associated with non-adherence was as high as 300 billion US dollars a year. There are a multitude of factors contributing to the lack of compliance and despite the effort that has been made to understand the reasons behind drug adherence problems in pediatrics, many questions still linger [10]. Despite this fact, some key factors have been recognized and they include not only socio-economic circumstances and adverse effects of the medication, but also attributes of the dosage form itself, such as palatability [10], [12] and dosage form. Taste was indicated as the greatest barrier to completing treatment by more than 90% of pediatricians[13], as drugs often exhibit an unpleasant bitter taste, frequently perceived as a “bad taste”[13]–[15].

The oral route is still the preferred route of administration in children[2], [14], [16], [17]. Liquid oral pediatric dosage forms (oral suspensions and solutions) are the most common formulations found in the market. Usually, to disguise the bitter taste, high-intensity sweeteners, flavors and acids are added to the formulation[13], [14]. The addition of these excipients might help reduce the bitterness, but it will not eliminate it[14]. Liquid preparations have identified shortcomings regarding palatability, stability (chemical, physical or microbiological) and transport to lower-income countries[17]. One needs to take into account that the lack of access to medicines is mostly in children living in developing countries[2], as it has been highlighted by the WHO initiative: “Make Medicines Child Size”. Consequently, there is a growing preference to adopt solid oral dosage formulations. Not to say that these dosage forms are without their challenges, such as chocking and chewing risks, but they have the potential to overcome the issues of traditional liquid preparations.

Many solid oral dosage forms have the advantage of masking or encapsulating the taste. However, inability to swallow tablets and capsules is a common problem within the pediatric population, as such, these dosage forms are usually perceived as being appropriate for older children[18]. The ability to swallow varies greatly within the pediatric population. Chewables and (oro-) dispersable tablets are easier to swallow, but taste masking is still an issue that needs to be addressed[14].

As first reported by Sam *et al.*[19] the ideal pediatric formulation will have to be an integrated approach where formulation, manufacturing process, packaging and administration device meet the

needs of the patients, caregivers, healthcare providers and manufacturers[20]. Being that the final oral dosage form should be flexible, convenient to handle, have acceptable taste, minimal administration frequency, adequate bioavailability, minimal number of excipients, have a robust manufacturing process, be stable, be commercially viable at an acceptable cost for the patient and payers and finally be easily transported and stored[20].

This view is well aligned with the concept of Quality by Design (QbD), as it is defined in the ICH Q8 “a systematic approach to development that begins with predefined objectives and emphasis product and process understanding and process control, based on sound science and quality risk management”[21]. Process analytical technology (PAT) is under the QbD framework blanket as it can act as a facilitator to the process of knowledge transfer from a research and development space to production[22]. PAT is commonly used to refer to the ability to monitor a process real-time, improve process understanding and control the quality of the manufactured product[23]. PAT has been established as a scientific approach to support innovation and development within the pharmaceutical industry[24] in order to ensure quality and consistency of the final product. In early stage process development, PAT applications focus on establishing a measuring system to help identify and understand relationships among critical formulation, process factors and critical quality attributes. This knowledge is then used to establish a robust control strategy during robust manufacturing to control and supervise the process.

This work aims at developing fundamental knowledge of the parameters that affect the properties of the particle coating and at determining their impact on the Active Pharmaceutical Ingredient (API) release.

1.2 Problem statement and definition

Microspheres (Figure 1.1), as well as other multiparticulate systems, have been identified as a flexible dosage form that can be used as a platform technology [14], [17] for oral medicine requiring precise dose measurement. Platform technology is defined, in Annex 5 of the 46th WHO report on Specifications for Pharmaceutical Preparations, as a “technique, including formulation and related processes, which can be used to obtain different dosage forms, different strengths and/or accommodate different APIs”[2]. Microsphere drug delivery systems consist of a plurality of discrete small dosage units, each exhibiting some desired characteristic where the API is dispersed in a matrix[25]. Microspheres can be a starting point for the dosage form, offering the possibility of being further processed into a wide range of alternative pediatric drug delivery systems, providing the opportunity of

taste masking. The topic of microsphere manufacturing is further developed in sub-chapter 2.2.1 Making microspheres.

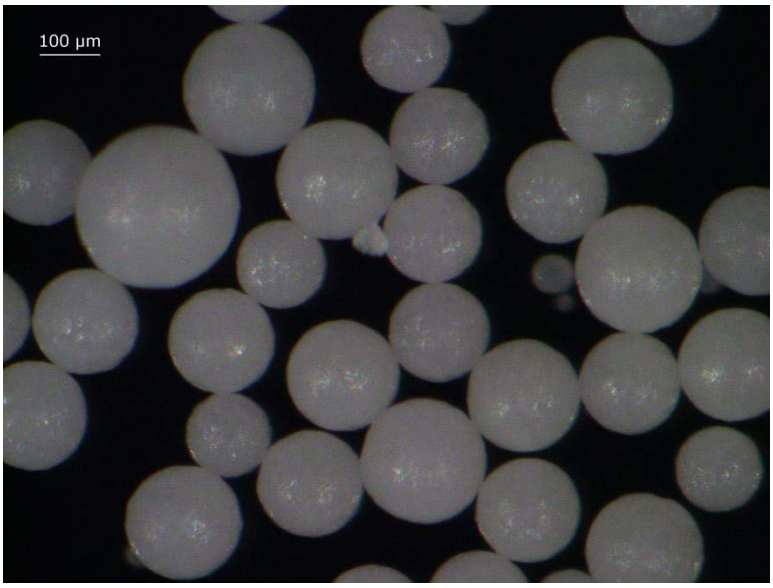

Figure 1.1 Melt spray congeal microspheres

On the subject of the taste masking technologies, there are several strategies that can be adopted: modifying the drug molecule, modifying formulation pH, barrier approach, drug complexes, disguising bad taste or blocking taste receptor[14], [26]. It is important to mention that the barrier approach is the most widely used, accounting for 27% of patents and patent applications[26] in the field of taste masking technology in the period between 1997 and 2007. The barrier approach, in taste masking, consists of applying a coating (or barrier) to the core containing the API. This approach will prevent the API from going into solution while in the oral cavity. However, one must ensure the release of the drug afterwards (in the gastro-intestinal track) so that pharmacokinetics are not adversely affected[14].

As several factors influence the choice of coating to use, selection of the taste-masking coating needs to be done on a case-by-case scenario that takes into account the properties of the API, the dose level, the dosage form and the release profile among other factors. For taste masking purposes, the polymer should not allow the release of the API in the oral cavity, but it should allow the release of the drug in the expected absorption site (intestine or stomach)[27] in order not to hinder bioavailability of the drug. In the particular case of this work, the chosen solution was to study a reverse enteric polymer system, this is, using polymers that are insoluble at mouth pH, but soluble in gastric pH [27]. They are

cationic polymers with a defined number of tertiary amino groups, that dissolve under protonation in acidic media of pH 5.5[28] and below. The solubility pH-dependency should ensure an effective protection in the mouth and a quick release in the stomach.

Kollicoat®Smartseal 30D is a novel aqueous dispersion developed specifically for taste-masking applications and moisture protection for orally administered pharmaceutical products by BASF and Colorcon[29]. Kollicoat®Smartseal 30D has type IV *("*excipient, colorant, flavor, essence, or material used in their preparation*"*[30]) and type V (*"*FDA accepted reference information*"* [30]) drug master files, a submission to the FDA that contains the chemistry, manufacturing and controls of a substance used for drug formulations, making Kollicoat®Smartseal 30D a strong candidate for future "new drug application" filings. Kollicoat®Smartseal 30D was chosen in this study because it is representative of the methacrylic acid polymer family that is commercially available on the market and no work was found in the literature that links coating formulation and process parameters to the dissolution performance of this coating. With a proper understanding of the impact of the critical process parameters (CPPs) and critical material attributes (CMAs) on the critical quality attributes (CQAs), effective taste masking of pediatric coated microspheres with Kollicoat®Smartseal 30D reverse enteric should be possible to achieve. This is assuming that:

1. The bad taste is exclusively due to the API release in the mouth
2. By coating the microspheres we eliminate the contact of the "bad-tasting" API with the taste buds, and thus the taste is no longer perceived.

This work aims at answering one question: "How do the methacrylic acid coating formulation and processing conditions in the fluid bed with a Wurster insert, affect the quality of the taste masked melt-spray congeal microsphere's coating?"

1.3 Objectives

The main objectives of this work are:

- To develop further understanding of parameters that affect microspheres coating properties with a methacrylic acid-based aqueous dispersion (reverse enteric polymer blend) and to determine their impact on the API release profile at pH 6.2;
- To develop a robust barrier membrane and barrier membrane manufacturing process to produce taste masked microspheres for pediatric use. This requires simultaneously studying coating formulation parameters such as, plasticizer concentration and solids'

in suspension, and fluid bed coating with a Wurster insert unit operation process parameters: product bed temperature, air flow, spray rate, atomizing air pressure, coat weight gain and curing. In order to determine which are the CPPs and/ CMAs and their impact on the required CQAs:

- Coating thickness – 4 to 20µm
- Coating uniformity – non-porous film
- Taste masking performance (neutral taste in the mouth), evaluated by the non-dissolution of API in 0.05M Potassium Buffer at pH 6.2
- API release in hydrochloric acid pH 1.2

It is essential to select the PAT tool(s) that are able to monitor the above mention CQAs. The use of PAT tools will help monitor the coating process, and thus develop a systematic understanding of it.

1.4 Original contributions

The most relevant contributions of this work include:

- Demonstrate the robustness of a methacrylic acid-based polymer coating membrane and process after curing. Within the chosen design space from the seven initial key variables, the remaining CPP and CMA is coating level, percentage of plasticizer, spray rate and temperature, with the curing being a crucial part of the process as it allows for a complete film formation and reduces overall variability within the batch.
- Demonstrate that when studying coating performance, the microstructure of the coating is of great importance. Coating thickness helps explain the majority of the variation in coating performance. Nevertheless, coatings of the same thickness can sometimes display very difference taste masking performance. It is the microstructural differences within those coatings that help understand how the variations in formulation and process impact the dissolution performance.
- Determine if Multiblock Partial Least Squares (MBPLS) can provide a visually simplistic way to compare different sources of information (or even combine them). The potential benefits of using near infrared (NIR) spectroscopy, Raman spectroscopy, focus beam reflectance measurement (FBRM), process data or raw material properties to predict taste masking performance of reverse enteric polymer applied to melt-spray congeal microspheres was investigated. It would not be feasible to integrate all these

tools in a control strategy in an industrial context, MBPLS was helpful demonstrating that, within the evaluated blocks of information and the current set-up, Raman outperformed the other sources of information.

- Show how Raman could be potentially used to establish a control strategy for fluid bed coating: by demonstrating that variation in Raman signal correlates to the variations in product performance, showing that Raman can be used to monitor the coating process (beginning to end) and to identify process disruptions (such as spray rate changes).
- Aid the development of platform manufacturing technologies that can produce high quality dosage forms for the pediatric population in a reliable and replicable manner.

1.5 Thesis outline

This thesis is organized into five main chapters that will follow the outline described below.

This initial chapter (Chapter 1) is a small introduction that defines the framework, motivation and original contributions of the work developed.

Chapter 2, consists on a literary review of the foundations and evolving perspective on taste masking, with special focus on coating, which is of central interest for this project. It covers the state of the art on some of the critical concepts used throughout this thesis, namely on the coating suspension formulation, Wurster coating process, QbD and multivariate data analysis.

Chapter 3 and Chapter 4 detail the carried out research work. First the employment of QbD concepts/tools to define the critical process and formulation attributes for the taste masking performance. Showing how the *in vitro* performance of the coating, evaluated by dissolution testing at pH 6.2 is greatly influenced not only by thickness, but also by the microstructure of the coating. The second step was to demonstrate the usefulness of PAT tools to compute in-line prediction of the coating performance. Both chapters are based in submitted paper to peer-reviewed journals. For consistency purposes minor changes were made to both documents.

Chapter 5 summarizes the main conclusions from the work and draws recommendations for future work.

CHAPTER 2 STATE OF THE ART

2.1 Taste masking

Since the European medical agency has included the palatability of the product as an acceptability criteria in its Guideline on Pharmaceutical Development of Medicines for Pediatric Use[31], there has been a lot of emphasis on taste masking to try and improve compliance among the pediatric population.

The extent to which taste masking is required, is dependent on the physiochemical properties of the API, as well as its taste threshold[14]. In addition, measures to mask the taste of oral dosage forms must include degree of effectiveness, but also avoid negative effects over any sensory awareness[32], such as mucosa irritation, roughness in the mouth or hindered swallowing.

The factors taken into account during the taste masking formulation development include: extent of the bitter taste of the API, number of excipients, dose load, drug particulate shape and size distribution, drug solubility and ionic characteristics, required disintegration and dissolution rate of the finished product, desired bioavailability, desired release profile, stability (shelf-life and in-use), required dosage form and commercial viability [20], [27]. There are generally four taste masking principles[15] modification of formulation and/or pH, solid dispersions, chemical or solubility modification and physical barrier.

2.1.1 Modification of formulation and/or pH

The most used principals in liquid formulations to mask bad-taste are: 1) modification of formulation, by adding sweeteners and flavors[13]–[15] or 2) modifying pH. It is known that children have a higher tolerance threshold to sweetness (compared to adults), which explains the generalized use of sweeteners in pediatric formulation. Liquid dosage forms also have intrinsic limitations, such as, stability issues, higher transportation costs and challenging controlled release. In order to maintain chemical stability of medication that is prone to hydrolysis, pH modification is a commonly used strategy in liquid formulations[13]. For bitter drugs with a low detection taste threshold, these modifications do not provide adequate means for taste masking[15]. The lack of controlled-release formulations results in the need to administer multiple dosages throughout the day[20].

2.1.2 Solid dispersions

Solid dispersions are characterized by having one or more APIs randomly distributed, or dispersed, in an inert solid carrier[15], [26], such as polymers, sugars, waxes or other suitable carrier agents[33]. The granules can be formed by either solidifying the molten mixture, as in spray congealing, melt granulation and hot melt extrusion. Reported drawbacks[15] of these technologies include their unsuitability for heat sensitive products. Taste masking by solid dispersion can also be achieved by precipitation followed by solvent evaporation.

However, like in the case of modification of the formulation by adding sweeteners or pH, depending on the taste threshold of the API, taste masking is often incomplete. Frequently, these approaches require the addition of taste-modifying agents or further coating of the pellets produced by solid dispersion.

2.1.3 Chemical or solubility modification

Solubility modification is used to decrease the solubility of the drug in the mouth, the hypothesis is that if the drug does not dissolve in the mouth, then the perception of the drug's bitter taste will also be reduced, or even eliminated. Although solubility modification is a simple process, its applicability is limited as it is only applicable to those drugs that have a pH-dependent solubility[15]. Developing a new molecule, that will still have the same pharmacokinetics but a different solubility, is a time consuming route.

Another option for taste masking is inclusion complexation. In this application, the API is entrapped into the "cavity" of a complexing agent, this is to say the host molecule, thus forming a stable complex[33]. The most common used complexation agents are cyclodextrins[15]; theoretically they either enclose the drug to inhibit its interaction with the taste buds, or interact with the gatekeeper proteins of the taste buds (bitter blockers)[26] to block them. There is still limited understanding of the tasting mechanism and bitter blockers[14], a reason that justifies the unfeasibility of the latest approach for a commercial product for the time being.

Ion exchange resins are crosslinked water-insoluble polymer carrying ionizable functional groups[34], that in turn can be either cationic or anionic[35]. The drug can be bound to the resin through weak ionic bonding, to an oppositely charged resin[26], so that dissociation of the drug-resin complex does not occur in the oral cavity[15]. Drug release from the resin depends on the properties of the resin itself and the ionic environment of the gastro intestinal tract[33]. The drug's release involves

ion exchange between those ions present in the gastro intestinal tract and those of the drug attached to the resins[15], which can have a negative impact on the bioavailability of the drug[14].

All in all, these approaches imply high development costs and lengthen timelines, with a variable success rate[14], which justifies the limited use of this technology for taste masking. In the period between 1997 and 2007 less than 5% of the total taste masking patents and patent applications focused on these technologies.

2.1.4 Physical barrier

A uniform physical barrier coated onto the API is the most efficient way of successfully providing a palatable oral dosage form. For this reason in the period between 1997 and 2007, coating (application of a physical barrier) accounted for 27% of the patents[26], making it the most commonly used technique of that decade[26].

The coating system can be classified accordingly to the type of coating material (molten or polymeric), coating solvent system (aqueous, organic or dry)[26] or by the coating technology. The discussion on coating material and formulation is made in sub-section 2.3 of this same document. Let us start by reviewing the available coating technologies.

Dry coating is an alternative that has been progressively gaining attention, as wet coating methods have become less desirable due to environmental concerns over resulting waste streams and possible volatile organic compound emissions[36], as well as typically longer process times for aqueous coating systems[37] or even for moisture sensitive APIs. In dry particle coating, submicron-sized guest particles are typically attached to micron-sized particles without using any solvents or binders[36]. Based on the above definition, it is reasonable to assess that the difference in particle size of the coating material and the core is a key parameter. There has been some work reported in the field of taste masking for tablets[37]–[41], and more recently on pellets with the purpose of taste masking[42], [43]. Capece *et al.*[44] have used a solventless dry coating process that makes use of high-intensity vibrations (laboratory resonance acoustic mixer, LabRAM), in order to avoid the use of plasticizers, binders and heat treatments to coat APIs.

The work to be developed will focus on fluid bed coating, as it is a well-established technology in the pharmaceutical industry due to its versatility[15]. In fluidized beds, the coating solution is usually sprayed onto particles by a two-fluid nozzle located at the top, bottom or horizontally in relation to the product bed[45]. Top spray coaters have been reported to present high porosity coatings and difficulties in achieving uniform film application[27]. Tangential coaters, also sometimes called,

rotor coating systems[46], consist of a disk rotating in the fluidizing chamber and a spray placed horizontally in the reactor. Centrifugal force causes the product to move toward the wall of the chamber, air velocity through the gap provides acceleration upward, and gravity and turbulent eddies force the product inward and toward the disc center[46].The combination of the rotation and the air flow provides specific properties, such as higher spherical shape and density to the resulting coated particles[47]. The main drawback of this technology is its applicability. Due to the high level of agitation in the reactor, it is not suited for coating materials that are crumbly or friable[48]. Given that Wurster coaters will be the focus of this work, sections 2.4 Fluid bed with Wurster coating will elaborate on the description of the system and the influence of several parameters.

2.2 Multiparticulate drug delivery systems

Multiparticulate drug delivery systems consist of a plurality of discrete small dosage units, meaning that a single dose of an API is subdivided into a multiplicity of small independent subunits[14], [16], each exhibiting some desired characteristic. Contrary to single-unit forms, which retain their structure in the digestive tract, multiparticulates will disperse in the gastro-intestinal track after administration[49]. Generally they are small easy to swallow spherical particles with diameters in the range of 0.05 (or smaller) to 2.00 mm[16], [49]; they comprise microcapsules, microspheres and pellets[20].

To deliver the total dose, the small discrete particles are combined into a single dosage form, that can range from ‘sprinkles’ to (less commonly) compressed tablets[50]. A numerous combinations of dosage form and administration options can be used[14]. This flexibility of dosage form and dosage administration gives multiparticulate systems a great advantage over single-unit systems (such as non-disintegrating dosage forms). It allows for an easy adjustment of the strength of a dosage unit by simply changing the number of multiparticulates[14], [50]. It also allows for the combination of multiparticulates with different drug release rates to obtain the desired overall release profile[50], or to obtain the same result by layering different drugs onto a starting core[14]. In allowing the development of sustained release solutions, multiparticulates can potentially reduce the burden of repeated administration by offering the opportunity to develop fixed-dose combination (where two or more drugs are combined in a single dosage form[51]).

Failure of a drug delivery unit can be caused by a multitude of reasons. For example, it can be due to lack of disintegration of the unit or non-dissolution of the API, or by the early release of the API, the cause and definition of failure of a dosage form will depend on the end goal of the

formulation. Regardless, in multiparticulate systems, the API is divided into many subunits. Failure of a few units may not be as critical as the failure of a single-unit system[16]. Due to their small size, multiparticulates are less dependent on gastric emptying, because they can pass the pyloric sphincter easily[50], even when it is closed[16]. By enabling a good distribution along the gastrointestinal tract and improving absorption, multiparticulate systems reduce intra- and inter- subject variation in gastrointestinal time, plasma levels, bioavailability and reduce irritant effect that may be induced by single-units if lodged at a particular site for a prolonged period of time[50]. All in all, multiparticulate drug delivery systems have shown to give superior reproducible pharmacokinetic behavior in comparison to monolithic drug formulations[52].

The multiparticulate approach is not without some disadvantages, to name the two major ones: gritiness/mouthfeel and co-administration with food. Pour mouthfeel (gritiness) can make a formulation unacceptable to the patient. As for administrating the microspheres with food, it is a double edge sword. On the one hand it has been reported to have had helped improve organoleptic properties, on the other hand it might have an impact on drug's bioavailability[14].

Nevertheless, multiparticulates stand out as the flexible solid dosage form for pediatric use[53] with the great advantage of being suitable for taste masking by film coating, which will also help to improve patient's compliance.

2.2.1 Making microspheres

Microspheres consist of multiparticulates system of a fairly homogeneous mixture of matrix and API[54]. They are not to be confused with microcapsules as they differ in morphology and internal structure (Figure 2.1). Microcapsules have at least one discrete domain of API (or more) and are reservoir systems[54].

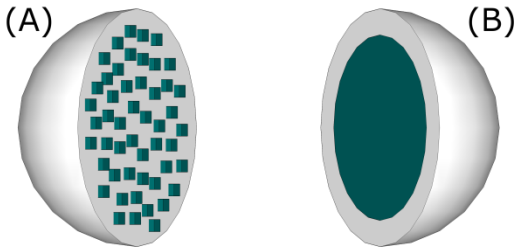

Figure 2.1 Schematic representation of (A) microsphere and (B) microcapsule.

In making microspheres, the API is mixed with the excipients, before or during the manufacturing process. The most common processes are: spray drying, granulation, complex perfect

spheres and spray congealing. Granulation is a process in which particles are made to adhere to each other, resulting in larger particles. In the absence of liquids this is called dry granulation, in the presence of liquids this is called wet granulation. Therefore there are many methods for granulating particles, high shear granulation, roller compaction, hot melt granulation, to name a few. The appropriate method needs to be chosen based on the material to be granulated andthe desirable granules properties. More recently, complex perfect spheres (CPS^{TM}) have emerged as a proprietary method by Glatt where the mixture of API and excipients is densified and spheronized by an orbital motion created by air suspension[55]. Spray-drying refers to a solution or suspension sprayed into a hot chamber where the microspheres are formed by evaporation of the solvent in the hot environment during the downward fall in the chamber[50]. The microspheres produced by spray-drying generally have irregular geometry and porous surfaces due to the evaporation of the solvent[56]. Spray congealing is a similar process to the aforementioned spray drying, but in this case molten waxes or fats are sprayed into a cooled chamber, which solidify during their fall towards the bottom of the chamber where the microspheres are collected. The API might be insoluble or soluble in the matrix. If the API is soluble in the matrix, upon cooling, the API will be dispersed in the matrix. If the API is insoluble in the molten matrix, it will be embedded in the core or distributed in the matrix[56]. A specific case is melt-spray congealing (MSC). MSC (Figure 2.2) is a process in which a hot molten mixture is atomized by a spinning disk atomizer and the molten droplets congeal to form solid microspheres. The major disadvantage is that one must ensure API stability at high processing temperatures, but if this is assured, it produces microspheres within a tight span of particle size distribution.

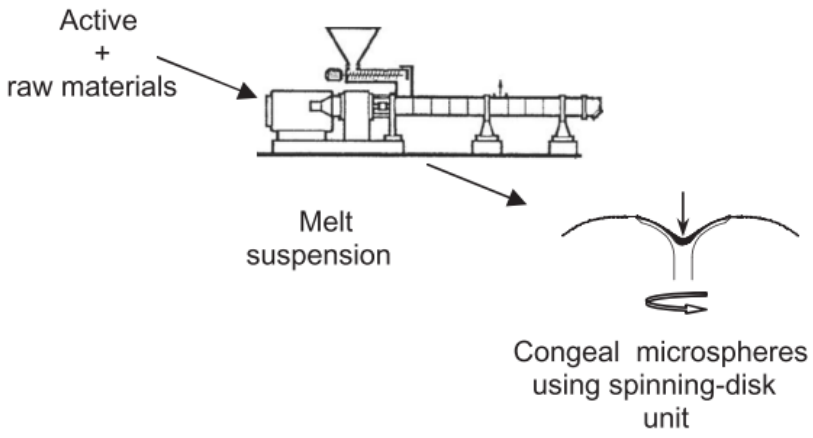

Figure 2.2 Schematic representation of MSC to produce microspheres. Adapted from Lo *et al.*[57]

2.3 Coating formulation

There are numerous applications of coating, including drug layering, modified release coating, physical and chemical protection, aesthetic purposes, taste masking and enhanced identification of drugs[58]–[61]. The properties of the coating material are essential to the successful coating of microspheres. It is essential to select a coating formulation that exhibits good film forming properties but low agglomeration tendencies[62] to ease processing of the coating. This section will focus on the main constituents of a coating formulation: solvent, polymer type, placticizer, anti-tack agents and water-soluble additives. This section also aims at introducing the main coating formulation aspects (viscosity and solid content) impacting film-formation and the ability of the coating to be processed to achieve efficient taste masking.

2.3.1 Solvent

Polymers may be applied in organic or aqueous solution or suspension. The use of organic solvents has been decreasing since the 1970's[50], as a result of toxicity and environmental pollution concerns, danger of explosion and occupational hazard for the workers having to handle the volatile solvents[50], [60]. This helps to explain the growing popularity of aqueous based coatings, even though aqueous coatings also lead to problems of their own, such as long drying times at higher temperatures than organic solvents[50].

2.3.2 Polymer

It should not come as a surprise that the film coating polymer is the most critical component of the coating solution, as different polymers may impact different drug release profiles[50].

Some of the key attributes that the film polymer should possess are listed below[61]:

1. Provide uniform film forming capacity (low porosity)
2. Be compatible with the product substrate, providing chemical and physical stability of the end dosage form
3. Allow drug release at the intended action site
4. Have low viscosity (in order to facilitate atomization)
5. Be stable in the desired solvent

For taste masking purposes, the polymer should not allow the release of the API in the oral cavity, but it should allow the release of the drug in the expected absorption site (intestine or

stomach)[27] in order not to hinder drug bioavailability. Bioavailability is defined as the fraction of an administered dose that reaches the systematic circulation[32].

Traditionally, water soluble polymers (polymeric solutions) have been used for taste masking[32]. They are used as physical barriers to delay drug release. However, their efficiency to block the interaction between the bitter API and the taste receptors is quite limited. They are expected to enable a fast dissolution rate irrespectively of the medium, being that the thickness of the coating will be the main factor determining the rate of release[25]. Joshi *et al.* [32] have reported that a minimum coating thicknesses of 10µm needed to be applied for this type of polymer. Water-soluble polymers used for taste masking include derivatives of cellulose (hydroxyethyl cellulose, hydroxypropyl methyl cellulose), polyvinyl alcohol and polyethylenglycol[32].

Polymeric suspensions of water-insoluble polymers have also been used for taste masking, like, ethyl cellulose, cellulose acetate and polyvinyl acetate [32]. They have mostly been used in controlled-release dosage forms. Advantages of these systems include decreasing dosing frequency and thus enhancing adherence to the therapeutic regime[63]. Film thickness is especially critical in the use of water-insoluble polymers as there is a higher risk of affecting bioavailability. The other extreme situation of system failure would lead to dose dumping, this is when the coating is compromised and the entire drug load is rapidly released.

A third category of polymers used for taste masking is pH dependent polymers. pH dependent polymers have ionizable functional groups. They will dissolve when a sufficient number of those functional groups are ionized. Films of reverse enteric polymers are cationic polymers that have a ionizable tertiary amine as functional group. Making these polymers insoluble at the neutral pH and ionizable in acidic pH, providing an effective barrier against the movement of drug molecules to the surface and water molecules to the core[32] at saliva pH. Saliva pH is generally in the range of 6.2 to 7.6[64]. Examples of these polymeric systems are methacrylic acid copolymers, based on methacrylic and acrylic acid[65], such as Eudragit E® 12.5, Eudragit® E 100, Eudragit® E PO, Eudragit® E PO ReadyMix and Kollicoat SmartSeal® 30 D. Films of enteric coatings (anionic polymers) on the other hand are highly stable under acidic pH, but break down rapidly at less acidic pH[66]. They are generally used to target drug release in the intestinal track, protect the API from hydrolysis in the stomach and protect the stomach to irritating APIs. Enteric polymers used in taste masking are sodium alginate, shellac, cellulose acetate and carboxymethyl cellulose to name a few[32].

2.3.3 Plasticizer

The suitability of a plasticizer depends on its interaction with the polymer chains[50]. A suitable plasticizer must be soluble with the polymer. For aqueous-based dispersed systems, the plasticizer must partition into the polymer phase to ensure miscibility.

The plasticizers action is based on molecular interactions with the polymer chains. Plasticizers weaken intermolecular attractions between polymer chains[63]. Plasticizers facilitate coalescence of discrete polymer spheres of aqueous based dispersed systems in film forming processes, by increasing film elongation.

The glass transition temperature (T_g) is the temperature at which the mechanical properties change from stiff and brittle to soft and elastic[60]. At temperatures above the T_g, polymer chain movement is increased and the film behaves as flexible material[60]. By lowering the T_g of the polymer, plasticizers decrease both elastic modulus and tensile strength[50].

Plasticizers are thus a key excipient of the coating formulation, as they reduce the brittleness of the polymer and reduce the propensity of cracking[61] by promoting the formation of an uniform film.

Attention should be paid to the level of plasticizer used, because high plasticizers amounts might lead to agglomeration problems during the coating operation due to the ease with which the coat can deform[50]. Joshi *et al.* [32] reported that above the optimum level of plasticizer the deposited film would present molecular scale holes, reducing the films taste masking efficacy.

Generally, polymer suppliers will have recommendations regarding the plasticizer to use and its level for the coating formulation[61]. Some of the most common plasticizers include: Polyethylene Glycol (PEG), Propylene Glycol (PG), Triethyl citrate (TEC), Tributyl citrate (TBC), Acetyl triethyl citrate (ATEC), Acetyl tributyl citrate (ATBC) and Dibutyl sebacate (DBS).

2.3.4 Anti-tacking agents

Anti-tacking agents are materials that are able to reduce agglomeration or sticking of particles during processing and subsequent storage. They can be used directly in the coating solution or added in a dry blending step at the end of the coating, to prevent agglomeration during overtime. Magnesium stearate, talc and kaolin are frequently used anti-tack agents[50].

2.3.5 Water-soluble additives

Water-soluble additives include low and high molecular weight compounds. Low molecular weight water-soluble additives include sucrose, lactose, sorbitol, mannitol, sodium chloride and calcium phosphate[50]. While high molecular coat weight gain compounds commonly used are polyethylene glycol, hypromellose and hydroxypropylcellulose, both classes of additives have the same end goal – to enhance drug release rate, but slightly different mechanisms of action. Pores are channels that form in the coating and increase the water permeability, thereby accelerating the API release. While low molecular weight compounds will dissolve in aqueous medium and leach out of the coating forming pores, high molecular coat weight compounds will also form pores, but not leach out of the coating, the latter can also result in the swelling of the coats, compromising the coating integrity.

2.3.6 Viscosity

The viscosity of the coating is intrinsically related to its composition as it is dependent on the solid content, the type of polymer and weight of polymer used. Viscous coating preparations have poorer flow properties and may increase tendency for nozzle clogs (see Figure 2.3), forcing several stops during the coating process and promoting unwanted agglomeration of the particles being coated[50].

As the viscosity of a solution increases (above 200-250 cps[61]), for a constant atomization pressure, the droplet size distribution produced by the spray guns will increasingly become wider, due to the production of larger droplets. If the atomization air pressure is adjusted, it can compensate this effect. Larger droplets may overwet the surface of the particles, potentially resulting in agglomeration or, under extreme conditions, wet quenching of the bed, that is if wet agglomerates are too strong to be fragmented and too large to be fluidized, then regions of the bed may de-fluidize and stick together as large wet clumps[67]. For coatings with a viscosity greater than 350 cps[61], the presence of larger droplets will have to be compensated with an increase of temperature to promote evaporation and prevent the over-wetting of the product. Viscous coating preparations are also difficult to spread onto the cores, hindering coalescence of the film and thus forming inconsistent coats[50]. All in all, this will lead to a lower-mass coating efficiency and a rougher film surface[61].

2.3.7 Solid content in film formation

The concentration of solids in the coating suspension has an influence on the quantity of solvent that must be removed from the coating during the process. A low level of solids can increase the process time required to provide a protective film coating. A high level of solids can potentially

reduce the volume of coating formulation to be used and thus, reduce process time. However, when trying to coat with a coating formulation based on a high solid content at low coating level (low percentage of weight gain), it can be difficult to achieve an acceptable film coating uniformity[61]. A high level of solids can also lead to an increase of viscosity, which in turn might lead to the processing issues mentioned in the above sub-section.

2.4 Fluid bed with Wurster coating

In the 1950s, coating was performed in top spray granulators, where the spray nozzle is placed on top of the product chamber[47].The spray nozzle is located in the expansion chamber and the spraying droplets travel countercurrently to the fluidizing air[68].

During the 1960s, work was done towards the modification of the fluid bed coating unit to spray coating liquid from the bottom. Wurster invented bottom spray coating with an insert, also called the Wurster system (in his honor), which reduces the potential for agglomeration[47]. When coating without the insert, it was observerd that the spray system increased considerably the collision between particles and droplets, resulting in a higher material efficiency for tablet coating. For smaller particles, such as microspheres, the risk of agglomeration is increased, as particle motion becomes disorganized and loses its regular and circulatory pattern[68]. As such, due to the high concentration of wet particles, agglomeration is favoured.

In Wurster systems, a column is placed above the gas distributor plate which promotes the circulatory movement of the particles being coated. In order to promote a higher central air velocity through the column, the area of the air distribution plate located directly under the column has higher perforated area than the periphery region, creating a region of lower pressure to which the particles are drawn and lifted up the column[45]. The nozzle is placed in the center of the gas distributor plate and the liquid droplets are sprayed concurrently with the fluidization air[68]. Contact between droplet and particle, spreading of the droplet of coatings onto the particle, coalescence of the coating and evaporation of the solvent (Figure 2.3 (B)), are occurring almost simultaneously during the coating operation[46], [47]. The drying of the wetted particles is done with the hot air that is also helping the fluidization[45], [47]. The dried solid matter which remains on the surface of the particle forms the film coating. As on the exit of the partition the fluid bed cross-section is suddenly enlarged, air velocity decreases and the particles decelerate in the expansion chamber, falling outwards freely in an inverted U-shape trajectory back onto the product bed staging area[45], [47]. The particles flow downwards in the annulus (staging area)[69]. Note that in order to avoid sticking and agglomeration, the coating film

must be dry enough when reaching the staging area. The cycle starts over when the particles re-enter the partition column through the partition gap and repeat the fountain-like cyclic flow until the desired coating level is achieved[45]. A layer of coating is applied with several passes through the spray, in order to produce complete coverage of the surface (layering)[46]. In coating, the main goal is not to change the particle size distribution, but to functionalize the particles being coated. When coating, the aims are to have an uniform distribution of the film and consequently particle size, to achieve an efficient evaporation, to inhibit core penetration by solvents and agglomeration[46], [61]. Agglomeration is something that is unwanted in a coating operation. It happens if a liquid bridge is established between two particles and remains until complete drying. So the now solid bridge has to be strong enough to resist mechanical stresses from collisions with other particles[45].

Figure 2.3 (A) is a schematic representation of the above described particle trajectory and the coating process occurring in a Wurster coater.

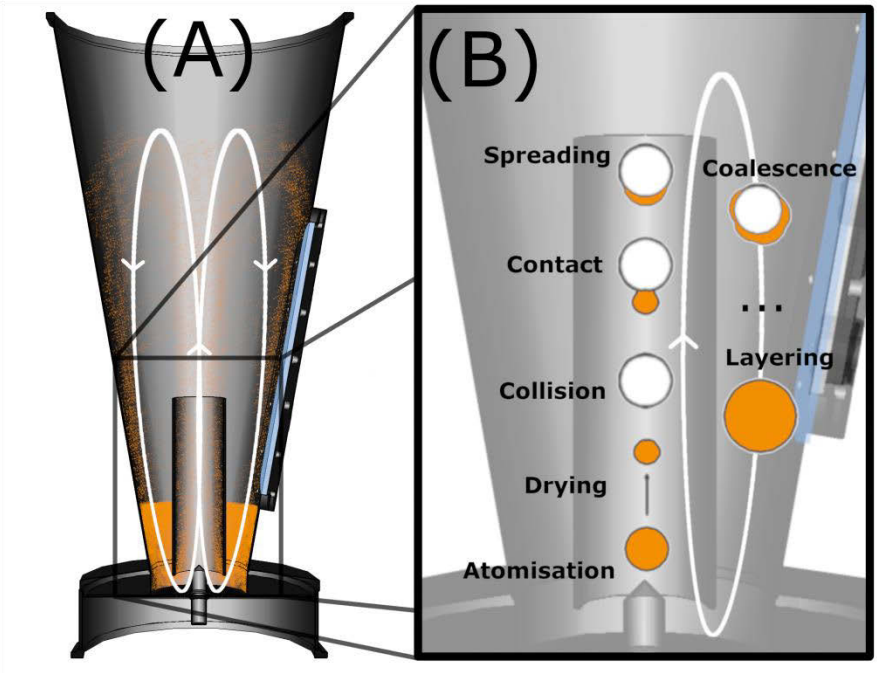

Figure 2.3 (A) Particle trajectory during the coating process in a fluid bed with a Wurster insert and (B) microlevel process occurring during coating adapted from Werner et al.[70]

The application of a film to a solid is a complex process, involving several phenomena – particle dynamics, mass and heat transfer[47]. The performance of the coating operation should take all these aspects under consideration, however the most usual approach is to define coating efficiency as simply material efficiency (E_c), defined in equation (2.1) [47].

$$E_c = \frac{W_c}{W_{cs} Dm} \quad [dimensionless] \tag{2.1}$$

$$W_c = W_p \left(\frac{w}{1-w}\right) [Kg] \tag{2.2}$$

In equations (2.1) and (2.2) [47], W_c is the deposited mass of coating [Kg], w the coating content of the microspheres [Kg/Kg], W_p the mass of core material [Kg], W_{cs} the mass of coating solution [Kg] and Dm the coating solution dry matter content [Kg/Kg]. Note that, in the above mentioned equations, there is no information regarding the energy balance or the quality of the coating itself, hence the name material efficiency.

2.4.1 Batch size

Fluidization is affected by batch size. A useful limit to consider is working capacity. Working capacity refers to the final batch weight. In the case of the Wurster coating process, this capacity refers to the volume outside the column. At least 40-50%[46], [61], [71] of the working capacity of the Wurster column should be occupied by when initially loading the batch. This loading is a guideline that aims at having a sufficient quantity of particles inside the partition to accumulate the maximum coating solution droplets and to avoid the premature coating drying phenomenon or depositing of the coating in the partition walls[69].

It should be referenced that the 40% limit is typically used for high coating levels. When the coating level is less than 10% w/w, then the advised range should be 60-70%[71] of working capacity.

Working capacity can be calculated by equation (2.3)[61], where B is batch size (g), r_1 the radius of the chamber [cm], r_2 the radius of the Wurster partition [cm], L the length of partitions [cm] and ρ_p the bulk density of the particles [g/cm^3].

$$B = \pi(r_1^2 - r_2^2) L \rho_p \, [g] \tag{2.3}$$

In the case of production scale, it is possible for the coaters to have multiple Wurster columns, thus it becomes necessary to multiply the radius of the partition in Equation 2.3 by the number of partitions[69].

2.4.2 Air flow rate/Air velocity

The air flow that fluidizes the cores within the coating chamber will also dry the liquid film coat deposited onto cores during drying[50]. Promoting adequate fluidization depends on, not only the mass of material to be coated, but also, the tackiness of the coating being applied[71]. Note that as more coating is applied, the mass increases, which might lead to an increase on the requirements for fluidizing air. On the other hand, tacky coatings can increase the drag forces on coated particles and potentiate agglomeration. In both cases an increase of fluidizing air can be used to offset these issues[71]. However, if set too high it may increase the erosion of friable cores.

Starting from a fixed bed (at a fixed tube-to-bottom height), particle flow is secured by the air flow rate[47], orifice plate configuration and Wurster height. When increasing the gas velocity, a point will be reached where the drag force exerted by the gas upon the particles counteracts the weight of the bed: this is the beginning of the fluidization and the corresponding gas velocity is called minimum fluidization velocity. Since the substrate is transported up through the Wurster partition, the air must be well above the minimum fluidization velocity. The upbead region was characterized by Geldart and Rhodes[72] as a vertical pneumatic conveyor. The process is an entrainment of particles in the fluidization medium (usually air). The flow of particles into the upbed region (and thus the solid mass flow per unit of area in the upbed region) is controlled by the Wurster partition height[73]. In the Wurster column, typically, it will be a dilute pneumatic conveying process. Due to the usual height of the Wurster, the flow is not fully developed when the particles leave the column[73]. When the particles leave the upbed region to enter the expansion region, the air velocity should drop to a level well below the minimum fluidization velocity (u_{mf}). This is what allows the particles to fall in a counter-flowing fluidization medium, towards the downbed region[73]. When leaving the Wurster, a minimum height (the transport disengagement height) is required to avoid entrainment of the particles[73], [74]. This is the reason why most fluid-bed apparatus are designed so that they have a significant larger diameter in this region. This will enable the air velocity to be well lower than the minimum fluidization velocity. The downbed region is a slightly expanded bed. Depending on material type (in Geldart's classification of powders[73]), the bed will expand more or less[73]. It is in this region that the particles will most likely tend to agglomerate, if the film is not fully dried. The control of the air flow rate in this downbed region is achieved by the hole area in the bottom plate under the downbed region versus that under the upbed region.

The choice of velocities, and consequently of air flow, will have to take the above considerations of the desired fluidization pattern. By making use of flow regime diagrams one can

make an initial choice of the appropriate air flow to be used. Figure 2.4 [75] shows the charts to map the different flow regimes in terms of the dimensionless variables d_p* and u*, defined in equations (2.4) and (2.5), respectively; d_p* is the dimensionless particle size and u* is the dimensionless gas velocity. In the equations, d_p is the particle size [m], ρ_g is density of the gas [Kg/m^3], ρ_s is the density of the solids [Kg/m^3], g is the gravitational constant [m^3.Kg.s^{-2}],μ is dynamic viscosity [Kg.(m.s)$^{-1}$].

$$d_p^* = d_p \left(\frac{\rho_g(\rho_s-\rho_g)g}{\mu^2}\right) \ [dimensionless] \tag{2.4}$$

$$u^* = u\left(\frac{\rho_g^2}{\mu(\rho_s-\rho_g)g}\right)^{1/3} \ [dimensionless] \tag{2.5}$$

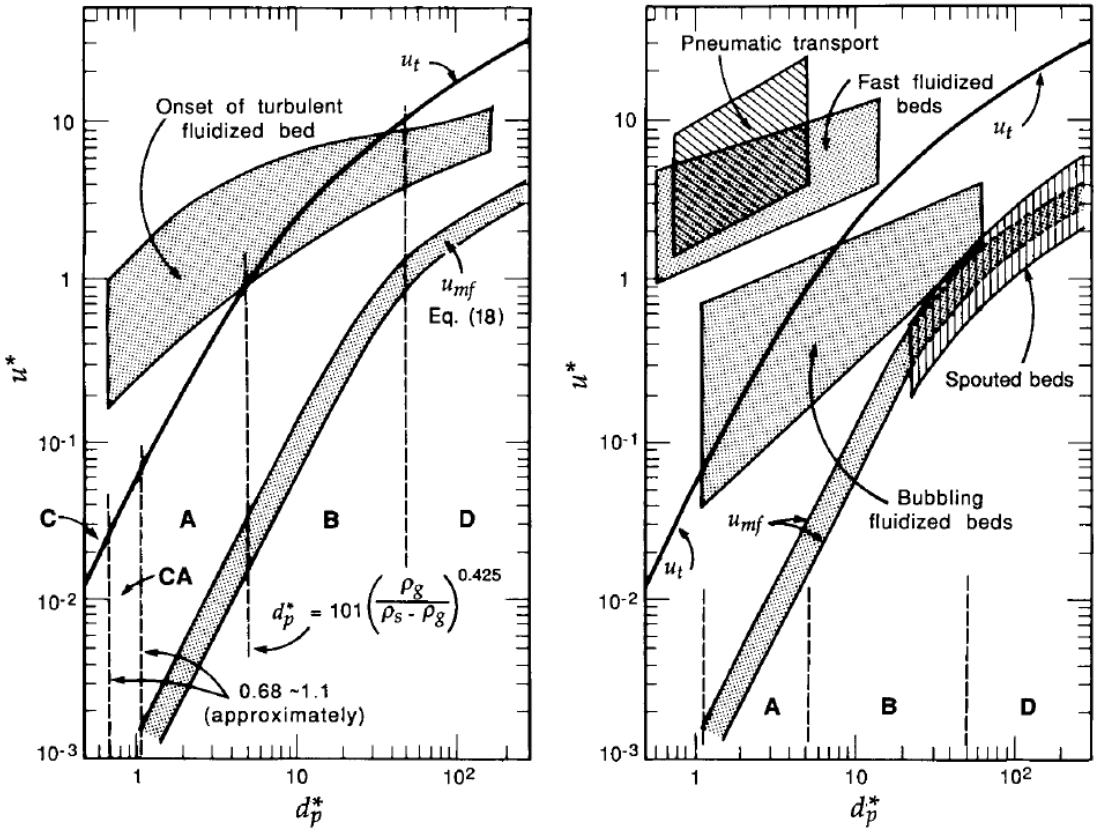

Figure 2.4. Flow regime diagram for whole range of gas-solid contacting. Letters C, A, B and D refer to the Geldart classification of solids[75].

The charts have been put together by the works of several researchers to show the onset of fluidization and terminal velocity (u_t) in bed of single-sized particles and include Geldart classification of solids. Geldart[74] classified powders into four groups according to their fluidization properties at ambient temperature. From smallest to largest particle size they are groups C, A, B and D. Group C

comprises cohesive or very fine powders where normal fluidization is extremely difficult to achieve, due to high interparticle forces. Group A powders fluidize easily at low gas velocities and controlled bubbling at higher gas velocities. Group B powders fluidize well with vigorous bubbling. Finally group D powders are difficult to fluidize giving rise to large exploding air bubbles or severe channeling (spouting) behavior.

In conclusion, proper product circulation should be safeguarded by adjusting (among others) the air velocities (or rather air flows) in the different transport regions of the bed.

2.4.3 Coating Temperature

The coating temperature, that is the temperature in the product bed, is an indirect parameter, as it cannot be adjusted directly. The product bed temperature results from interplay of inlet air temperature and spray rate. Nevertheless, as the film coating is forming in the product bed, it directly affects the end product quality.

At optimal coating temperature, solvent evaporation happens at a rate that is slow enough for adequate coalescence of the polymer to the cores[50], but fast enough to avoid agglomeration.

The minimum film-forming temperature (MFFT), is the minimum required temperature to cause coalescence of a polymeric solution to form a film[60]. Below this temperature, a polymeric dispersion will form an opaque, discontinuous material upon solvent evaporation. At temperatures above the MFFT, a clear continuous film will be formed.[76] If the operating temperature is lower than the minimum film-forming temperature, polymer particles may dry before coalescing, forming discontinuous porous films. An opaque or white powdery material is formed upon water evaporation[60].

2.4.4 Liquid flow rate and atomization pressure

Typically the nozzles used in the fluidized air are pneumatic binary nozzles: liquid is supplied at a low pressure and is sheared into droplets by air[46]. Pneumatic atomization is the process of producing sprays by the disruptive action of a high velocity gas upon a liquid stream[77]. In binary nozzles, the two fluids involved are air and coating. One can control droplet size distribution, simply by adjusting liquid flow rate and atomization pressure. The atomization of a liquid is accomplished by creating a high relative velocity between the liquid and the surrounding air[77]. In general, higher relative velocities will result in smaller size droplets. However, when set too high the droplets might end up being so small that they might dry before they reach the core[50]. Yet if set too low, larger

spray droplets will form, which can more easily form liquid bridges between cores[50]. A drawback of using this type of nozzle is that the atomized air will also contribute (to some extent) to the evaporation of the coating solvent, thus increasing the droplet's viscosity, which in turn can inhibit spreading and coalescence once in contact with the raw material[46].

Dybahl Hede *et al*.[77] have presented a comprehensive literature review with empirical mathematical correlations that can be used for the determination of mean droplet size and droplet size distributions by different authors. However, as it is stated by the authors of this review, "it is not in any way obvious which correlation that predicts the mean droplet size best in a given situation"[77], as many of this correlations have been developed for specially designed nozzles. The usefulness of the correlations needs to be assessed on a case-by-case basis.

Maximal liquid spray rate depends on coatings' and particles' physiochemical properties such as surface tension, viscosity and specific area, and of drying characteristics such as glass transition temperature and minimum film forming temperature[45]. Nevertheless, the value for maximal liquid spray rate can be obtained in an experimental basis and it is defined as liquid spray flow rate used just before agglomeration or collapse of the bed is observed[45].

2.4.5 Humidity

Drying capacity for aqueous coating systems is affected by the fluidization air, temperature and absolute humidity, being that air is the drying agent. Like in any drying operation, the drying of the coating onto the particles contains two fundamental and simultaneous processes: heat transfer to evaporate the solvent and mass transfer as liquid or vapor within the solid and as a vapor from the surface of the solid to the air.

During the drying, the rate of evaporation from the wet surface to the surrounding air is determined by the difference between the water vapor pressure at the liquid surface and the vapor pressure in the surrounding air. In an enclosed space, evaporation will continue until the two vapor pressures are equal. However, in a case like the one of a fluidized bed, unsaturated air is constantly being supplied, and thus the wet surface will reach an equilibrium temperature at which the cooling effect due to evaporation is equal to the heat transfer to the liquid by conduction and convection by the air.

An indication of the water content in the air is relative humidity that is defined as the percentage of partial pressure of water vapor in the air divided by the saturated vapor pressure of water

at the same temperature[78]. As the name indicates, relative humidity measures the amount of moisture in the air against a maximum amount of moisture in saturated air.

Another point to consider is that if the air is too humid, the spray rate that can be used is limited, otherwise overwetting will occur. If the humidity is too low, static might build up[61] and affect particle flow.

2.4.6 Curing conditions

After coating, it is usual to perform a curing step, which allows more residual water to evaporate and help the polymer particles to coalesce[50] which leads to a denser film coat. This phenomenon is accelerated at elevated temperatures, reason why this operation is typically done in an oven at controlled temperature and relative humidity. The curing temperature should exceed the minimum film forming temperature but not the glass transition temperature, as beyond the latter, the polymer will become soft and sticky, leading to agglomeration.

2.5 Quality-by-design and process analytical technology

Traditionally, the pharmaceutical industry has been reluctant to introduce innovative systems into the manufacturing sector. One of the reasons often pointed out is the rigid regulatory system surrounding the drug approval process, where the company must provide a detailed manufacturing plan and any alteration to it must be approved by the regulatory body around the world[79]. This mindset has gradually been changing over the past decade, or so, and we are now in a new era for the pharmaceutical industry, where the regulatory bodies give incentives to improve product quality and process performance. Figure 2.5 attempts to illustrate the main milestones in the evolution of QbD, being that the International Conference Harmonization of Technical Requirements for Registration of Pharmaceuticals for Human Use (ICH) is of special importance, given that it brought together the regulatory authorities of United States, Europe and Japan.

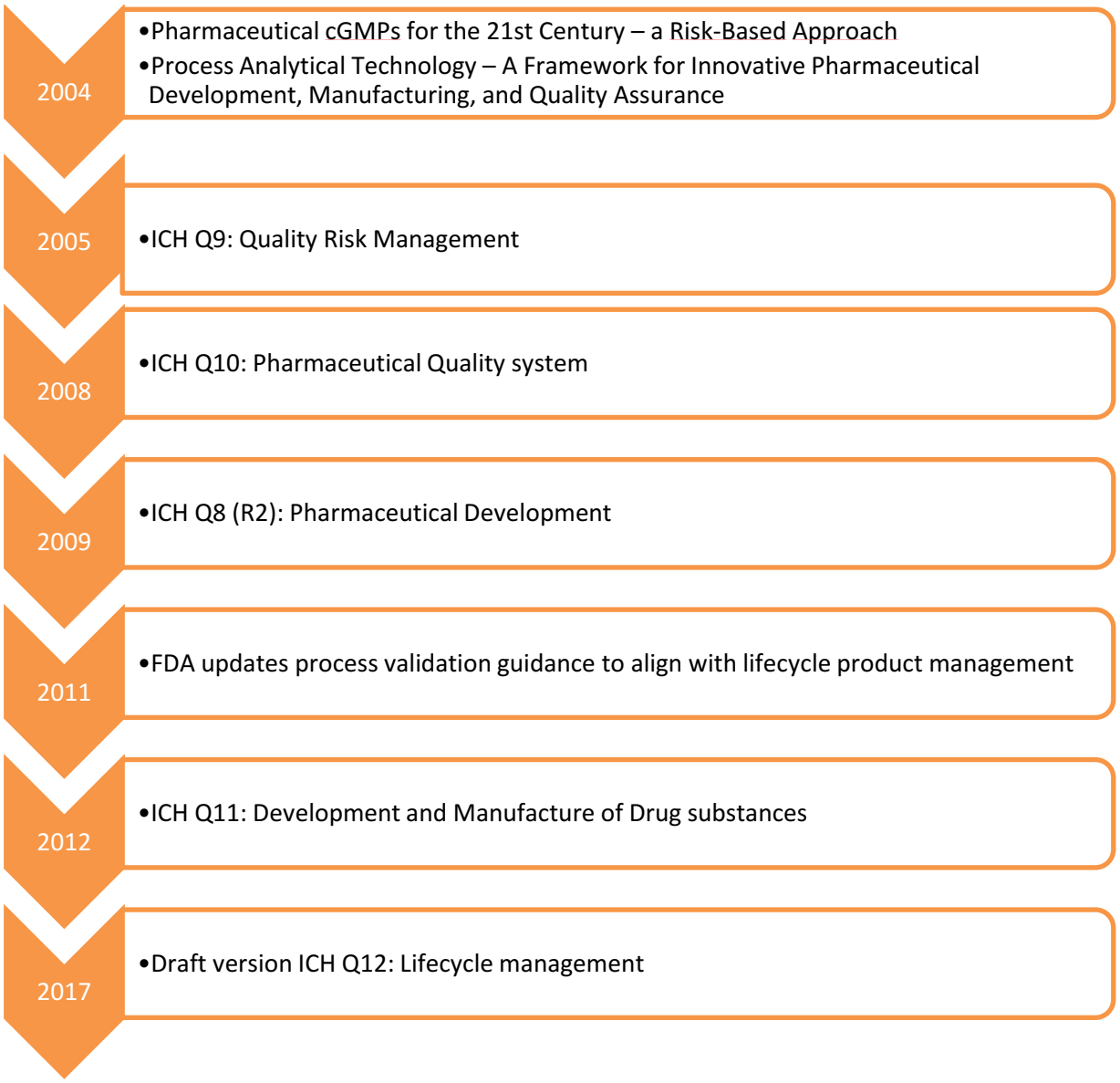

Figure 2.5 Evolution of the regulatory framework for pharmaceutical products.

In the 1950s, Juran was a pioneer in developing the QbD principle[80]. The QbD approach makes use of sound science and quality risk management to develop both product and process so that the process is developed to meet the desired quality specifications [21]. The main idea is that if the relationships between process settings and material attributes are fully understood, quality issues can be anticipated and promptly mitigated. A process is generally considered well understood when[81]:

1. Product quality is based on clinical performance;
2. All critical sources of variability are identified and explained;
3. Variability is managed by the process;

4. Product-quality attributes can be accurately and reliably predicted over the design space established for materials used, process conditions, manufacturing, environmental and any other relevant condition.

Quality risk management is defined in the ICH guideline Q9 as "a systematic process for the assessment, control, communication and review of risks to the quality of the drug product across the product life cycle"[82]. Some of the recommended tools are Ishikawa diagrams, failure mode analysis, effects and criticality analysis, fault tree analysis, hazard analysis and critical control points, hazard operability analysis, preliminary hazard analysis, risk ranking and supporting statistical tools. The usefulness of each of these tools depends on the prior knowledge of the process, risk assessment stage and complexity of the issue to be addressed.

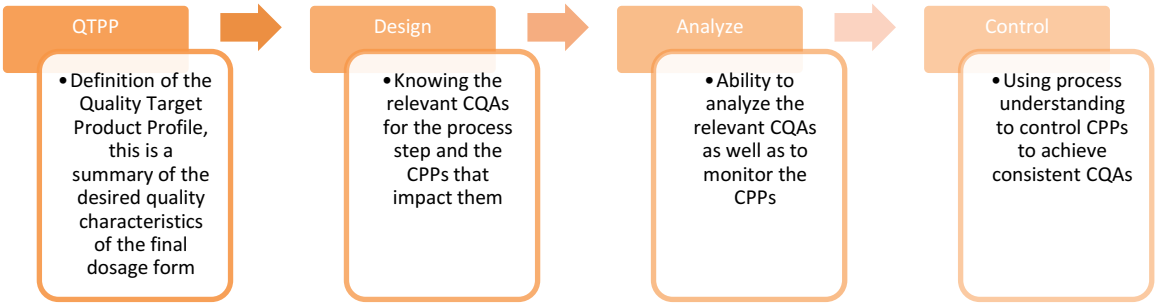

Figure 2.6 Three step implementation of QbD, with the objectives of each step[81].

Figure 2.6 illustrates the stages of implementation of QbD: Design, Analyze and Control. The design stage starts with the identification of the CQAs that are being affected by the process step along with the CPPs that have been determined to affect the CQAs. This step aims at creating (or further developing) process understanding and it is critical for the next phase: the choice of a suitable analyzer. In the analysis stage, a suitable analyzer is chosen to monitor the CQAs and the CPP. The final stage is control. It involves a control scheme design based on process understanding such that the data from the analyzer can be used for making real-time process decisions, so that consistent process performance and product quality can be achieved.

Process Analytical Technology (PAT) has been defined as "a system for designing, analyzing, and controlling manufacturing through timely measurements (i.e., during processing) of critical quality and performance attributes of raw and in-process materials and processes, with the goal of ensuring

final product quality" [24]. A goal of the PAT framework is to identify and handle sources of variability of the process to provide a foundation for QbD implementation.

Process analysis measurements can be classified as: in-line, sample is analyzed *in situ*[24]; on-line, sample is diverted from the main process, analyzed and may be returned; at-line, the sample is removed and analyzed close to the process; and off-line, the sample is removed and analyzed away from the process. Traditional methods to monitor the above mentioned parameters are limited to either endpoint analysis or limited sample collection. With the implementation of PAT tools, the goal is to get real-time analysis of the whole process (in-line monitoring). For PAT tool applications, it is necessary for the analytical results to be available in the time-frame necessary to facilitate making decisions in real-time[81].

2.6 Design of experiments

Design of experiments (DoE) is a structured, organized method to plan and conduct experiments and analyze the resulting data using the statistical approach in order to determine the factors that affect a process, its interactions and how they affect the output of that process[83]. DoE is a much more efficient way to achieve process knowledge[84] when compared to changing one factor at a time. Risk analysis should be the starting point for allocation of resources for this activity. Prior knowledge about the process should be used to define the appropriate range to define the design space, so that areas where it is impossible to operate are excluded[23].

Montgomery[83] has described a process by the means by which we transform a series of inputs in outputs, under the influence of a series of factors that can be categorized as controlled or uncontrolled. Noise corresponds to uncontrolled unavoidable variation which is expressed through the experimental error. Nuisance factors are factors that may influence the experimental response but in which we are not particularly interested. It is still important to be aware of what these factors might be so that we can reduce or even eliminate the variability transmitted from these nuisance factors to our response. Blocking is a basic design technique that is used to this effect. A block is defined as a set of homogeneous experimental conditions.

The impact of controlled factors on the quality of the product can be used to help identify CMAs and CPPs. In DoE approach, the controlled inputs are systematically varied in order to determine their effect on the responses. DoE can also be run for the purpose of optimization, that is to find a set of CMAs and CPPs level that will result in the desirable quality target product profile (QTPP). In confirmation experiments, DoE is used to confirm that the system behaves in a way that is

consistent to previous knowledge. In discovery experiments, DoE is used to determine the impact of new variables, materials or levels in the CQAs. Finally, DoE can be used for robustness testing in order to address how we can set control variables to minimize the variability in our response to factors that we are not able to control very well.

The choice of the design is dependent on the type of parameters under study, the number of replicates and the run order for the experimental trial, determining if blocking is required or not. Choosing a design also implies thinking of the quantitative relationship (empirical model) that will describe the results. DoE seeks to approximate reality with a mathematical model, the simplest of which is a linear model. The model is a quantitative relationship that is established between inputs and output. Linear models are often called main effect models and are used extensively in screening and characterization experiments[83]. Another type of design that is used in screening experiments is the D-optimal design[85]. Generally, a D-optimal design is a computer-aided design that minimizes the variance of the model regression coefficients[83]. It does so by maximizing the determinant of **XX**', where **X** is the data matrix of independent variables, that is the controlled factors under study evaluated at specific levels in the design space. They are especially useful in situations where the design matrices are not orthogonal and the effect estimates are correlated[86].

2.7 Multivariate data analysis

Chemometrics, as defined by Massart *et al.*[87], "is a chemical discipline that uses mathematics, statistics and formal logic (a) to design or select optimal experimental procedure; (b) to provide maximum relevant chemical information by analyzing chemical data; and (c) to obtain knowledge about chemical systems".

Multivariate data analysis (MVDA) is thus involved in the process of collecting and extracting information from data. The first step is to collect "good data", meaning data with a reasonably low amount of error for the purpose that is being given to the data. Otherwise the information may be uncertain or even worst, wrong.

As stated in point (a) of the chemometrics definition, there is a need to choose which experiments are relevant to the problem being studied. To this end, the chemometrician will resort to design of experiments (DoE). The experiments will generate data which the chemometrician will use to extract information (point (b)) and which will give information about the system, as stated in point (c) of the same definition.

The first step for extracting information or for a data analysis is to display the data. Usually, the objects (samples) are represented as rows and the variables as columns. In many cases there will be more variables than objects since chemical systems are usually multivariate systems. Simplistically this means that several measures are made simultaneously. That is why chemometrics falls into the "multivariate analysis techniques" category. [88] One of the main advantages of chemometrics is that it offers methods that allow reducing the dimensionality of the data, such as Principal Component Analysis (PCA).

The data analysis will often lead to the formulation of hypothesis that will need to be tested (hypothesis testing), or it may have the goal to describe quantitatively one variable (or more) in terms of the others (calibration/regression), or even to try to group the objects according to the variables measured (classification). The obtained models always have to be validated. This is often achieved by the development of statistical tools, numerical methods, computer technology together with chemical and biological knowledge (in order to make interpretations).

Before describing some of the chemometric methods used in this work, the nomenclature will first be explained. In this document, vectors are indicated by bold lower-case characters, two-way matrices by bold capitals and finally three-way arrays by underline bold capitals.

2.7.1 Principal component analysis

PCA is a favorite tool for data exploration, that is to say, to compress and retrieve the essential information and to display (the relevant information) in a clearer way than displaying the same information of each of the variables individually.

Principal component analysis (PCA) is able to reduce the dimensions by projecting the data into a "new set of variables" called principal components (PCs)[87], which are linear combinations of the original **X** variables. The first principal component will capture the maximum variance of the data, in order to preserve, as much as possible, the structure originally presented.[87]

Of course there will be some variation that is not captured by this first component (this will be in the residuals) thus one can calculate a second component that captures the second maximum source of variance in the data. This second principal component will be orthogonal to the first. Thus, the variable reduction is done by making linear combinations of the original variables. [87]

Mathematically, PCA can be described in the following way[88]: given a **X** data matrix with *n* rows and *m* columns, PCA decomposes it as the sum of *r* $\mathbf{t_i}$ and $\mathbf{p_i}$, where r is the rank of the matrix. **X** will be given by equation (2.6)[88].

$$\mathbf{X} = \mathbf{t_1 p_1^T} + \mathbf{t_2 p_2^T} + \cdots + \mathbf{t_k p_k^T} + \cdots + \mathbf{t_r p_r^T} \tag{2.6}$$

The rank of a matrix is the number of the non-zero rows obtained by reducing a matrix to its echelon form, so trivially *r* must be less or equal to the smaller dimension of **X**. The $\mathbf{t_i}$ and $\mathbf{p_i}$ vectors are known as scores and loadings, respectively. While the $\mathbf{t_i}$ gives information about how the samples relate to each other, the $\mathbf{p_i}$ gives the same information about the variables. The principal components (PCs) are the outer product between the $\mathbf{t_i}$ and $\mathbf{p_i}$ ($\mathbf{t_i p_i^T}$) and they are ordered according to the variance captured.

When one is performing a PCA analysis, the goal is to explain the main sources of variation in the data and not to explain each detail and particularity of every sample. Therefore, the model is generally truncated leaving out a small amount of variance in a residual matrix. **X** will be now given by equation (2.7)[88].

$$\mathbf{X} = \mathbf{t_1 p_1^T} + \mathbf{t_2 p_2^T} + \cdots + \mathbf{t_k p_k^T} + \mathbf{E} = \mathbf{T_k P_k^T} + \mathbf{E} \tag{2.7}$$

The scores ($\mathbf{t_i}$) form an orthogonal set $\mathbf{T_k}$ and the loadings ($\mathbf{p_i}$) form an orthonormal set $\mathbf{P_k}$ with **E** being the residuals.

The projection of the score vectors on a plan is called score plot, whereas the projection of the loading vectors on a plan is called loading plot.

2.7.2 Regression analysis in the context of multivariate data analysis

The regression problem: how to model one (or more) dependent variables, responses **Y**, by means of a set of predictor variables, **X**, is one of the most common problems that can be encountered in science and technology[89].

In handling numerous and collinear **X**-variables, or predictors, and response profiles (**Y**), Partial Least Squares (PLS) Method allows for the investigation of more complex problems[89]. PLS seeks to find factors, latent variables (LV), which both capture and achieve correlation, by maximizing the amount of variance explained in **X** that is relevant for predicting **Y**[90].

The NIPALS (Non-linear Iterative Partial Least squares) algorithm is perhaps the most intuitive way of calculating the scores **T** and loadings **P**, and an additional set of vectors known as weights, **W**[90] (see Figure 2.7). The PLS decomposition is started by selecting a column of **Y**, as the starting estimation for $\mathbf{u_1}$ (score of the first latent variable of **Y**). Each model parameter is iteratively estimated until convergence is achieved. Convergence is checked by comparing the scores **t** in **X**. After convergence, the entire procedure is repeated for the next latent variable (the NIPALS algorithm is given in for example, Westerhuis *et al.*[90]).

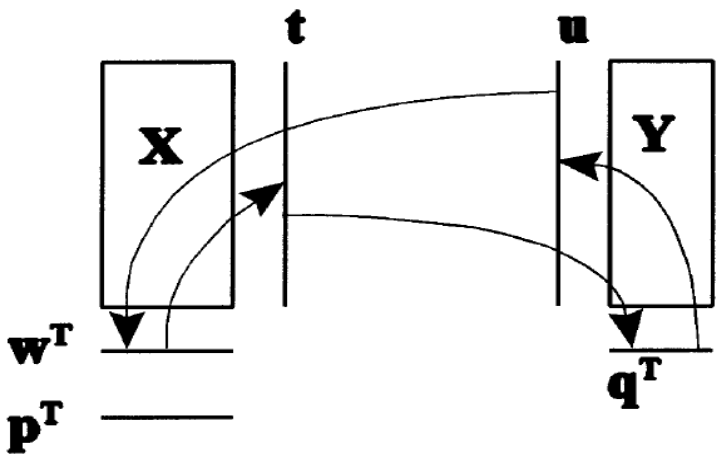

Figure 2.7 PLS method. The method will start by a first estimate of u, until convergence of t.

PLS can also be written to look as a multiple regression model, given by equation (2.8)[89], where **W*** is **W** in terms of non-deflated **X**, $\boldsymbol{\beta_{PLS}}$ the "PLS regression coefficients" and **F** the **Y** residuals.

$$\mathbf{Y} = \mathbf{X}\mathbf{W}^{*}\mathbf{Q}' + \mathbf{F} = \mathbf{X}\boldsymbol{\beta}_{\mathbf{PLS}} + \mathbf{F} \tag{2.8}$$

The variable influence on projection (VIP) was developed as a parameter which summarizes the importance of the **X**-variables, both for **X**- and **Y**-models. The VIPs are a weighted sum of squares of PLS weights taking into account the amount of explained **Y**-variance in each dimension.

Extensions to the PLS model, where additional sources of information could be added, have been found to be useful in the literature to monitor chemical processes[91], [92], particularly in cases where the number of variables measured on the same observations is very high and/or there are several groups of variables[93]. The advantage is that in addition to monitoring the whole process, we are

keeping the information segmented making it easier to detect, isolate and identify causes for when a fault happens[90]. It seems only logical to break up a process that consists of many distinct sections (sources of information) into several **X**-blocks, one corresponding to a different source of information about the process. Nevertheless, it is ideal for the data to be analyzed jointly. For example, when acquiring multivariate data from different processing units within an industry, it is often relevant to determine how each processing unit influences final product quality along with assessing the impact of any given process variable occurring within that unit.

An extension of PLS capable of taking these blocks into account is multiblock PLS (MBPLS), first proposed by Wangen and Kowalsky[94]. In MBPLS, the blocks are typically scaled to unit variance before being scaled a second time to compensate for varying block dimensions. While the blocks must all have the same number of observations, the number of variables may vary widely. To achieve this, they are divided by the square root of the number of variables in the blocks to achieve block scaling and allow a direct comparison between the blocks[90]. In MBPLS model, different scores for each data block are calculated; these are called sub-level-scores. With the block scores, it is possible to calculate the super-level scores. If the super-scores are used for the deflection of **X** and **y** blocks (Figure 2.8), then the predictive capacity is equal to an unfolded PLS model. Blocking the information like in MBPLS has the great advantage of simplifying the interpretation of the data by looking at smaller blocks of information and the relationship between them[95].

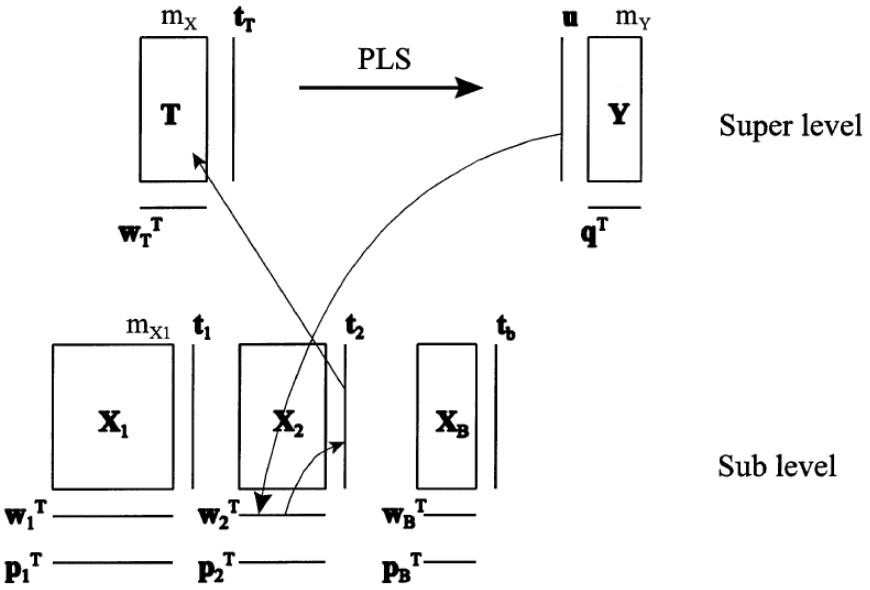

Figure 2.8. MBPLS method. Adapted from Westerhuis *et al.*[90]

Block importance for prediction (BIP)[93] is an extension of the variable importance on the projection (VIP). The general rule used is that when the blocks have been scaled, a block with a BIP much higher than 1 represents an important contribution to the model[93].

Statistical indicators should be used to evaluate the generated models. The root mean square error of calibration (RMSEC) gives an estimate of the average deviation of the model from the data, giving us an idea on how well the model fits the data. In contrast, cross-validation is a practical way to test the significance of a model[96]. In cross-validation, typically the data set used for calibration is splitted into different training sets to try to evaluate how the model would perform when applied to new data. The root mean square error of cross-validation (RMSECV) can be used to measure the predictive power of a model, making it a useful tool for initial model comparison. In order to be able to calculate the root mean square error of prediction (RMSEP), one needs to have available independent prediction set of samples that have known **Y** values.

CHAPTER 3 BUILDING PROCESS UNDERSTANDING OF FLUID BED TASTE MASK COATING OF MICROSPHERES

Title page

Authors and affiliations:

Barbara Santos Silva, Department of Chemical and Biotechnological Engineering, Sherbrooke University, Pfizer Industrial Research Chair, Sherbrooke, CANADA

Matthew Santangelo, Pharmaceutical Sciences, Drug Product Development, Pfizer Global Research and Development, Groton, USA

Marie-Josée Colbert, Department of Chemical and Biotechnological Engineering, Sherbrooke University, Pfizer Industrial Research Chair, Sherbrooke, CANADA

Clémence Fauteux-Lefebvre, Department of Chemical and Biotechnological Engineering, University of Ottawa, Ottawa, CANADA

Jeremy A. Bartlett, Pharmaceutical Sciences, Drug Product Development, Pfizer Global Research and Development, Groton, USA

Pierre-Philippe Lapointe-Garant, Manufacturing Process Analytics & Control Team, Pfizer Canada, Montréal, CANADA

Ryan Gosselin, Department of Chemical and Biotechnological Engineering, Sherbrooke University, Pfizer Industrial Research Chair, Sherbrooke, CANADA

Date of submission: October 24th, 2018

Journal: AAPS PharmSciTech

Note: For consistency purposes minor changes were made to this section.

Contributions to the thesis: This chapter is focused on describing the adopted methodology to study the relevance of coating formulation and Wurster process variables in the taste masking performance of a novel reverse enteric polymer (Kollicoat® Smartseal). It is important to point out that dissolution at pH 6.2 was used as a surrogate test for taste masking performance. This work allowed us to conclude that Kollicoat® Smartseal is a robust polymeric system (within the studied design space) and that the final microstructure of the applied film is critical for coating performance.

Titre en français : Étude du procédé d'enrobage de microsphères par lit d'air fluidisé dans un but de masquage de goût

Résumé en français :

Le goût est souvent cité comme un des principaux facteurs ayant un impact négatif sur l'adhésion thérapeutique des enfants. Les systèmes composés de microsphères enrobées sont des solutions prometteuses car ils fournissent des doses de PA divisées en de nombreuses unités posologiques plus petites permettant un dosage mieux adapté à la grande variabilité de poids des enfants de bas âges. Aux fins des présents travaux, les microsphères ont été enrobées avec du Kollicoat® Smartseal, un polymère entérosoluble inverse, qui agit pour minimiser ou empêcher la libération de PA à pH neutre dans la cavité buccale. Il en résulte un effet masquant du goût désagréable du PA. Sept variables clefs du procédé d'enrobage avec Wurster ont été sélectionnées puis évaluées par un plan d'expérience D-optimal et une analyse de la variance. Le pourcentage de PA libéré à pH 6,2 a été utilisé comme méthode de substitution pour déterminer la performance au chapitre du masquage de goût du Kollicoat® Smartseal. Les sept variables étudiées sont : la température du lit de produit, le débit d'air entrant, la pression d'air atomisé, le débit de l'atomiseur (paramètres du procédé), le taux d'enrobage, le niveau de plastifiant, la présence de solides dans la suspension d'enrobage (caractéristique du matériel) et le durcissement. Les résultats montrent que le niveau d'enrobage, le niveau de plastifiant, le débit et la température du lit sont les paramètres critiques du procédé et renforcent l'importance du durcissement pour réduire la variabilité entre les lots en favorisant la formation d'un film complet. Le lien entre les caractéristiques du matériau, les paramètres du procédé et les attributs de qualité a permis une meilleure compréhension des paramètres qui affectent le profil de libération du PA à pH buccal (*in-vitro*). Il a été démontré que tant l'épaisseur que la morphologie de l'enrobage ont un impact sur la dissolution dans 50 mM tampon phosphate de potassium.

Mots clefs : Kollicoat® Smartseal, enrobage, lit d'air fluidisé avec Wurster, plan d'expérience D-optimal, microsphères, forme posologique pour des fins pédiatriques

3.1 Abstract

Taste is routinely cited as one of the major contributing factors that negatively influence pediatric patient compliance. A promising solution is coated microsphere systems, which provide doses of active pharmaceutical ingredients (API) subdivided into a plurality of small dosage units. In this work, the microspheres were coated with Kollicoat® Smartseal, a reverse enteric polymer, which acts to minimize or prevent the release of API in the neutral pH of the oral cavity, which results in a masking effect of the unpleasant taste of the API. A screening of seven key variables in a Wurster coating process was evaluated by D-optimal design and by analysis of variance. The percentage of API released at pH 6.2 was used as a surrogate method for taste masking performance evaluation of Kollicoat® Smartseal. The seven studied variables were: product bed temperature, inlet airflow, atomizing air pressure, spray rate (process parameters), coating level, plasticizer level, solids in coating suspension (material attributes) and curing. Results show that coating levels and plasticizer levels are the critical process parameters and reinforce the importance of curing to reduce the overall variability within the batch by promoting complete film formation. The links between material attributes, process parameters and quality attributes were demonstrated to allow a better understanding of the parameters that affect the API release profile at mouth pH (*in vitro*). It was demonstrated that not only thickness, but also coating morphology have an impact on the dissolution in 50 mM potassium phosphate buffer at pH 6.2.

Keywords: Kollicoat® Smartseal, Wurster coating, D-optimal design, microspheres, pediatric formulation

3.2 Introduction

Depending on the ability of a child to swallow a tablet, the pediatric oral formulations might differ, with liquid oral formulations being preferred for younger children (from birth) and tablets being preferred for older children (from 7 to 8 years old)[53], [97]. Oral liquid dosage forms usually make use of sweeteners, flavoring agents and acids to mask the unpleasant taste of active pharmaceutical ingredients (APIs)[2], [13]. Yet, according to more than 90% of pediatricians[13], the greatest barrier to complete pediatric treatment is still the palatability of the dosage form[13]–[15]. Moreover with the pediatric population including preterm newborns up to 18-year-old adolescents[14] and with appropriate dosing being based on the patient's body surface area, it is not surprising that flexible oral dosage forms are preferred[2].

As it has been identified in 0, microspheres have been acknowledged as a flexible platform technology[14], [17], since they can be administered to a wide range of the pediatric population as long as precise dose measurement and particle size control are achieved.

As it was previously explained in section 2.1, there are four main taste masking principles: modification of formulation and/or pH, use of a physical membrane, chemical or solubility modification and solid dispersions[15]. In the field of pediatric oral dosage formulations, the two most common approaches are the use of physical membranes and modified formulations using sweeteners and flavors[26]. That being said, having the API dispersed into a matrix system, such as microspheres, can be classified as a solid dispersion approach. In theory, by having the API randomly dispersed within an inert solid carrier, the interaction between API and taste buds will be inhibited and thus mask the API's taste. However, taste masking by solid dispersion is often incomplete because API located in the exterior surface of the microsphere can quickly dissolve in the oral cavity and interact with the taste buds. In practice, the extent to which taste masking is required will always depend on the physiochemical properties of the API, as well as its taste threshold[14], meaning that depending on the API, other taste masking methods might need to be applied. For solid oral dosage forms, the application of a uniform physical barrier is the most efficient way of successfully providing a palatable dosage form. Several technologies are described in the literature for coating microspheres such as microencapsulation[98]–[100], dry coating[40], [44] and fluid bed coating (or air suspension coating[58]) . The present work will focuses on fluid bed coating with a Wurster insert. The coating layers are formed during the recirculation of the particles through the Wurster column. For further details on the Wurster coating process, the reader is advised to see section 2.4.

To produce an optimal coating, it is also essential to select a formulation that exhibits good film forming properties but low agglomeration tendencies[62]. Key coating formulation materials are polymer and additives. The polymeric system chosen for this work is the reverse enteric polymer Kollicoat®Smartseal 30D. Described in the literature is some work showing the effectiveness of this methacrylate acid copolymer [101]–[103] for taste masking. However, this work does not link the coating formulation and coating process to drug dissolution. Additives are generally used to facilitate processing of the polymer in order to promote film formation and improve mechanical properties of the polymer. Commonly used additives are described in sub-section 2.3.3 through 2.3.5 of this document.

When developing a taste-masked formulation, the formulation scientist should keep in mind the desired body site (stomach or intestine) for drug release and absorption. The chosen taste masking

strategy should not impair the bioavailability of the drug. As mentioned previously, reverse enteric polymers dissolve at acidic pH, making them ideal for stomach specific drug delivery given that the gastric pH for fasted state is pH 1-2[104]. Reverse enteric polymers do not dissolve at mouth pH 6.2 to 7.6[64].

One of the major challenges still associated with aqueous film coatings is the incomplete film formation that could lead to long-term physical stability issues[105]. To countervail this, it is usual to perform a thermal post-treatment (curing step), which results in stable release profiles upon storage[106]. This operation is typically done in an oven at controlled temperature and relative humidity. Figure 3.1 summarizes the key variables involved in the process[62].

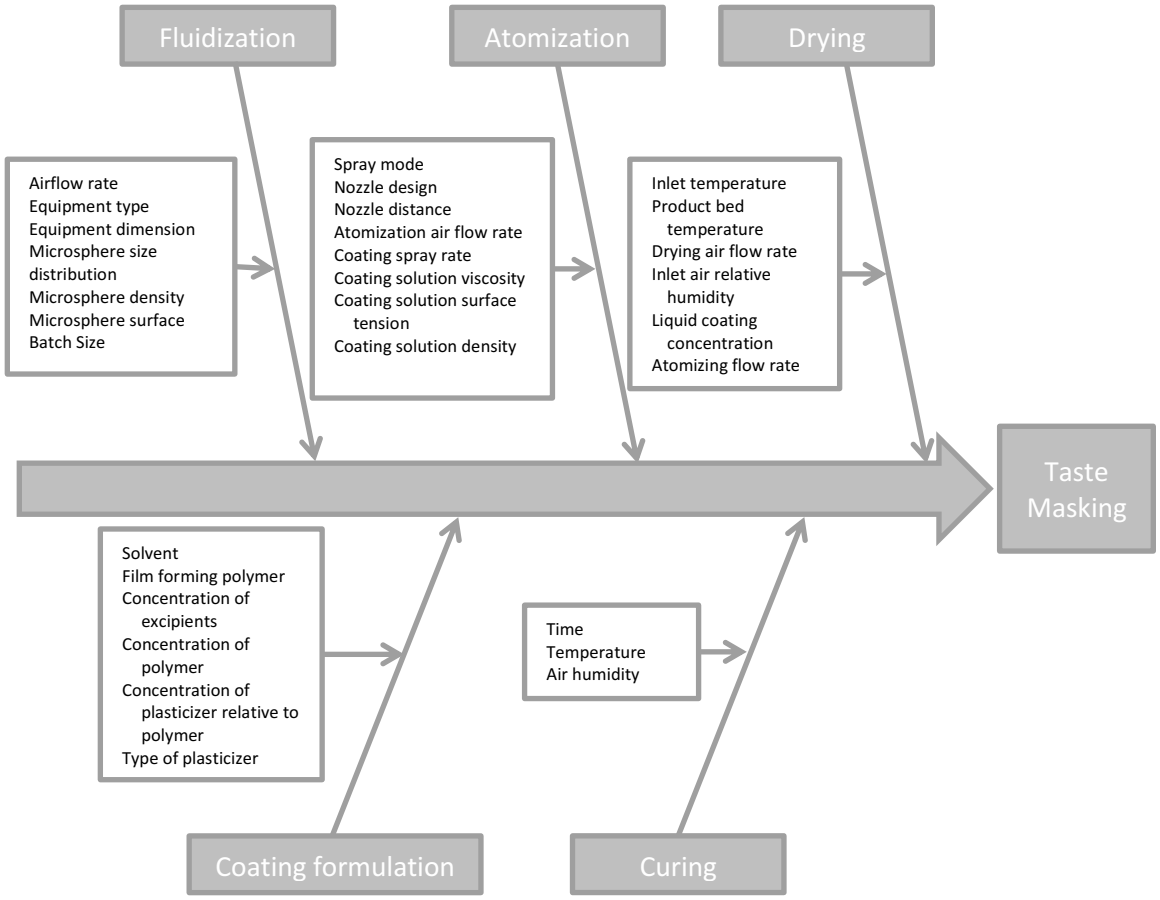

Figure 3.1 Ishikawa diagram for formulation and process variables for the fluid bed coating of microspheres.

The main objective of this work is to develop a fundamental knowledge of the parameters that affect the properties of the microsphere coating with a reverse enteric polymer (Kollicoat®Smartseal 30D) and to determine their impact on the API release profile at pH 6.2 (*in vitro* representation of the behavior in the mouth). *In vitro* dissolution provides insight on how efficiently the barrier membrane

coating prevents drug release into the oral cavity[107]. In the fasted state, the stomach pH is around 1.2[108]. The ability of the API to fully release at pH 1.2 was confirmed. However, it is not within the scope of this project to link processing conditions and bioavailability assessment. The parameters studied include both process parameters and coating formulation material attributes; curing and the quality of the coating was evaluated in terms of coating morphology. Coating morphology is also an important quality criteria, as an incomplete film will have pores and fissures in the coating[83] that impact the effectiveness of taste masking. The coating morphology is evaluated by thickness measurement, surface area analysis of the uncoated and coated microspheres as well as scanning electron microscope (SEM) imaging of cured microspheres.

3.3 Material and methods

3.3.1 Microspheres

The chosen microsphere composition was as follows: 10% w/w crizotinib (Pfizer Inc.) (API), 50% w/w stearyl alcohol (BASF, USA) (wax carrier), 10% w/w poloxamer 407 (Lutrol® F-127) (BASF, USA) (pore former) and 30% w/w microcrystalline cellulose (MCC) (FMC Corporation, USA) (filler).

The blend of materials was fed to a twin-screw extruder forming a molten mixture. The 18 mm co-rotating twin-screw extruder (model MIC18PH, Leistritz Group, Germany) had a total of seven barrels and the temperature profile was as follows (from drive to end): 40-40-40-60-80-80-80 °C. The molten material in which the API was suspended was kept at 80°C and fed to a 4” conical spinning-disk atomizer heated at 80 °C, spinning at 2250 rpm to form the droplets that, upon cooling at ambient air temperature, congeal to form the microspheres[57], [109] (MSC). The particles were then sieved to a diameter above 150 μm and below 600 μm.

The same microsphere formulation, composition and manufacturing procedures were also used throughout the batches. The mean volumetric microsphere cores particle size were was 304.4±6.3 μm with a span of 0.61±0.02 for batches 1 to 17 and 314.0±4.7 μm with a span of 0.56±0.01 for batches 18 to 21, after sieving. The span of a particle size distribution is a parameter that provides insight on the width of the distribution. Span can be defined as the difference of D90 and D10, divided by D50. Particle size distributions were determined by QICPIC (Sympatec GmbH, Germany), an automated particle analyzer based on dynamic image analysis. In QICPIC, the samples are fed (through VIBRI) to the RODOS, a dry disperser (Sympatec GmbH, Germany) that is used to ensure the effective

separation of the microspheres. A high-speed camera then captures the particles within the frame and information can be gathered relative to particle size and sphericity of the particle[110].

3.3.2 Preparation of coating suspension

The polymer system used for coating in order to achieve taste masking was Kollicoat®Smartseal 30D (BASF, Mississauga, Canada), an aqueous dispersion containing methyl methacrylate and diethylaminoethyl methacrylate co-polymer dispersion containing 30% of solids (dry polymer). Following BASF recommendations, the lipophilic antioxidant, butylated hydroxytoluene (Spectrum, Gardena, Canada) is dissolved in the plasticizer, triethyl citrate (Vertellus, Greensboro, USA) at 50 °C. The anti-tacking agent, talc (Sigma-Aldrich, Saint Louis, USA) was dispersed in distilled Milli Q water (Merk Milipore, Burlington, USA) by a homogenizer (Polytron PT1300, Kinematica, Switzerland). Stirring continuously, the talc and subsequently the mixture of antioxidant and plasticizer were added to the Kollicoat®Smartseal 30D. The suspension was stirred for at least two hours and then subsequently passed through a 200 μm sieve just before starting the coating operation to ensure no lumps were being introduced in the coating line that would potentially obstruct the nozzle during the coating operation.

3.3.3 Experimental design

Taking Figure 3.1 as a starting point, parameters related to the equipment design were excluded from this study given that only one coater was available to perform the experiments.

As it is not feasible to include all the variables in a screening analysis, the curing conditions (time, temperature and air humidity) were not included in the study. Rather, the impact of curing was included as a binary choice: subsamples of the batches were either cured or left uncured.

Thus, from the state of the art in fluid bed coating[62], [70], and by a process of elimination, it was decided that it was relevant to study the following seven process and formulation parameters:

1. Product bed temperature (selected levels: 25.0-28.5-32.0 °C): 32 °C was the level established for a maximum inlet temperature of 65 °C, so that the bottom plate would not heat to melting-point temperature of the microspheres and 25 °C was chosen taking into account the minimum film forming temperature (MFFT) of the polymer dispersion[28]. The product bed temperature provides a more precise overview of the conditions at which the sprayed droplets coalesce and form a film barrier when compared to inlet air temperature.

2. Inlet airflow (selected levels: 40-50-60 m^3/h): levels were chosen so that the flow regime[75] within the Wurster column[45], [47] would allow appropriate material transport in the upbed region. The two studied regimes were: fast fluidization, when airflow was set at 40 m^3/h, and pneumatic transport, when airflow was set at 60 m^3/h. Visual assessment of the flowability of the particles in the fluid bed confirmed the choice.
3. Atomizing air pressure (selected levels: 1-2-3 bar): levels were chosen in order to promote different droplet to particle ratios, given that the size of the droplets must be significantly inferior to the size of the microspheres to promote layered growth[67].
4. Spray rate (selected levels: 5-8-11 g/min): levels were chosen simultaneously with airflow and product bed temperature. Ensuring that product bed temperature could be kept within the chosen levels (above 11 g/min the temperature drops below 32 °C at maximum inlet temperature) and to keep to reasonable processing time (with 4 g/min the processing time to achieve a 23.6% w/w coat weight at 15.68% w/w solids in suspension would take 4 h).
5. Coating levels (selected levels: 7.00-15.3-23.6% w/w): were chosen in order to promote a significant difference in coating thickness that would have an impact on the dissolution profile, but still keep relatively thin coatings (<20 µm).
6. Plasticizer (selected levels: 12-16-20% $w/w_{dry\ polymer}$): levels were chosen based on mechanical properties of the film[28], namely the minimum film forming temperature (ranging from 21 °C to 7 °C[28]) (helped chose the product bed temperature) and the percentage of elongation at breaking point (spanning from 50 and 250%[28]).
7. Solids in suspension (15.68-19.60-23.52% w/w): levels were chosen in order to reduce the processing time. Total solids are considered as 30% of Kollicoat®Smartseal 30D, butylated hydroxytoluene, triethyl citrate and talc. By using a coating suspension with 23.52% w/w solids versus a 15.68% w/w the process time is reduced by 70%.

Based on those parameters, a seven factors D-optimal design[111] using two levels (high and low) as well as three center points was carried out in randomized order to identify and classify the critical formulation and process variables (Annexe I). The D-optimal design was calculated using Matlab R2010b (MathWorks, USA).

3.3.4 Coating of the microspheres

The twenty-one batches were run in a GPCG-2 (Glatt GmbH, Germany) fluid bed fitted with a 4" Wurster insert. Column gap was fixed at twenty mm from the air distribution plate (plate B). The coating suspension was continually stirred throughout the coating process and atomized by a Sclick970 (model 0 S3) with a 4 mm spacer and 0.8 mm liquid tip. The initial batch size was 400 g. Process parameters were recorded manually every 5 min until the desired suspension coat weight loss was achieved and the duration of the runs spanned from 20 min to 3 h.

The coating weight to be applied was determined using equation (3.1):

$$m_{suspension} = \frac{w_c m_{core}}{(1 - w_c)\varepsilon_c x_s} \tag{3.1}$$

Where w_c *[%*$w_{coating}$*/*$w_{uncoated\ cores}$*]* is the coat weight, m_{core} [g] is the mass of uncoated cores, ε_c [-] is the mass efficiency of the process, x_s *[%*$w_{solids\ in\ suspension}$*/*$w_{suspension}$*]* is the fraction of solids in suspension and $m_{suspension}$ [g] is the coating suspension to be applied. The coating suspension was continually stirred throughout the coating process.

3.3.5 Curing

Preliminary studies showed no significant changes to the dissolution profiles of coated material (results not shown) after being cured at 40 °C and 75% relative humidity for 16 hours. From these results, it was inferred that these conditions should promote stable film and adequate curing conditions. Each batch was divided into two sub-sample sets. One of the subsamples was subjected to a curing step at 40 °C and 75% relative humidity for 16 hours in a stability chamber. Both uncured and cured subsamples were kept refrigerated at 4 °C in amber glass bottles while held for further characterization.

3.3.6 Dissolution testing

The equivalent of 100 mg API was subjected to release testing using the USP/Ph.Eur dissolution Apparatus II (paddles), rotational speed 100 rpm, 900 mL of 50 mM potassium phosphate buffer, pH 6.2 (Chata Biosystems, USA), N=3. The detection was done by UV-VIS at 320 nm with baseline correction at 380 nm using dip style probe (Pion, USA) with a 1 cm cell path length collecting 120 spectra every 30 sec for 120 minutes.

3.3.7 Film thickness

Following the mounting procedure for EpoxyCure2 (Buehler, USA), it was possible to entrap a portion of cured microspheres in an epoxy mold. After 6 h to 10 h hardening, the microsphere-epoxy-puck was sanded with a 240 grit sandpaper until the microspheres were exposed at the surface followed by 360 and 600 grit sandpapers and MetaDi II 3 and 1 μm diamond paste (Buehler, USA) to smooth the surface. The surface was then analyzed by a polarized light microscope Leica DMRX-POL (Leica Microsystems Wetzlar GmbH, Germany) to measure the thickness of the coating on five microspheres (per puck) on an average of six locations per microsphere. An average of the six locations results was used for this analysis.

3.3.8 Data analysis software

Results from dissolution tests, i.e. amount of API released at 30, 60, 90 and 120 min were used as response variables for data analysis of variance (ANOVA). The software used to assess the influence of the main factors under study on taste masking was Design Expert® version 8.0.1 (Stat-Ease, Inc. Minneapolis, MN, USA).

3.3.9 Surface area analysis

Nitrogen adsorption isotherms at 77 K were measured in an accelerated surface area and porosimetry system (ASAP 2020) (Micromeritics, USA). Cured samples were previously degassed at 30 °C in order to preserve their integrity, under vacuum (3 μmHg) for 72 hours. Specific surface area was calculated using Brunauer-Emmett-Teller (BET) equation using 0.14 to 0.30 P/P^0 adsorption values range[112].

3.3.10 Scanning Electron Microscopy

Scanning Electron Microscopy (SEM) (S-4700, Hitachi, USA) was used to investigate the microstructure of the coating on three microsphere cross-sections at different locations. Each of the analyzed pucks (prepared as per section 3.3.7 Film thickness) was sputtered with gold-platinum using argon in a partial vacuum chamber. SEM images were obtained at an acceleration voltage of 5.0 kV.

3.4 Results and Discussion

3.4.1 ANOVA of MSC coated microspheres dissolution for 30, 60, 90, 120 min.

Uncured

The DoE was used to estimate the magnitude and direction of the main effects on the percentage of API released at 30, 60, 90 and 120 min from MSC microspheres coated with Kollicoat®Smartseal 30D at pH 6.2 for uncured microspheres. As the DoE was a screening design with a limited number of experimental conditions, higher order interactions were not considered. Using the data generated from the DoE batches to fit the overall model (Table 3.1), the critical formulation and process parameters on final performance were estimated by means of analysis of variance (ANOVA). ANOVA for main factors is presented in Annexe II. The analysis was conducted taking into consideration that effects with a p-value less than 0.05 give an indication that the term is significant[83].

Table 3.1 Model factor of ANOVA analysis of average dissolution responses at pH 6.2 of uncured microspheres for 30, 60, 90, and 120 min.

	30 min	60 min	90 min	120 min
	Estimated model factor in terms of actual factors (not coded) (p-value)			
Intercept	140.6	137.3	132.5	127.1
Coating Level (%w/w)	-2.4 (<0.0001)	-2.0 (<0.0001)	-1.8 (<0.0001)	-1.5 (<0.0001)
Plasticizer Level (%w/wdry polymer)	-3.4 (<0.0001)	-2.5 (<0.0001)	-2.0 (<0.0001)	-1.6 (<0.0001)
Atomizing Air Pressure (bar)	4.4 (0.0025)	4.8 (0.0002)	4.8 (0.0002)	4.5 (0.0002)

The ANOVA results show that the coating level, plasticizer level and atomizing air pressure all have a statistically significant effect on the percentage of API released. The other factors were not found to have a statistically significant effect within the studied levels. Let us therefore discuss these three factors in turn.

The coating level is an indirect measurement of the coating thickness being applied to the microspheres, which explains its impact: a higher coating level implies a thicker barrier membrane and more complete coating coverage across the batch which translates to the dissolution being suppressed

at pH 6.2. Figure 3.2 shows the clear effect of coating level for the API release from MSC microspheres coated with Kollicoat®Smartseal 30D at pH 6.2.

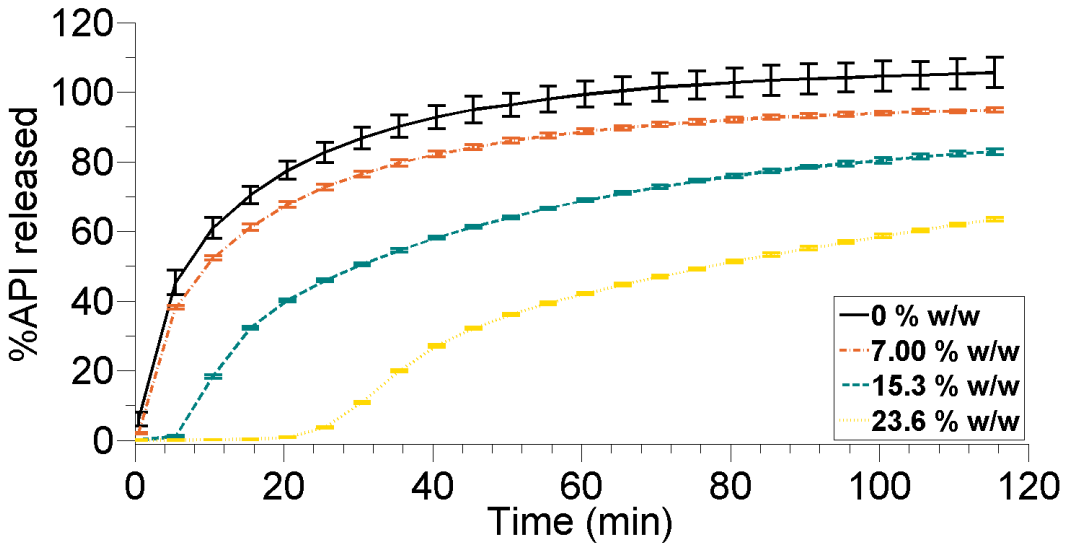

Figure 3.2 Percentage of API released as a function of time for representative coating weight gain: 0% w/w (uncoated microspheres, solid black line), 7.00% w/w (batch 20, dash-dotted orange line), 15.3% w/w (batch 2, dashed teal line) and 23.6% w/w (batch 17, yellow dotted line) for uncured coated microspheres with Kollicoat®Smartseal 30D at pH 6.2. Each point represents mean ± standard deviation calculated from three subsamples of each batch.

At the same coating level, variations of around 6.0% (for the lowest coating level, 7% w/w) and 22% (for the highest coating level, 23.6% w/w) were measured in release of API at 60 min of dissolution. Indicating that other parameters, besides coating level, may be influencing the API release. As the ANOVA model indicates, we also have to take into consideration the effect of plasticizer levels and atomizing air pressure.

The level of plasticizer used had a negative impact on API dissolution. That is to say that the amount of API released is greatest at lower plasticizer concentrations. For example, at 60 min the average percentage of API released for the lower level of plasticizer (12% $w/w_{dry\ polymer}$) was 83% and was 60% at the higher level of plasticizer (20% $w/w_{dry\ polymer}$). The percentage of plasticizer is calculated in relation to the dry polymer content in the suspension, meaning that an increase in plasticizer level corresponds to an increase of the plasticizer to polymer (film former) ratio. Higher levels of plasticizer give the polymer chains more elasticity[28] and facilitate the coalescence of discrete polymer particles, favoring a more complete film formation.

Higher atomizing air pressures lead to smaller droplet sizes, which in turn lead to a more uniform coating being applied and lower API release[70]. However, the model shows that the atomizing air pressure seemed to cause an unwanted increase in API release. When analyzing the batch records, results show that batches with an atomization pressure of 3 bar had a mass coating efficiency on average lower (79.4%) than for batches with atomization pressure of 1 bar (91.1%). This seems to indicate that some proportion of the spray dried prematurely for batches with higher atomizing air pressures, possibly resulting in less polymer being applied to the microspheres than anticipated, which would lead to increased API release.

Cured

The overall estimated model results of cured microspheres from release studies at 30, 60, 90 and 120 min (Table 3.2) show the effect of curing on critical formulation and process parameters on final performance. Curing decreases the overall percentage of API dissolved. After curing the average percentage of API released at 60 min is approximately 32% when compared to 72% before curing.

Table 3.2 Model factor of ANOVA analysis of average dissolution responses at pH 6.2 of cured microspheres for 30, 60, 90, and 120 min.

	30 min	60 min	90 min	120 min
	Estimated model factor in terms of actual factors (not coded) (p-value)			
Intercept	96.8	118.1	163.1	167.6
Coating Level (%w/w)	-3.1 (<0.0001)	-3.9 (<0.0001)	-4.1 (<0.0001)	-4.3 (<0.0001)
Plasticizer Level ($\%w/w_{dry\ polymer}$)	-2.6 (<0.0001)	-2.8 (<0.0001)	-2.9 (<0.0001)	-2.7 (<0.0001)
Spray Rate (g/min)	1.6 (0.03)	1.9 (0.01)	2.3 (0.001)	2.2 (0.0004)
Product Bed Temperature (°C)	-	-	-1.3 (0.03)	-1.3 (0.01)

For cured samples, the main effects controlling drug release are the coating level, plasticizer level, spray rate and product bed temperature. The reason why coating level and plasticizer impact the percentage of API at the studied times has already been discussed in the previous section. Unlike

uncured samples (Table 3.1), atomizing air pressure was not found to be significant. Note that the uncured film cast onto the microspheres is not yet in its final form and as such the stability of the coated dosage form is compromised. Caution should be taken when drawing conclusions using the uncured dissolution data as a response variable, because of the transient nature of the uncured coated microspheres. Nevertheless, the comparison between uncured and cured dissolution profiles comes to confirm the importance of curing for complete film formation when coating with aqueous suspension[63].

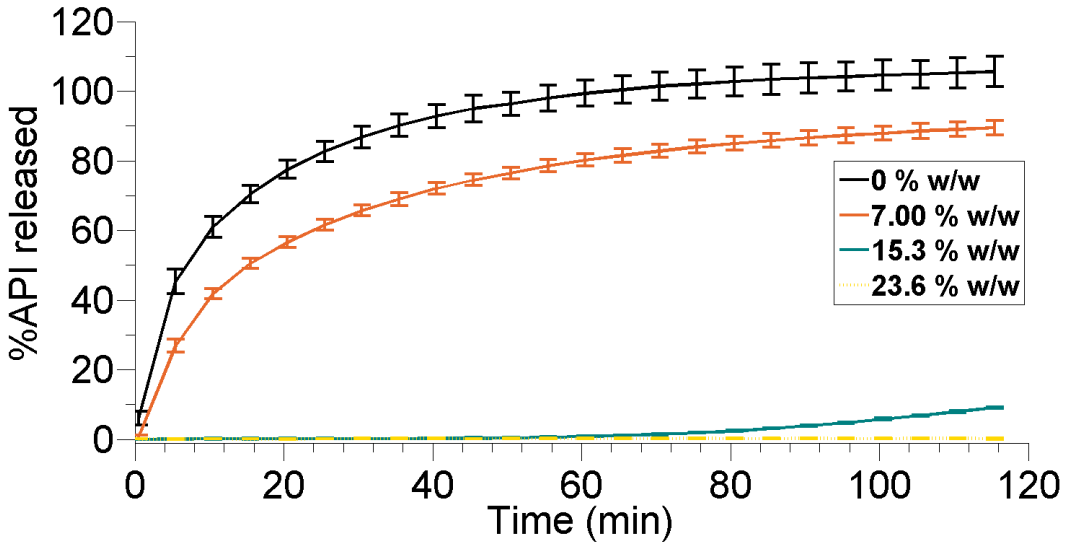

Figure 3.3 Percentage of API released as a function of time for representative coating weight gain: 0.00% w/w (uncoated microspheres, solid black line), 7.00% w/w (batch 20, dash-dotted orange line), 15.3% w/w (batch 2, dashed teal line) and 23.6% w/w (batch 17, yellow dotted line) for cured coated microspheres with Kollicoat®Smartseal 30D at pH 6.2. Each point represents mean ± standard deviation calculated from three subsamples of each batch.

Figure 3.3 shows the effect of coating levels for the API release from MSC microspheres at pH 6.2 of cured coating. When comparing Figure 3.2 and Figure 3.3 it is observable that for the same coat weight gain, the percentage of API released at a given time decreases significantly after curing. These results clearly indicate that at the end of the coating process the polymeric film is not fully formed. By exposing the coated microspheres to higher temperatures (after coating) the fusion of neighboring polymeric particles[105] is promoted, allowing the polymeric coating particles to coalesce and form a more compact film around the microsphere. This phenomenon may explain why atomization air pressure is no longer a critical factor, as the spray dried droplets might partially coalesce during curing which would in turn decrease the effect of atomization air pressure seen in the uncured samples.

At increased spray rates the percentage of API released increases. The inverse effect was observed for product bed temperature. This is to say, lower product bed temperatures resulted in higher percentage of API being released. In both cases (higher spray rates and lower product bed temperature) the resulting microsphere should have higher residual moisture. It has been previously reported by Williams III, *et al.*[113] that product bed temperature and spray rate have influence film formation during curing.

The accepted mechanism for film formation when using aqueous polymer dispersions is that after the spraying of the aqueous polymer dispersion onto the microspheres' surface, water evaporates and the polymeric particles deform and approach leading to coalescence[105]. Dry sintering and capillary forces are pointed as possible drivers for coalescence[113], [114]. Higher water content in the microspheres generally promotes film coalescence, leading to continuous and well-packed films. However this is the inverse effect of what is observed in this case. It has also been reported that higher spray rates and lower temperatures can produce cracks in the film[114]. Solvent loss beyond the solidification point can cause shrinkage of the coating and subsequently contribute for the internal stress within a coating and the formation of cracks[115], which could potentially be the explanation for the appearance of spray rate and product bed temperature as significant factors after curing.

It has been shown that curing promotes complete film formation[105], [106], [116], [117], nevertheless the initial number of polymeric layers still plays an important role on the percentage of API release, so much so that, for particles coated with a low number of layers (lower coat weight gain) there is a considerable amount of drug release even after curing.

3.4.2 Thickness and surface area impact on dissolution of cured microspheres

As discussed previously, the amount of coating applied onto the microspheres will act as a diffusion barrier and prevent the API from being released into the oral cavity[62], explaining why thickness is considered a critical quality attribute for the coating process. The mean coating thicknesses of the cured microspheres ranged from approximately 4.2 μm to 19 μm between batches. In Figure 3.4, as expected, thicker coatings released less when compared to thinner coatings. However, there are still variations in terms of release profiles between batches that have similar coat weight gains (or thicknesses). Given the lengthy sample preparation time for specific surface analysis measurement, it was chosen to sample across the DoE and only measure a few critical samples, which is why not all batches have a measured surface area in Figure 3.4.

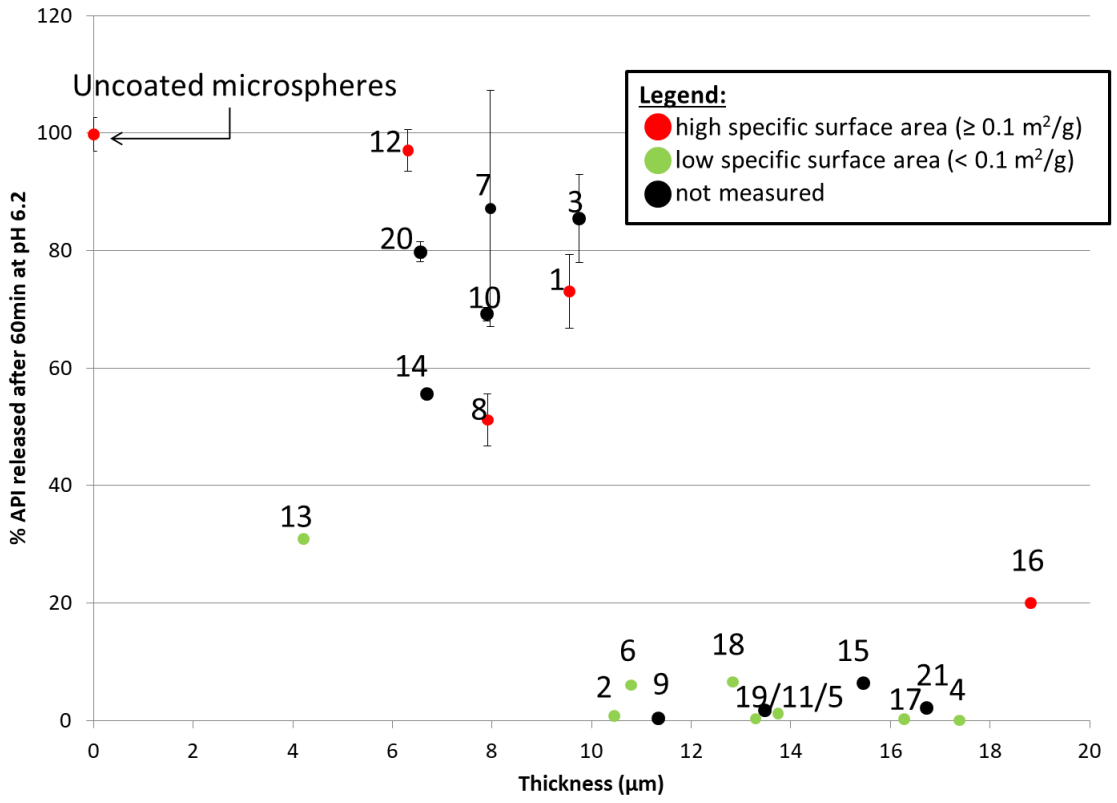

Figure 3.4 Effect of thickness on percentage of API released from cured MSC coated microspheres with Kollicoat®Smartseal 30D at 50 mM potassium phosphate buffer pH 6.2 at 60 min. Color code based on the results of surface analysis: red are batches with high surface area (≥0.1 m2/g), in green with low surface area and in black are points where surface area was not measured.

Specific surface area is the total surface area of a material per unit of mass (or volume). An increase in particle size (due to coating) corresponds to a decrease in specific surface area. It is interesting to look at the specific surface area because it gives insight on how a solid interacts with its surroundings. In this case it clarifies how microspheres might interact with the dissolution media and help hypothesize on the structure of the coating. In the case of non-uniform or highly porous coating layers (and the MSC microsphere core) the specific surface area exposed to the dissolution media is higher. If there is higher specific surface area exposed, higher amounts of API will be dissolved for the same amount of time, because as it was first described by Bruner and Tolloczko[118], the dissolution rate is directly proportional to the surface area of the undissolved solid in contact with the solvent. As such, for porous coating layers (high specific surface area) the probability that continuous dissolution-media-filled channels exist is higher[116], [119] than for non-porous coating layers (low specific surface area).

In Figure 3.4 one can see that for batches with similar levels of coating thickness, the ones that release the least also had a lower specific surface area. A hypothesis that would help us explain this phenomenon would be that when comparing batches with the same thickness the high specific surface area batch should present a more porous (or non-uniform) coating than the one presenting low specific surface area. Analyzing SEM images of coatings with similar thicknesses but significantly different surface areas helped us to qualitatively (visually) confirm this hypothesis. A comparison was made between average batches, batch 16 (19±0.8 μm, high surface area) and batch 17 (16±2 μm, low surface area), with batches that have thicker coatings, batch 1 (9.6±2 μm, high surface area) and batch 2 (10±1 μm, low surface area) as well as with batches which have thinner coatings, batch 13 (4.2±0.3 μm, low surface area) and batch 12 (6.3±2 μm, high surface area). SEM images are shown in Figure 3.5 (for clarity the reader is advised to consult the online version of this document).

For batches 16 and 17, where a thicker coating was applied, given the higher percentage of API dissolved and specific surface area of batch 16, it was expected to have a highly porous film when compared to batch 17. In Figure 3.5 (A) (batch 16) one can see that the coating presents more cracks than in Figure 3.5 (B) (batch 17). Aligning these observations with the ANOVA results from the previous section it was verified that in batch 17 a higher amount of plasticizer was used (20% $w/w_{dry\ polymer}$) than for batch 16 (12% $w/w_{dry\ polymer}$).

When compared to batches 1 and 2, coating thickness is approximately the same (approximately 10 μm). As can be observed in Figure 3.5 (C) and (D), the surface of the coating in batch 1 is more irregular than in batch 2, thus implying a more porous coating. Interestingly, in batch 1, the atomizing pressure was of 3 bar, versus 2 bar in batch 2. Figure 3.5 (C) seems to suggest that the coating spray dried prematurely, given that the structure of the droplets is still present even after curing. A layer of coating is applied with several passes through the spray, in order to produce complete coverage of the surface (layering)[46]. Mechanisms known to lead to layered particle growth include the agglomeration of semi-dried droplets on particle surface[120], a phenomenon that may have happened under batch 1 conditions as higher atomizing air pressures resulted in smaller spray droplets that dried before reaching the core[50]. This is in agreement with the conclusions from the ANOVA analysis of uncured microspheres dissolution, when it was verified that atomizing air pressure caused an increase in API release.

Batch 13 seemed like a particularly interesting batch to analyze because an extremely thin coating was applied (4.2±0.3 μm) and a relatively low API release at pH 6.2 when compared to the thicker coatings (31% API released at 60 min). As such, a non-porous coating layer was to be expected

for batch 13 (low surface area) when comparing it to batch 12 (97% API released and high surface area), especially when considering that in batch 13, a higher amount of plasticizer was used (20% $w/w_{dry\ polymer}$) than for batch 12 (12% $w/w_{dry\ polymer}$). Additionally, when looking at the SEM images and the thickness values standard deviation (0.3 μm), it seems that the coating applied to batch 13 was thin but uniformly applied onto the surface of the coated microsphere (Figure 3.5 (F)). Batch 12 (6.3±2 μm) has higher variability of coating thickness (a higher standard deviation) and from the SEM, it seems that the coating did not cover the whole microsphere Figure 3.5 (E). However, the authors consider that the SEM results were inconclusive as the coating is too thin and it was not possible to clearly differentiate the coating structure.

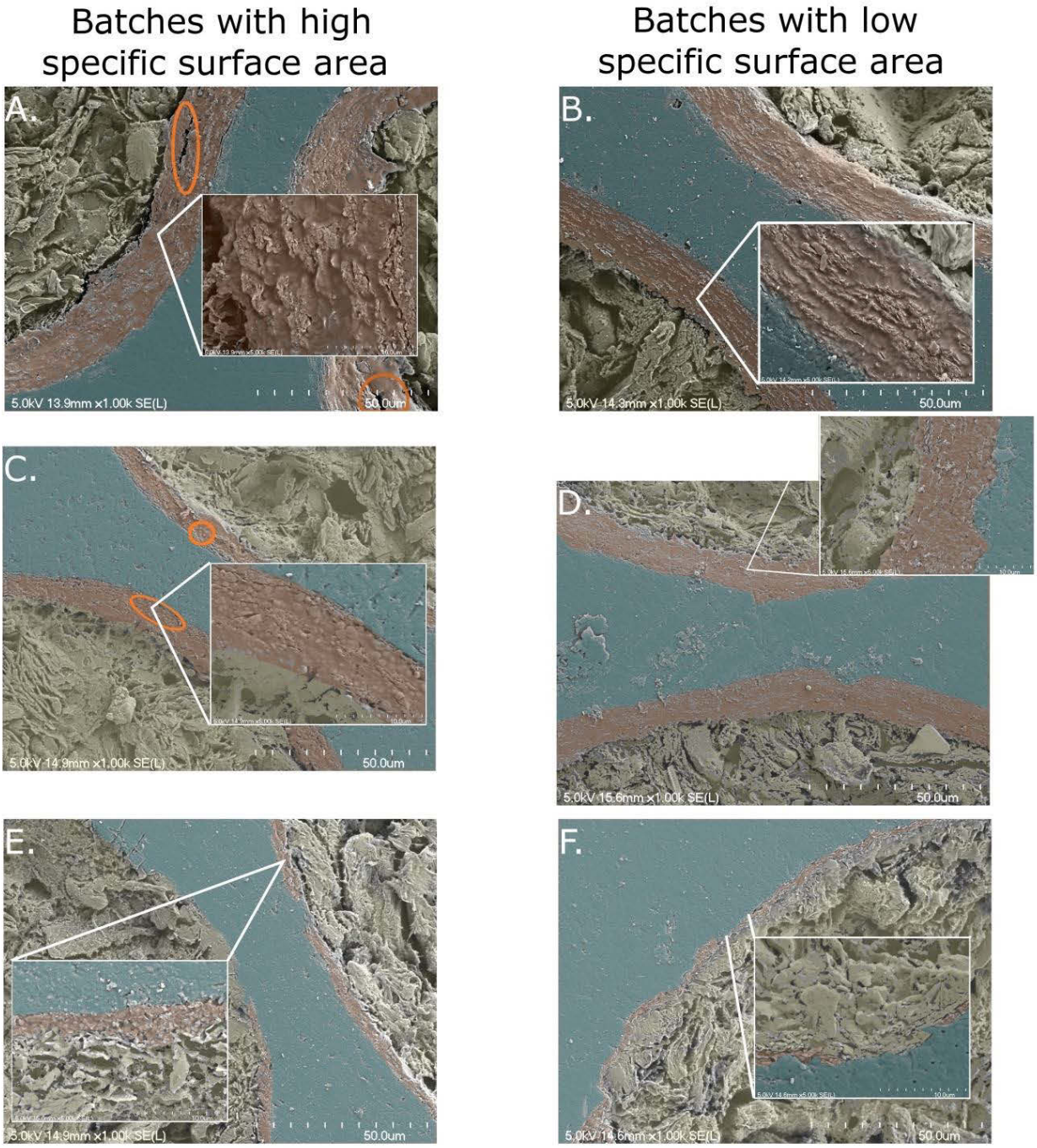

Figure 3.5 SEM images of a cross section of cured coated microspheres (A) Batch 16, mean coating thickness = 19±0.8 µm (B) Batch 17, mean coating thickness = 16±2 µm (C) Batch 1, mean coating thickness = 9.6±2 µm (D) Batch 2, mean coating thickness = 10±1 µm. (E) Batch 12, mean coating thickness = 6.3±2 µm and (F) Batch 13, mean coating thickness = 4.2±0.3 µm. False color was added to highlight the different regions in the images, color scheme is as follows: Blue: epoxy, orange: coating, yellow: MSC microsphere core.

3.5 Conclusion

This research aims at understanding how the coating process using a reverse enteric polymer (Kollicoat®Smartseal 30D) can be used to facilitate the development of pediatric formulations designed to overcome one of the major limitations with current pediatric medications, poor palatability.

The significance of the studied variables on the amount of API released in simulated saliva, which is a surrogate for taste masking, was evaluated by ANOVA. Results from this study indicate that within the chosen design space, out of seven key variables, atomizing air pressure, coating level and plasticizer levels are the critical process parameters and critical material attributes to be controlled for optimal taste masking. However, once the coated material is submitted to curing, the only remaining critical process parameters are coating level and percentage of plasticizer with the appearance of spray rate and product bed temperature. Indicating that curing is a crucial part of the process for this polymer system as it allows for a complete film formation and reduces overall variability within the batch. In future work, it would be important to understand the fundamental mechanisms behind the curing step in order to facilitate the formulation, development, choice of an adequate coating level and understand the role of relative humidity to the curing process.

It was also shown that even though coating thickness helps to explain the majority of the variation in coating performance, the coating microstructure also has an important impact on dissolution. BET analysis and SEM were used to characterize the microstructure of the coating, showing that in the future porosity should be considered as a critical quality attribute. Even for low specific surface areas, BET analysis using N_2 adsorption can still provide a useful qualitative measurement regarding the surface area of the microspheres. For the present study, SEM was used to visually confirm how the qualitative differences in specific surface area impact coating structure and its effect on dissolution. Future work in this area should include investigations on quantitative characterization of the porosity of the coatings being applied, as well as the influence of key variables on the porosity to gain a better control on the impact of the porosity on the critical quality attributes.

Future work in this field should also include the understanding of the API release mechanism of the Kollicoat®Smartseal 30D coated microspheres, not only at pH 6.2 (to evaluate the API release in the mouth), but also at lower pHs in order to simulate gastric conditions, as a surrogate test to ensure bioavailability.

3.6 Acknowledgements

This project was financed by an NSERC-FQRNT Industrial Innovation Scholarship (FQRNT application number 191551 and NSERC application number 475318) and the Industrial Chair Pfizer on PAT, the Collaborative Research and Development Grants and Pfizer Inc. (449123-13). This work has also received important contributions from Professor Nicolas Abatzoglou of Sherbrooke University, as well as Charles Bertrand, Carl St-Louis and Stéphane Gutierrez from the Centre de Caractérisation des Matériaux at Sherbrooke University. The authors would also like to acknowledge the numerous colleagues from Pfizer who made many contributions to this work, namely Jean-Sébastien Simard and Steve Hammond for their time and feedback on the developed work and the ones from Pfizer's Pediatric Network, such as Eddie Ebrahimi; Yangzhen Ciringh; and others such as Kevin Girard; Yong Zhou; Yang Angela Liu and Andrew Prpich. Finally, but not least, we would like to thank Philip Butler, from BASF, for supplying Kollicoat® Smartseal 30 D.

CHAPTER 4 MONITORING MICROSPHERES COATING PROCESS USING PAT

Title page

Authors and affiliations:

Barbara Santos Silva, Department of Chemical and Biotechnological Engineering, Sherbrooke University, Pfizer Industrial Research Chair, Sherbrooke, CANADA

Marie-Josée Colbert, Department of Chemical and Biotechnological Engineering, Sherbrooke University, Pfizer Industrial Research Chair, Sherbrooke, CANADA

Matthew Santangelo, Pharmaceutical Sciences, Drug Product Development, Pfizer Global Research and Development, Groton, USA

Jeremy A. Bartlett, Pharmaceutical Sciences, Drug Product Development, Pfizer Global Research and Development, Groton, USA

Pierre-Philippe Lapointe-Garant, Manufacturing Process Analytics & Control Team, Pfizer Canada, Montréal, CANADA

Jean-Sébastien Simard, Manufacturing Process Analytics & Control Team, Pfizer Canada, Montréal, CANADA

Ryan Gosselin, Department of Chemical and Biotechnological Engineering, Sherbrooke University, Pfizer Industrial Research Chair, Sherbrooke, CANADA

Date of submission: November 21st, 2018

Journal: European Journal of Pharmaceutical Sciences**Note:** For consistency purposes minor changes were made to this section.

Contributions to the thesis: In the previous chapter the criticality of coating thickness and coating microstructure for the *in-vitro* API dissolution at pH 6.2 were demonstrated. Therefore, monitoring fluid bed coating operation is of crucial importance in order to ensure consistent coating performance. This chapter provides a methodology that allows a one-to-one comparison between three different PAT tools, process data and raw material attributes in order to be able to recommend a process monitoring strategy that could in the future facilitate the development of a control strategy. Work was carried out on a bench-scale fluid bed coating unit (GPCG-2) where the window of the unit was replaced by a PAT adaptor able to accommodate multiple PATs simultaneously. Results show that

in-line Raman spectroscopy has a superior predictive performance (even better than process data) to monitor the coating process.

Titre en français : Suivi du procédé d'enrobage des microsphères par outils PAT

Résumé en français:

Parmi les facteurs qui influencent l'acceptation de la médication dans la population pédiatrique, le goût et l'irritation ont été identifiés comme des obstacles critiques pour l'adhésion thérapeutique des patients. Afin d'améliorer cette adhésion, les microsphères (systèmes matriciels dans lesquels le médicament est dispersé) peuvent être enrobées avec un polymère entérosoluble inverse qui empêche la libération de médicament dans la cavité buccale mais maintient une libération immédiate lorsque le médicament atteint l'estomac, et ce, dans le but d'obtenir un profil neutre pour le goût. Dans le cadre de ces travaux, la performance en ligne de trois technologies d'analyse des procédés (PAT) a été évaluée pour suivre le procédé d'enrobage des microsphères. Ces technologies sont la spectroscopie Raman, la spectroscopie proche infrarouge (*near infrared : NIR*) et la mesure de la réflectance du faisceau focalisé (*focused beam reflectance measurement: FBRM*), avec les données du procédé et les caractéristiques des matières premières. La performance des différentes sources d'information pour prédire les performances de la barrière d'enrobage est évaluée en utilisant une approche combinée des données : *multiblock partial least squares* (MBPLS). Les résultats montrent que la spectroscopie Raman a une performance de prédiction supérieure et qu'elle peut permettre de suivre le procédé d'enrobage des microsphères ainsi que de détecter les écarts par rapport au procédé, démontrant son utilité pour suivre l'enrobage par lit d'air fluidisé. Ce suivi est considéré crucial pour assurer la performance continue d'un enrobage par des membranes bloquantes composées de films fins.

Mots clefs : spectroscopie proche infrarouge, spectroscopie Raman, mesure de la réflectance du faisceau focalisé, MBPLS, enrobage dans un lit d'air fluidisé avec Wurster

4.1 Abstract

Among the factors that influence adherence to medication within the pediatric population, taste/irritation has been identified as a critical barrier to patient compliance. With the goal of improving compliance, microspheres (matrix systems within which the drug is dispersed) can be coated with a reverse enteric polymer that will prevent the release of the drug in the oral cavity while maintaining an immediate release once the drug product reaches the stomach, thereby achieving a taste neutral profile. In this work, the in-line performance of three process analytical technology (PAT) tools is evaluated in order to monitor the microsphere coating process. These tools are Raman spectroscopy, near-infrared spectroscopy and focused beam reflectance measurements, together with process data and raw material attributes. The ability of these different sources of information to predict the coating's barrier performance is evaluated by using a combined-data-approach: multiblock partial least squares (MBPLS). Results show that Raman spectroscopy has had a superior predictive performance and that it has the potential to monitor the coating process of the microspheres as well as to detect process discrepancies (such as spray rate changes), demonstrating its usefulness for the monitoring of fluid bed coating processes. It was also demonstrated that Raman can also be used to clearly differentiate batches with significantly different *in-vitro* dissolution performance. This monitoring is considered critical to ensure consistent coating performance for this thin film barrier membrane that is essential to patient compliance.

Key words: NIR, Raman, FBRM, MBPLS, Wurster coating

4.2 Introduction

Due to its convenience, the oral route is the preferred route of drug administration both for adults and children[17]. Taking into consideration the span of the pediatric population, it is desirable to design a dosage form that can provide the necessary dosage flexibility and overcome a limitation for pediatric patient compliance: the bitter (and sometimes burning[107]) taste of active pharmaceutical ingredients (API)[13]–[15]. Microspheres have been pointed out in the literature as a possible solution[14], [17]. In this work, microspheres were produced by the use of melt-spray-congeal (MSC), a continuous manufacturing process that produces highly spherical particles with a narrow particle size distribution [121].

Reverse enteric polymer(s) are cationic polymers with amino groups[122] that are less water soluble at neutral pH than at acidic pHs[32]. This property makes them ideal for taste masking applications, given that saliva pH is generally in the range of 6.2 to 7.6[64] and gastric pH for fasted

state is pH 1 to 2[104], thus ensuring that the drug will release upon exposure to acidic environment while minimizing release in the oral cavity. It should be noted that gastric pH can vary with food intake, pathophysiological conditions and concurrent drug therapy (such as proton pump inhibitors)[104].

Like other SODs, microspheres can also be coated to guarantee patient compliance. When coating small particles, Wurster coaters are a popular unit operation within the pharmaceutical industry[58]. For further details on the Wurster coating process, the reader is advised to see section 2.4. For further information on fluid bed coating with Wurster insert process, an overview of the macro[62]- and micro[70]-level processes was compiled by Werner *et al.* In a typical setting, the particles get coated by successive passes through the Wurster insert until the desired coat weight gain is achieved. The mass of coating deposited onto the microspheres has a direct impact on the thickness of the coating, and as such on its biopharmaceutical performance[123], [124]. Even though a direct measurement of the coating thickness would be desirable, the most common approach is to measure the coating solution/suspension weight loss[125] to determine the endpoint of the process, which does not necessarily provide information regarding coating uniformity or thickness (as the mass coating efficiency of the coating process will always be inferior to 100%, due to spray mass coating losses). Additionally, in order to promote adequate coating coalescence of the polymeric particles and efficient control of process parameters (fluidization, atomization and drying), film coating composition and curing needs to be ensured[47].

In past years, the paradigms of pharmaceutical and bio-pharmaceutical manufacturing have been changing. Examples of this are the United States Food and Drug Administration's application of the process analytical technology (PAT) guidance[24] and the use of the quality by design (QbD) approach by the International Conference on Harmonization[21], [82]. Linking product quality to the desired clinical performance allows to design a robust formulation and process to consistently deliver the desired product quality[80]. Traditional methods of monitoring the critical quality attributes are typically limited to either endpoint analysis or infrequent sample collection. With the implementation of PATs, the goal is to achieve real-time analysis of the process via in-line monitoring. For PAT applications, it is necessary for the analytical results to be available immediately in order to facilitate real-time decision making[81]. A systematic understanding of the coating process is required for the development of new products to be consistent with the PAT initiative[21], [24], as PAT process analyzers can bring many benefits in design, evaluation and control of film coating processes.

Knop and Kleinebudde[125] and more recently Korasa and Vrečer[126] have provided a thorough review of PATs in pharmaceutical film coating application as tools to monitor coating process critical quality attributes. Korasa and Vrečer[126] explicitly divided the above mentioned PATs by solid oral dosage form (either tablets or microspheres), highlighting that both near-infrared (NIR) and Raman are the most widely used process analyzers in film coating. However, in most works described in the literature for monitoring microsphere coating, only one PAT is evaluated at a time. The exception seems to be the work of Bogomolov *et al.*[127] where both NIR and Raman spectroscopy were compared based on the performance of the individual and combined (NIR and Raman) spectroscopic tools. In this work, three PATs were investigated: NIR, Raman and Focus Beam Reflectance Measurement (FBRM).

A molecule is NIR active when induced vibrational change results in change of the molecule's dipole moment. Typically, vibrational combinations and overtones of carbon-hydrogen, nitrogen-hydrogen and oxygen-hydrogen bonding produce NIR signatures. Interactions between atoms in different molecules alter vibrational energy states, thereby shifting existing absorption bands and giving rise to new ones, through differences in structure, which explains why NIR spectra contain information on the chemical composition as well as the physical information (such as particle size)[128]. This renders NIR spectroscopy unselective, as it is influenced by a number of physical, chemical and structural variables. Multivariate data analysis has helped to extract relevant information from the data. Anderson *et al.*[129] were the first to demonstrate the feasibility of quantitative in-line of film coating on pellet monitoring using NIR spectroscopy by use of the concept of multivariate batch calibration. Another good example of NIR being used to develop models to predict multiparticulates' performance is the work by Avalle *et al.*[123], where for a multiple-layer multiparticulate Partial Least Squares (PLS) models were developed to (a) determine the thickness of the API layer, (b) the API loading, (c) the functional coating thickness and (d) the release profile of 80% of the drug.

Raman spectroscopy involves a change in the electronic polarizability of the molecule[130] by irradiation of a sample with monochromatic light in the visible and NIR region and detection of the scattered light. Raman spectroscopy is often seen as complementary to NIR, as it allows the analysis of solids in the presence of water[125]. In contrast to infrared absorption, which is associated with polar molecules, Raman spectroscopy is associated with polarizable, delocalized electronic systems. Aromatic or conjugate structures, for example, produce strong Raman scattering[126]. Raman spectroscopy has many of the same advantages as NIR: non-destructive, high acquisition rate, minimal to no sample preparation and versatility. However attention should be paid to natural fluorescence,

which can cause interferences and potentially mask the Raman spectrum[124]. Works like the one develop by Hisazumi and Kleinebudde[131] in which the authors compared multiple curve resolution to PLS regression demonstrate the usefulness of Raman to determine (in-line) the film thickness of multi-layered pellets.

FBRM estimates chord length, which is defined as a geometric line segment whose endpoints lay on opposite edges of the particle under analysis. FBRM relies on measuring the light that is reflected back through the probe when a focused rotating laser beam hits a particle. The chord length is calculated by multiplying the duration of the reflection and the laser scan speed[132]. By measuring several particles (at random locations of the particles), a chord length distribution can be estimated, which corresponds to the number of times a given chord length was measured in the form of a probability density function. FBRM has successfully been applied to monitoring in-line particle growth in the granulation process in fluidized bed[133]. Most works evaluate FBRM in fluid bed granulation in comparison to traditional off-line technologies[132]. There is still very little research done in the field of In-line particle size measurement for coating process evaluation of coating thickness and the (in this case) undesirable tendency of agglomeration and/or attrition. It is however relevant to mention the work of Folttmann *et al.*[134] where spatial filtering velocimetry (another chord length distribution technique) showed reliable results to predict particle growth for the fluid bed coating process. Kukec *et al.*[135] performed an in-line comparative study between FBRM and spatial filtering velocimetry probe for monitoring the kinetics of particle growth in fluid bed melt granulation process. They were able to demonstrate the efficacy of both probes to predict process end-point.

In the present work, three PAT tools (NIR, Raman and FBRM) were installed on a bench-top Wurster fluid bed to monitor the coating process of MSC microspheres in real time. This work seeks to evaluate and compare strategies to monitor temporal variations of the fluid bed with Wurster insert bench-scale process of microsphere coating. The analysis is made by combining these PAT sources of information with the process and raw material data in order to predict the coating thickness and the API dissolution performance, based on multiblock partial least squares (MBPLS). From the model coefficients for each block and the block importance for prediction (BIP)[93], the usefulness of each data source can be established, making it possible to classify batches into within/outside product specifications categories and understanding the differences between process trajectories that lead to this variability.

4.3 Materials and Methods

4.3.1 Making microspheres and coating runs

In order to avoid redundancy the reader should refer to:

- Sub-section 3.3.1. Microspheres manufacturing, where the process of manufacturing microspheres and the materials used are described;
- Sub-section 3.3.2 Preparation of coating suspension;
- Sub-section 3.3.3 and 3.3.4 for a description of the coating process. Each batch was controlled to maintain the inlet airflow, the product bed temperature, as well as the spray rate and atomizing air pressure within the levels of the DoE (see Annexe I) in order to achieve the target coat weight gain by using the calculated coating suspension consumption. Note that due to Raman robustness issues it was not possible to monitor all 21 batches, batches 10 to 13 were excluded from the following analysis.

Given that coat weight gain, spray rate and solids in suspension were all parameters of the DoE, the duration of the batches was variable and spanned from 20 min to three hours. Process parameters were recorded manually at a frequency of 5 min until the desired suspension coat weight loss was achieved.

After coating, the samples were cured for 16 h at 75% relative humidity at the temperature of 40 °C in a stability chamber, like described in sub-section 3.3.5.

4.3.2 PAT data acquisition

In order to fit the PAT tools into the GPCG-2 fluid bed, an adaptor was custom-built to be interchangeable with the fluid bed equipment window (Figure 4.1), minimizing the modifications that needed to be made to the unit. The adaptor has five positions where the PATs can be mounted onto the fluid bed, each position being approximately 6 cm apart (center to center). The probes were inserted perpendicularly to the lateral surface of the product bed and the probe tip was flush mounted to the inner wall of the fluid bed in order not to disrupt the microsphere flow (Figure 4.1 C).

There was an initial effort to optimize the data quality by studying the impact of different positions and acquisition time on the PATs signal. The positions sought to reduce the noise in the spectra and maximize the number of counts. Initial tests showed that Raman signal was the least affected by position, not exhibiting significant differences between the three positions (counting from the base of the product bowl). The number of counts with FBRM was stable between positions one and

two, but then significantly decreased when the probe was inserted in position three. NIR signal was greatly affected by the positioning of the probe; the signal to noise ratio decreased when this probe was inserted in position number 2 from the bottom of the product bowl. For this reason the final configuration used throughout this study was NIR at the bottom position of the adaptor, position one, followed by FBRM in position two and finally Raman in position three (counting from the base of the fluid bed). The two other available positions were unused and kept close with a cap.

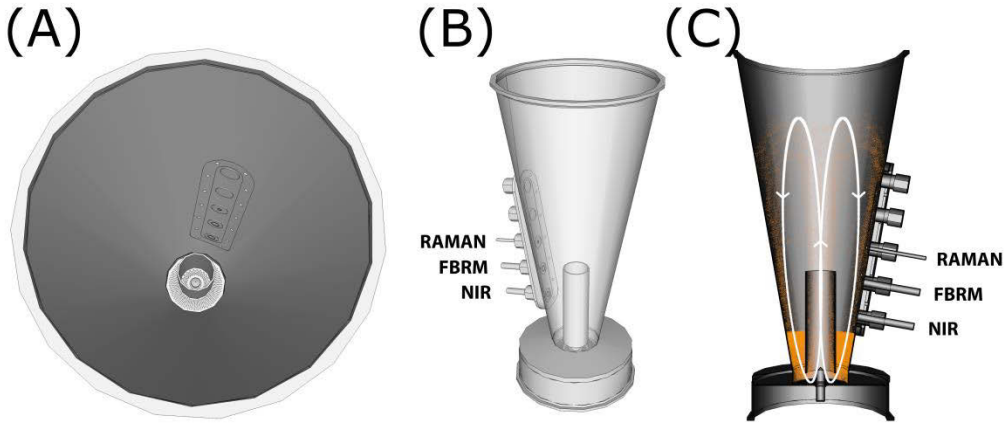

Figure 4.1 3D model of (A) Top view of (B)Product bowl of Glatt GPCG-2 with PAT window adaptor and the 3 PATs: NIR in position one, FBRM in position two and Raman in position three counting from the bottom. (C) Illustrative schematics of particle (in orange) movement (white arrows) inside the fluid bed.

The FBRM® D600 (Mettler Toledo, USA) chord length distributions were estimated using icFBRM (Mettler Toledo, USA) software that controlled the data acquisition rate at every 10 seconds (integration time set at 10 s).

The NIR ePAT611 (Expo Technologies LLC, USA) integration time was 25 milliseconds, the recorded spectra rate was 125 milliseconds. Each recorded spectra was an average of five spectra. NIR was controlled by the NovaPAC software (Expo Technologies LLC, USA). The spectral range was collected between 1096 nm and 2103 nm with a 4 nm spectral resolution.

The Pro-Raman Process Analyser (TSI, former ENWAVE Optronics, Inc., USA) was controlled by Symbion DX& RX suite (Symbion Inc., USA) to have a spectral acquisition every five seconds (integration time set at 5 s). The spectral region collected ranged from 250 cm^{-1} to 4428 cm^{-1} with a 2 cm^{-1} spectral resolution.

4.3.3 Reference methods

Thickness

To obtain a clear image of the cross-sections of the microspheres, these were entrapped in an epoxy mold, following the preparation procedure and analysis stated in sub-section 3.3.7. The measured coating thicknesses varied between 6.6 µm and 19 µm, between the 17 batches.

Dissolution testing

The dissolution testing at pH 6.2 methodology is detailed in sub-section 3.3.6. For the 17 batches, the average of the three replicas at 120 min was used to build the models, which varied between 0 and 97.6% of API released.

4.3.4 Summary of data

Figure 4.2 summarizes monitored variables that are descriptive of the process. The variables were classified in two groups: raw material and temporal variables. Raw materials are discrete variables set at the beginning of the process, while temporal variables are measured over the entire time history of the batch. A reminder of the nomenclature used: vectors are indicated by bold lower-case characters, two-way matrices by bold capitals and finally underlined bold capitals for three-way arrays.

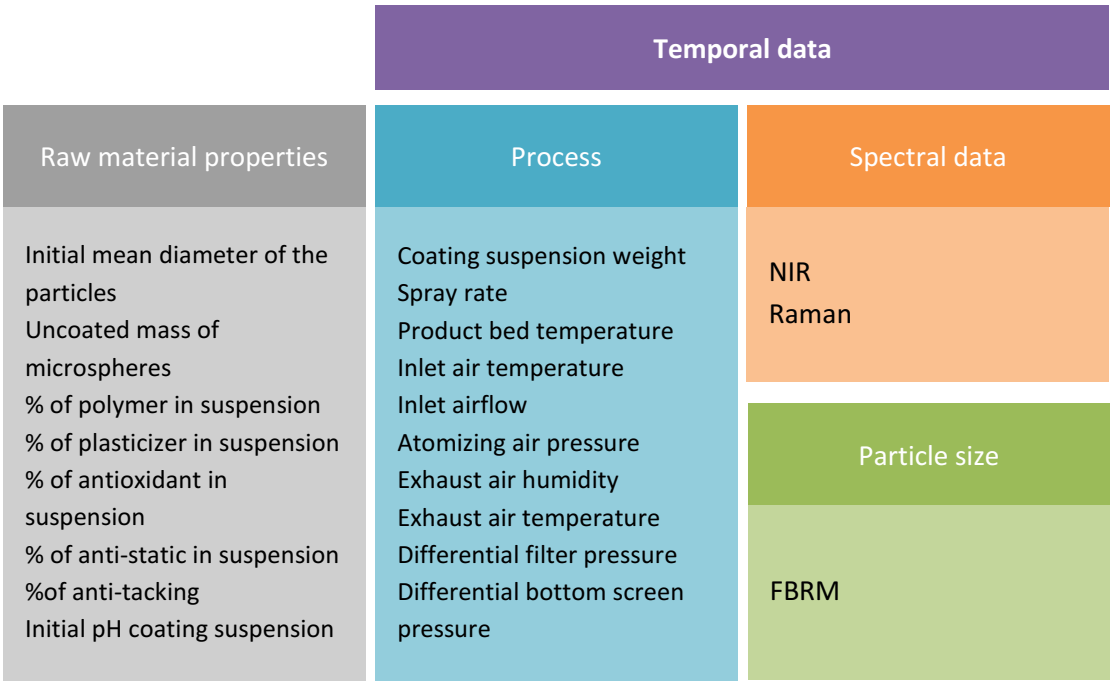

Figure 4.2. List of variables monitored during the coating runs.

The temporal data can thus be divided in four 3D matrices, Process (**P**), NIR (**N**), Raman (**R**) and FBRM (**F**) data, each with dimensions [batches × variables × time].

The selected wavelength for analysis in the NIR data ranged from 1136.8 nm to 1933.4 nm (202 data points), Raman ranges from 906 cm^{-1} to 1636 cm^{-1} (366 data points) and FBRM ranged from 1 μm to 331.13 μm (85 data points). Other regions were excluded from the analysis because they were uninformative or noisy.

Several data pretreatment methods were applied to the spectra, with the best results for NIR data obtained with a combination of standard normal variate (SNV, usually used for scatter correction)[136], followed by Savitzky-Golay estimate of the second derivative using 15 points and a first order polynomial (used to offset additive plus multiplicative effects)[136]. For Raman data, SNV alone was needed and FBRM required SNV and 15 point smoothing in order to normalize the differences induced by variations in air flow across the DoE.

In order to align/synchronize the batches that had different duration and the different sources of temporal variables that had different acquisition rates, the time series of all variables were linearly interpolated[137] by resizing the data from 0 to 100% batch completion.

As such, for the temporal data, the geometry dimensions of the four final matrices are **P** [17 × 10 × 100], **N** [17 × 202 × 100], **R** [17 × 366 × 100] and **F** [17 × 85 × 100]. The Raw material properties matrix (**M**) has dimensions of [17 × 8] and finally the reference (thickness and percentage of API released at pH 6.2 at 120 min) were treated as two separate vectors [17×1]. These last two vectors were mean-centered and divided by their standard deviation.

4.3.5 Multiway data unfolding

The original three-way data must be reshaped into a two-way array, also known as "unfolding"[91]. Unfolding is needed in order to perform the standard two-way principal component analysis (PCA) as well as the partial least squares (PLS) and multiblock PLS regression models. Two unfolding methods will be described here: batch wise unfolding (BWU) and observations wise unfolding (OWU).

BWU (Figure 4.3) is an unfolding technique that emphasizes the differences between individual batches. In BWU, the batches (rows) are left unchanged while the time and process data are combined (columns). This combination simply implies that a given process parameter, acquired at two different time points, will be considered to represent two different variables (columns). This allows an

easy comparison between the different batches[91] or endpoint prediction of quality attributes by making use of multivariate analysis. The four BWU unfolded matrices are $\mathbf{P}_{\mathbf{BWU}}$ [17 × 1000], $\mathbf{N}_{\mathbf{BWU}}$ [17 × 20 200], $\mathbf{R}_{\mathbf{BWU}}$ [17 × 36 600] and $\mathbf{F}_{\mathbf{BWU}}$ [17 × 8500].

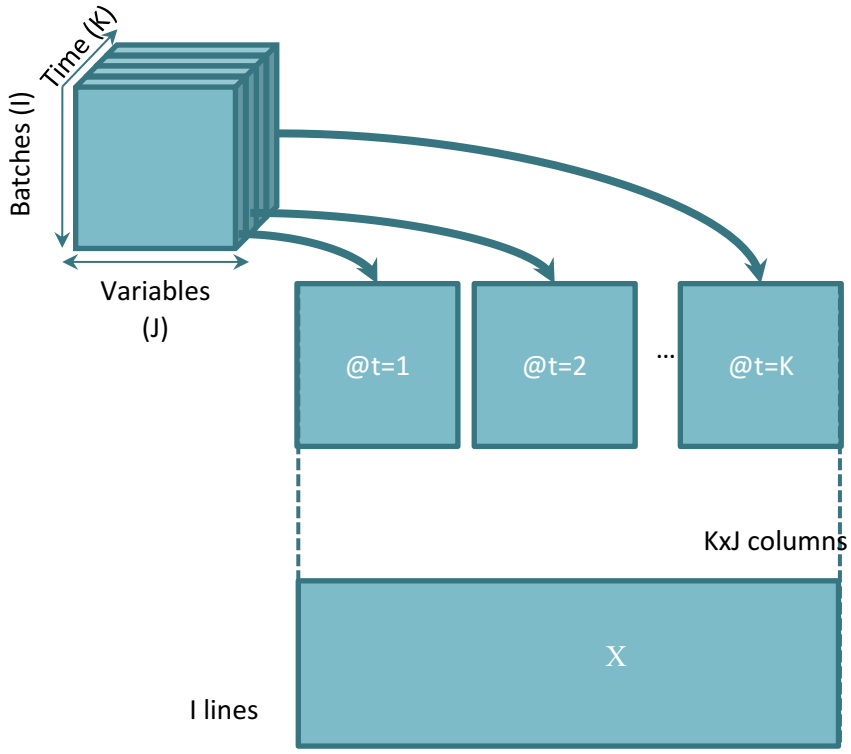

Figure 4.3. Illustration of batch wise unfolding (BWU) in which each batch represents one row in X and each process variable, for each time point, represents a column in X.

Within each batch, it is also possible to explore the process trajectory and how it relates to the changes in the process conditions using a method called OWU (Figure 4.4). In OWU, the process data (columns) are left unchanged while the time and batch data are combined (rows). The subsequent multivariate analysis provides a straightforward way to monitor batch process trajectories (displaying the evolving batch in terms of time)[138]. The four OWU unfolded matrices geometry dimensions are $\mathbf{P}_{\mathbf{OWU}}$ [1700 × 10], $\mathbf{N}_{\mathbf{OWU}}$ [1700 × 202], $\mathbf{R}_{\mathbf{OWU}}$ [1700 × 366] and $\mathbf{F}_{\mathbf{OWU}}$ [1700 × 85].

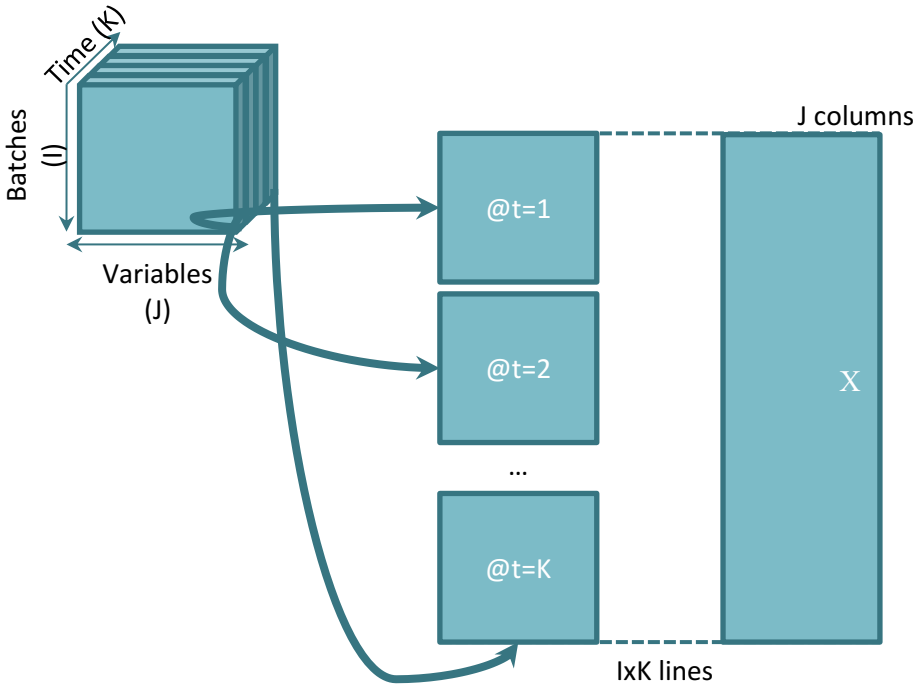

Figure 4.4. Illustration of observation-wise unfolding (OWU) in which each process variable represents one column in X and each batch, for each time point, represents a row in X.

Sub-section 2.7, provides the reader with an overview of the MVDA models used in this work. It is however important to specify how the RMSECV was determined. By randomly re-sampling the **X** and **Y** matrices (bootstrapping) a new set of model parameters can be estimated, allowing to measure uncertainty properties, such as confidence limits. In this work, the matrices **X** and vector **y** were re-sampled 50 times selecting a subsample size of 0.7 N, N being the number of batches (17 in this work), to estimate RMSECV. The same resampling strategy as to estimate RMSECV was used to estimate the distribution of BIP, in order to help estimate the dispersion in the calculated BIPs.

The computation of the models (PCA, PLS, MBPLS) were all done using in-house Matlab R2010b (MathWorks, USA) algorithms (see Annexe III to V).

4.4 Results and Discussion

4.4.1 MBPLS on coating thickness

All temporal variables recorded throughout each batch were included in this analysis as it was considered that the process trajectory may have an impact on the endpoint quality attribute. The quality of the information provided by temporal and raw materials for in-line quality attributes was evaluated.

This task is approached by predicting the endpoint thickness (that has been measured off-line). Simultaneously, the usefulness of the data sources (i.e. blocks) used to predict **y** (critical quality attribute) was assessed through the use of the MBPLS's BIPs.

The initial MBPLS model was calculated using two latent variables (LV) for ten descriptor blocks: $\mathbf{N_{BWU}}$, $\mathbf{R_{BWU}}$, $\mathbf{P_{BWU}}$, **M** and $\mathbf{F_{BWU}}$ in addition to five blocks of random variables for thickness (**y**) prediction. The additional random blocks were used to establish a reference with which the data blocks could be compared, random blocks (**Z**) 1 to 5 were created using Matlab function *rand* and the dimensions were [17 × 70600], [17 × 20200], [17 × 36600], [17 × 8400] and [17 × 100], respectively. The global **X**-variance captured by the calibration model is 22.7% and the model is able to explain 97.9% of the variance in **y**, with an R^2 of 0.98 and estimated RMSEC of 0.14 μm and RMSECV of 0.69 μm. However, it is important to stress that this model (given that it contains random variables) used solely to assess the quality of the gathered PAT data and rank them in order of importance to predict thickness.

As illustrated by the box plot (Figure 4.5(A)), the Raman data block has the highest BIP, followed by process conditions and raw materials, NIR and lastly FBRM and the random variables. The information captured by the FBRM is no more useful than a randomly generated variable, given that the median BIP value for FBRM is comparable to the random variables, even if FBRM has a wider spread.

It is also useful to analyze the loadings plot (Figure 4.5(B)). LV 1 (global **X**-variance 11.2% and 92% **y**-variance) clearly separates $\mathbf{R_{BWU}}$ from the other sources of information, having two distinct groups, one that clusters $\mathbf{N_{BWU}}$, $\mathbf{P_{BWU}}$, **M** and a second with $\mathbf{F_{BWU}}$ and the random variables ($\mathbf{Z_1}$ to $\mathbf{Z_5}$). Reinforcing the idea that Raman is the most useful source of information for endpoint prediction of thickness as the other useful sources of information prove to be redundant ($\mathbf{N_{BWU}}$, $\mathbf{P_{BWU}}$, **M**) or simply useless ($\mathbf{F_{BWU}}$ and random variables). LV2 (global **X**-variance 11.5% and 5.9% **y**-variance) breaks apart the groups formed in LV1, separates the FBRM data from the random variables and the process data from $\mathbf{N_{BWU}}$ and **M** and further puts $\mathbf{R_{BWU}}$ into evidence, showing that the information within the groups is somewhat different and could help explain certain differences within some batches. While RMSECV results indicated that LV 2 should be included in the model, it only provides a small contribution to the **y**-variance explained by the model (92% for LV 1 vs 5.9% for LV 2).

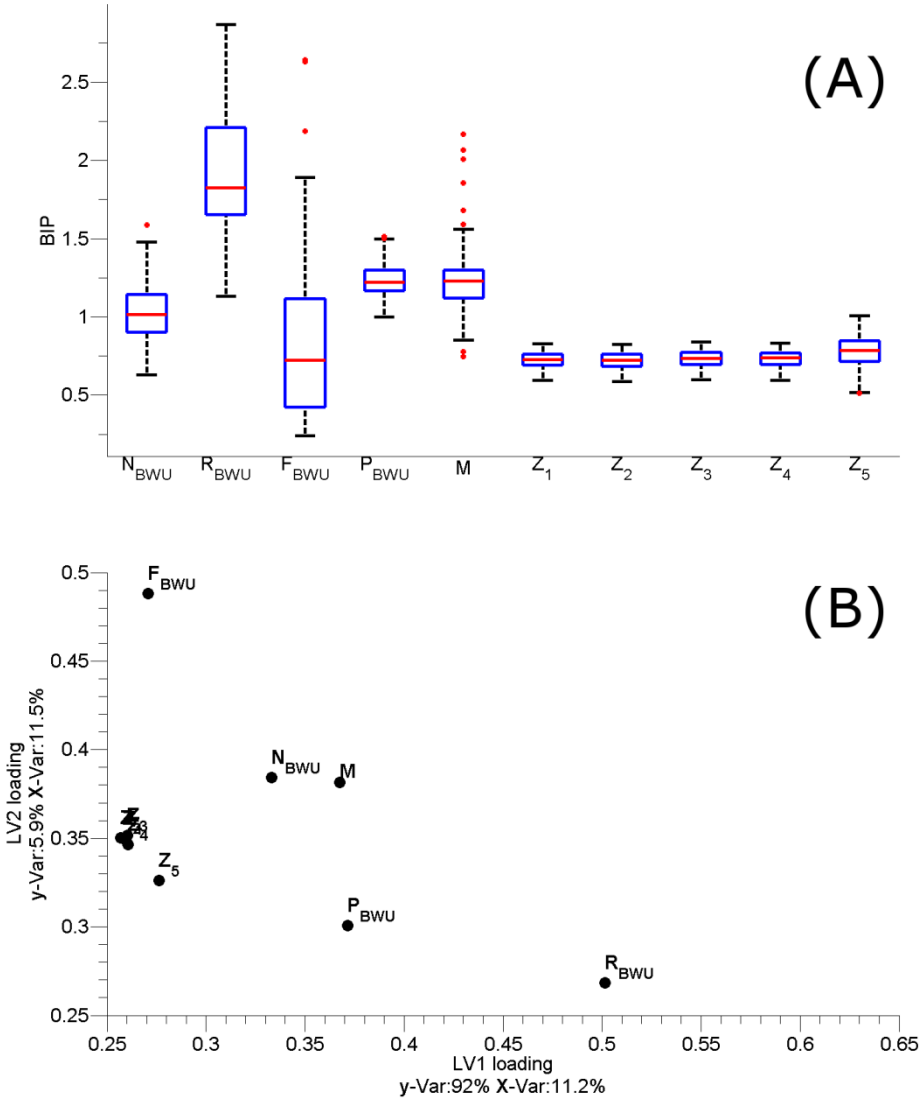

Figure 4.5 (A) BIP box plot of the 3 PAT (NIR, Raman and FBRM), Process data, Raw materials and five random variables for thickness prediction. For each box plot, the central rectangle spans from the first quartile to the third quartile, the segment inside the rectangle is the median, the "whiskers" above and below are the minimum and the maximum and the dots are the outliers. (B)Block-loadings plot for LV1 and 2 for MBPLS thickness model. Legend: NBWU (batch wise unfolded NIR matrix), RBWU (batch wise unfolded Raman matrix), PBWU (batch wise unfolded process matrix), M (raw material properties matrix), FBWU (batch wise unfolded FBRM matrix) and Z1 to 5 (random variable matrices).

From the discussion above it is possible to conclude that the current set-up of the FBRM is not able to provide enough resolution, which is necessary to measure particle growth. FBRM is limited by the fact that if the coating is very thin (6.6 µm to 19 µm) compared to the particle diameter (in this work either 304.4±6.3 µm with a span of 0.61±0.02 or 314.0±4.7 µm with a span of 0.56±0.01), the relative difference between particle size distributions throughout the coating is undetectable given the

width of the particle size distributions (given by the span). However, adjusting the position or the sampling strategy of the probe may have improved the results, as described by Alshihabi *et al.*[133] .

After this initial step, a second calibration model was built using only the useful blocks. When calculating a model excluding random variable blocks and FBRM, the four remaining blocks, $\mathbf{R_{BWU}}$, $\mathbf{P_{BWU}}$, $\mathbf{M_{BWU}}$ and $\mathbf{N_{BWU}}$, are used to compose **X**. The calibration model is shown in Figure 4.6. In this model, the same relative order of importance of the blocks is maintained (Raman > Process> RawMat> NIR). The global **X**-variance captured by the model is only 27.1%, but even so, the two-component model is able to explain 93.5% of the **y**-variance in which R^2 of 0.93, an RMSEC of 0.25 μm and RMSECV of 0.8 μm.

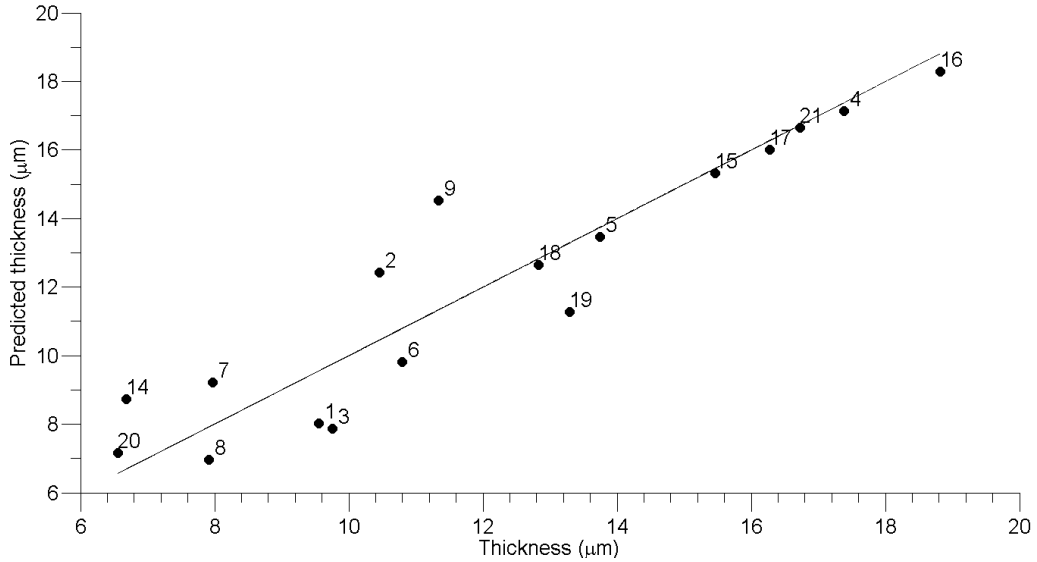

Figure 4.6 Measured vs predicted end-point thickness using only the significant data blocks (Raman, NIR, Process and Raw material data). The labels in the figure correspond to the batch identification number.

It is important to investigate the source of variance being used to build the MBPLS model. By further analyzing the sub-level loadings, it is possible to determine the main variables within the block contributing to the model. In the case of raw materials (data not shown) it is the percentage of anti-tacking agent in the coating suspension formulation and percentage of Kollicoat® Smartseal 30D, while for process data (data not shown), it is the suspension coat weight loss, which is in line with the traditional way to determine the endpoint of the process. In the case of Raman and NIR the signal intensity decreased throughout the coating process.

To further investigate spectral responses (both NIR and Raman) of the individual chemical, components were compared with spectra of microspheres (before and after coating). As illustrated in

Figure 4.7, the absolute intensity of the NIR signal decreases over time. In Figure 4.7 (A) the pretreated NIR signal is shown to ease visual interpretation. As the microspheres are coated, the StOH signal (main component of the core of the microsphere) is masked by the coating (decreasing signal intensity) (Figure 4.7 (B)). StOH that corresponds to approximately 37, 42 and 46% w/w of total microspheres at 23.6, 15.3 and 7% w/w coat weight gain, respectively. The polymeric coating material, which is the component that makes up the highest percentage in the coating suspension (12, 8 and 3% w/w for 23.6, 15.3 and 7% w/w coat weight gain), has no distinguishable spectral features and the remaining components of the coating are at much lower concentrations than the core material and the signal is much less intense.

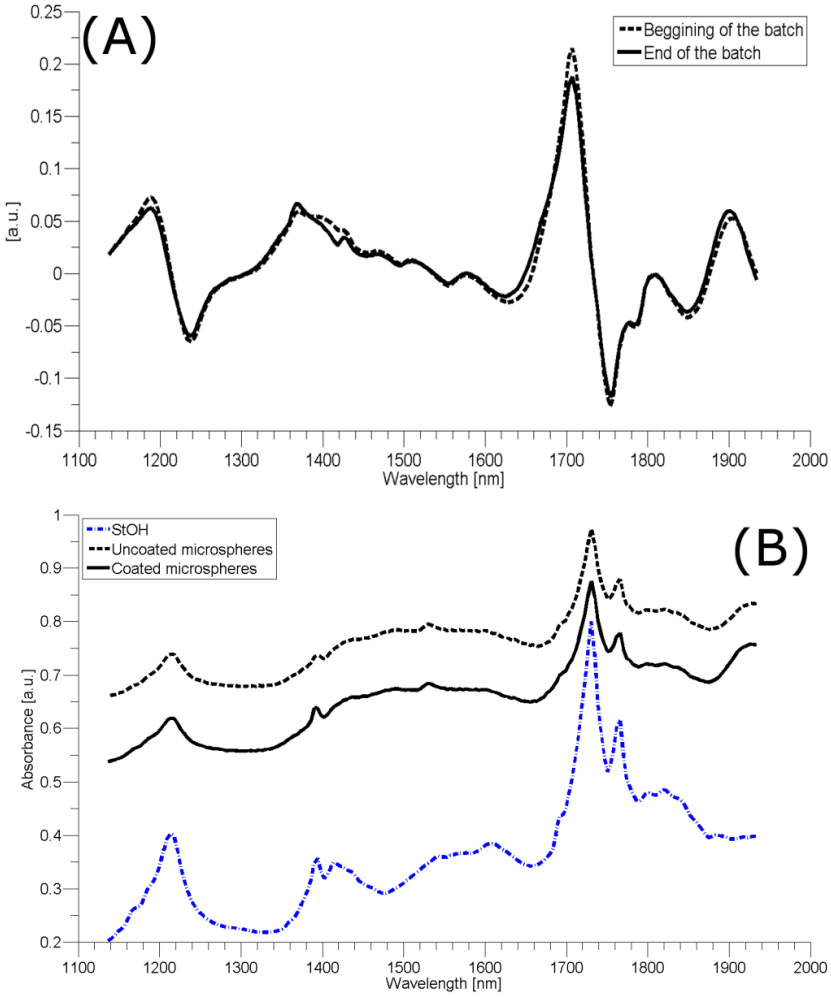

Figure 4.7 (A) NIR spectra at the beginning and at the end of the coating process for batch number 2 (SNV and Savgol 15 points, 1st order polynomial, 2ndderivative pre-processed). (B) Raw-NIR spectra collected off-line of uncoated microspheres (dashed line), coated microspheres (solid line) and stearyl alcohol (dash-dot line), which corresponds to 50%w/w of the uncoated microsphere composition.

Likewise, in Raman, the spectrum of coated microspheres shows a very similar shape resembling the spectra of uncoated microspheres (pretreated signal is shown in Figure 4.8(A)). As the microspheres are coated, the core signal is masked by the coating, decreasing the intensity of the signal as the thickness of the coating increases (Figure 4.8). As in NIR analysis, the polymeric blend has no distinguishable spectral features, and the remaining components of the coating are at much lower concentrations than the core material and have a less intense signal. For Raman, the main chemicals contributing for the microsphere Raman spectrum are attributed to the StOH and API (crizotinib), which is an aminopyridine base, and as such, a conjugated system with a strong Raman signal.

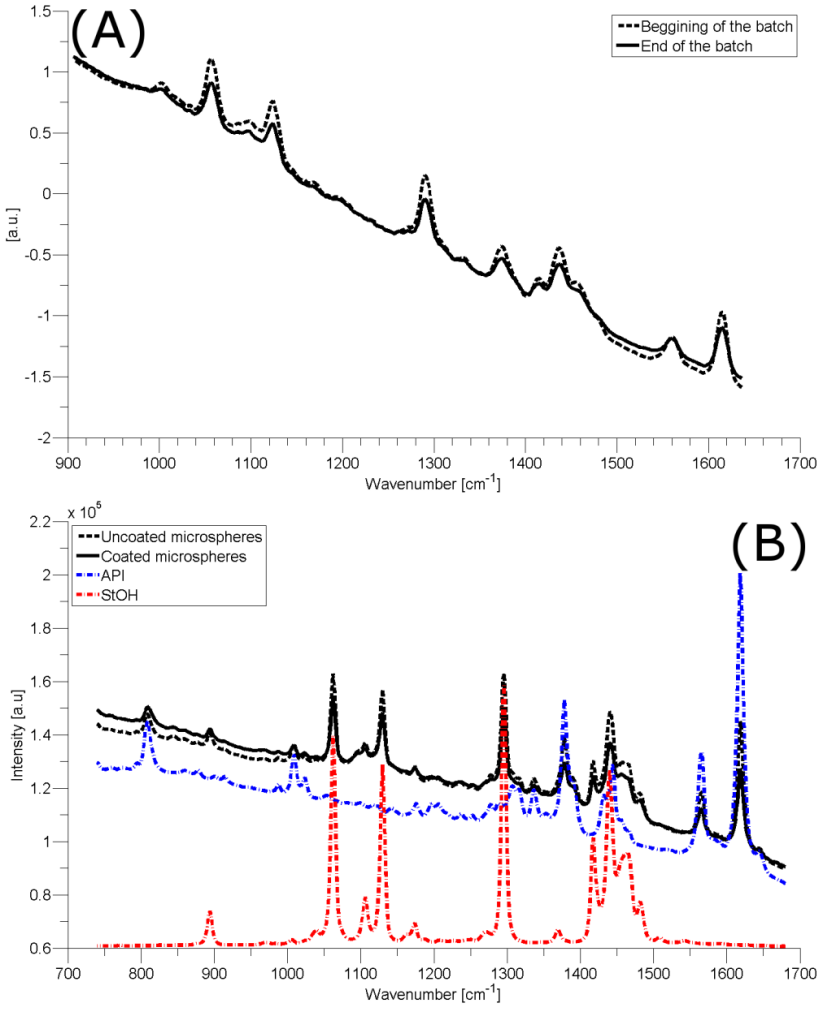

Figure 4.8 (A) Raman spectra at the beginning and at the end of coating run for batch number 2 (SNV pre-processed).(B) Raw-Raman spectra collected off-line of uncoated microspheres (dashed line), coated microspheres (solid line), stearyl alcohol (red dash-dotted line, 50%w/w of uncoated core composition) and API (blue dash-dotted line, 10%w/w of uncoated core composition). Coating spectrum is not presented as it does not have distinguishable peaks.

In conclusion, the Raman performance seems to be very satisfactory in that it outperformed the other blocks for endpoint prediction of coating thickness based on microscopy reference data.

4.4.2 MBPLS on dissolution at pH 6.2

Other coating properties (porosity and roughness[139]) and microsphere core properties (particle size, porosity, shape and roughness[139]) are going to determine the dynamic of API release. From the patient's perspective, the coating performance is determined by the *in vivo* taste of the microsphere. A simple estimate of *in vivo* taste masking performance is the use of API dissolution *in-vitro*. This justifies why the percentage of API released at pH 6.2 is considered to be a critical quality attribute for taste masking[32].

The same methodology was applied to the analysis of the dissolution results as for thickness. Initially a 2 LVs calibration MBPLS model was estimated using the $\mathbf{N_{BWU}}$, $\mathbf{R_{BWU}}$, $\mathbf{F_{BWU}}$, $\mathbf{P_{BWU}}$, $\mathbf{M_{BWU}}$ matrices and five random variables (same dimensions as mentioned before) to predict the percentage of API released at pH 6.2 at 120 min (**y**). The global **X**-variance captured by the model is only 15.9%, the model is able to explain 99.8% of the variance in **y** with an R^2 of 1.0, RMSEC 0.04% API released and RMSECV of 0.69% API released. As shown in Figure 4.9 (A), Raman is the block that has the highest BIP, followed by NIR and process conditions and raw materials. Once again, FBRM information is not much better than using random variables. Figure 4.9 (B) shows the loading plot. Where once again, LV 1 (global **X**-variance 10.6% and 93.1% **y**-variance) clearly separates $\mathbf{R_{BWU}}$ from the other sources of information. LV 2 separates the temporal from the discrete (**M** and **Z**) variables and $\mathbf{F_{BWU}}$. Although deemed significant when analyzing the RMSECV number of latent variables dependency, LV2 (global **X**-variance 5.3% and 6.7% **y**-variance) is helping to explain a much lower amount of variance than LV 1.

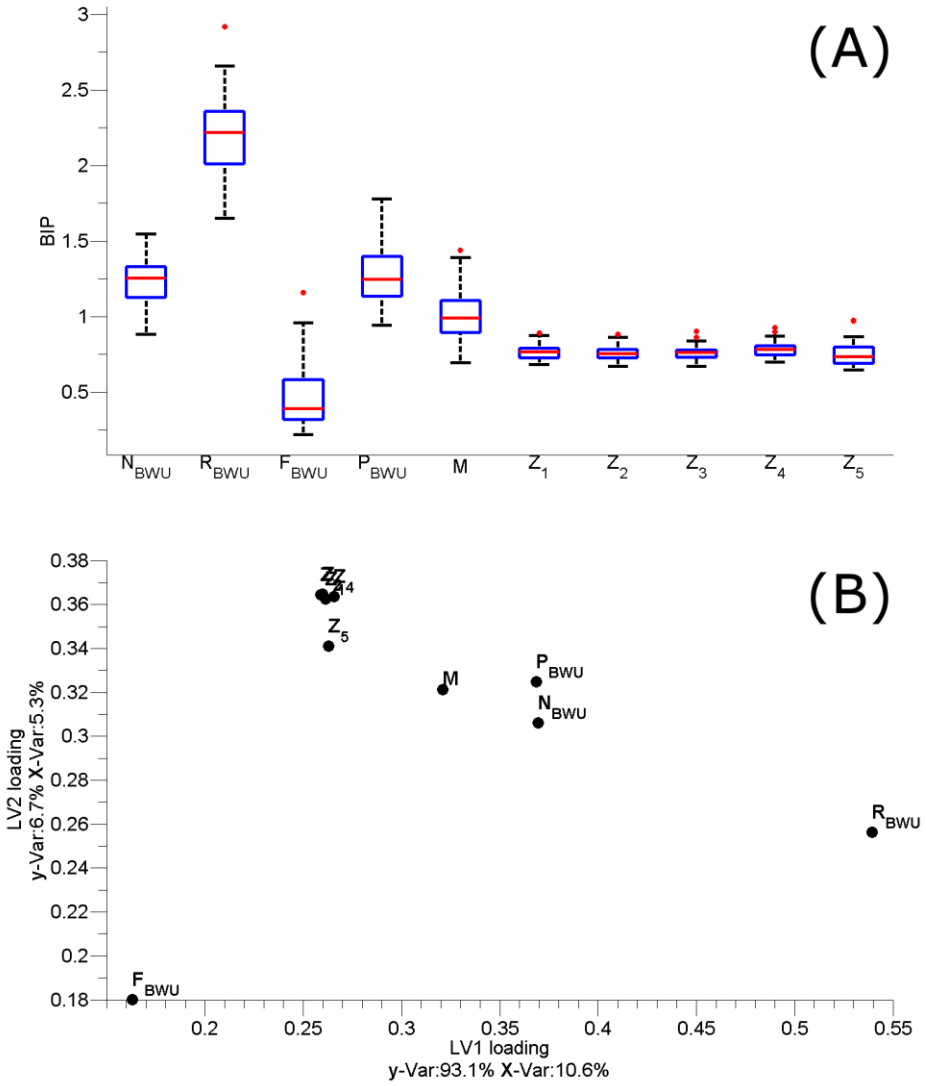

Figure 4.9 (A) BIP box plot of the 3 PAT (NIR, Raman and FBRM), Process data, Raw materials (RawMat) and five random variables for percentage of API released at 120 min in pH 6.2 prediction. (B) Block-loadings plot for LV1 and 2 for MBPLS dissolution model. Legend: NBWU (batch wise unfolded NIR matrix), RBWU (batch wise unfolded Raman matrix), PBWU (batch wise unfolded process matrix), M (raw material properties matrix), FBWU (batch wise unfolded FBRM matrix) and Z1 to 5 (random variable matrices).

This order is again verified when building a calibration model excluding random variables and FBRM, this is to say, for the MBPLS model using $\mathbf{N_{BWU}}$, $\mathbf{R_{BWU}}$ and $\mathbf{P_{BWU}}$ as set of predictor variables (**X**). The global **X**-variance captured by the model is 23%, and with a two-component model, the model is able to explain 98.5% of the variance in **y,** R^2 is 0.99, with RMSEC 0.12% API released and RMSECV 0.78% API released. The measured vs. predicted dissolution at 120 min and pH 6.2 for the selected model is shown in Figure 4.10. The sources of variation within the blocks were the same as previously explained in the previous section. The calculated model is able to predict and distinguish

between batches that have high and low percentage of API release. The loading plot once again shows that the information on $\mathbf{N_{BWU}}$, $\mathbf{P_{BWU}}$ and $\mathbf{M_{BWU}}$ blocks is redundant for prediction and putting into evidence the importance of the $\mathbf{R_{BWU}}$ block.

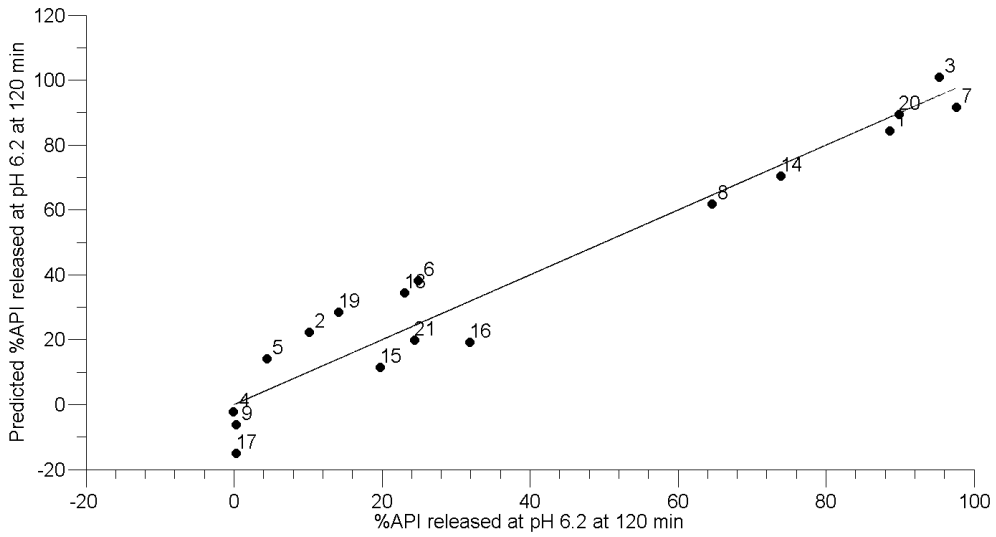

Figure 4.10 Measured against predicted dissolution values at pH6.2 at 120 min, using significant blocks: Raman, NIR, Process and Raw material data. The labels in the figure correspond to the batch identification number.

MBPLS has proven to be an effective tool to help decide the value of each PAT, being that Raman has been identified as being the best suited to monitor both endpoint thickness and dissolution performance. A thicker coating compared to a thinner coating with the same microstructure would provide a better barrier for dissolution of the API in conditions of the oral cavity and thus a slower API release. Intuitively, one would think that an in-line coating thickness measurement would have a great performance predicting percentage of API released. However, given the FBRM results, no in-line measurement was available and, as such, off-line coating thickness measurements using polarized light microscopy (**tt**) were used as a proxy to facilitate analysis. As illustrated in Figure 4.11, the **tt** block produced the highest BIP value, indicating that an in-line method that can directly measure the thickness of the coating (e.g. optical coherence tomography[140], high-speed cameras[141] or even in-line particle size measurement) would be the preferred method to monitor fluid bed coating when predicting the percentage of API released at pH 6.2. The two latent variable calibration model captures a global **X**-variance of 26.2% and 96.9% of the variance in **y**. The R^2 of the model is 0.97 with an RMSEC of 0.17% API released and RMSECV of 0.64% API released.

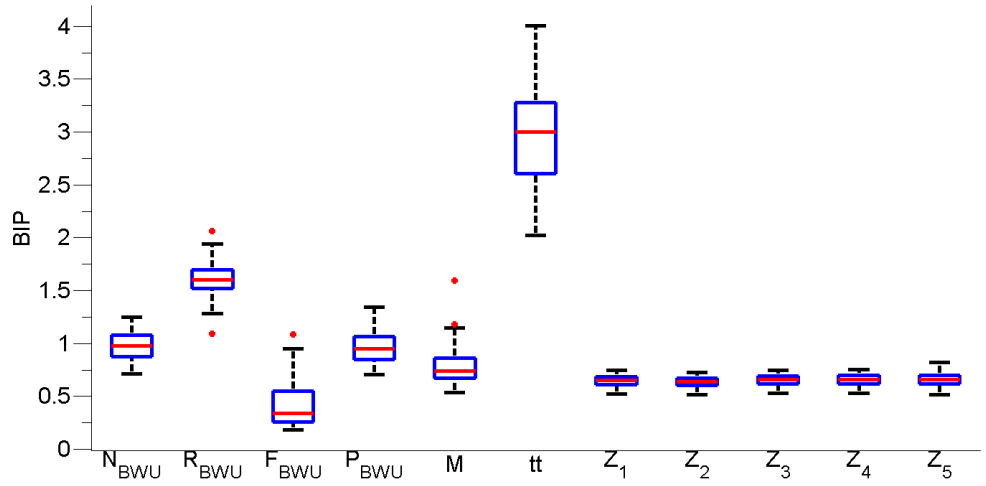

Figure 4.11 BIP of the 3 PAT (NIR, Raman and FBRM), Process data, Raw materials, Off-line measured thickness and five random variables for dissolution prediction. Legend: NBWU (batch wise unfolded NIR matrix), RBWU (batch wise unfolded Raman matrix), PBWU (batch wise unfolded process matrix), M (raw material properties matrix), FBWU (batch wise unfolded FBRM matrix) tt (off-line measured thickness vector) and Z1 to 5 (random variable matrices).

However, it should be noted that, as it has been referenced before in Chapter 3, the coating's performance will not only be dependent on its thickness, but also on the microstructure of the coating being applied. As such, a tool that is able to provide both types of information (i.e. coating thickness and properties) would be the preferred tool to gather the most relevant information for monitoring the Wurster coating process.

4.4.3 PLS on Raman

MBPLS showed that Raman has a superior performance to the other in-line process analytical tools. From this point on, the Raman spectra alone ($\mathbf{R_{BWU}}$) will be used in the calibration regression models.

Starting by modelling off-line thickness, the global **X**-variance captured by the PLS model is now 88.1%, and with a two latent variable model, the model explains 71.2% of **y**-variance. The RMSEC is 0.52 μm. It is interesting to see that even though the model has a lower R^2 than the previously calculated MBPLS for thickness in Figure 4.6 (0.71 vs. 0.93), the RMSECV is practically the same (0.67 vs the previous 0.8 μm). This indicates that even though it is harder to predict thickness, because there is less data to predict from (smaller **X**), the MBPLS and the PLS models are equivalent in terms of predictive power. We are able to conclude that the calculated model is able to predict within a reasonable error (approximately 1 μm) the coating thickness.

A second model was built to predict the percentage of API dissolved at 120 min at pH 6.2, the global **X**-variance captured is 78.8%, and with 1 latent variable model, the model is able to explain 73.8% of the **y**-variance with a calculated R^2 of 0.74, with an RMSEC of 0.5% API released and RMSECV is 0.55% API released. When comparing this to the previously calculated MBPLS model in Figure 4.10 (RMSECV 0.78% API released), it was possible to achieve a model with equivalent predictive power (RMSECV 0.55% API released). It is thus possible to build a reasonable PLS model to predict dissolution at pH 6.2 using only Raman data.

4.4.4 Exploratory data analysis

PCA is a tool often used for exploratory data analysis[142]. Process understanding and the ability of Raman to monitor the process can also be evaluated through BWU and OWU. As explained in section 2.6, the former technique will allow the visualization of variations within the batches and the latter will be useful to understand that variation by looking at the process trajectories.

From the score plot shown in Figure 4.12, we can clearly see a differentiation along the first principal component between the batches that have low percentage API release (colored in blue) versus the ones that have a high API release (colored in red). In this case, 78.8% of the variance between the Raman spectra corresponds to the variation in dissolution performance at pH 6.2 at 120 min, which explains the high quality of the correlation model for dissolution.

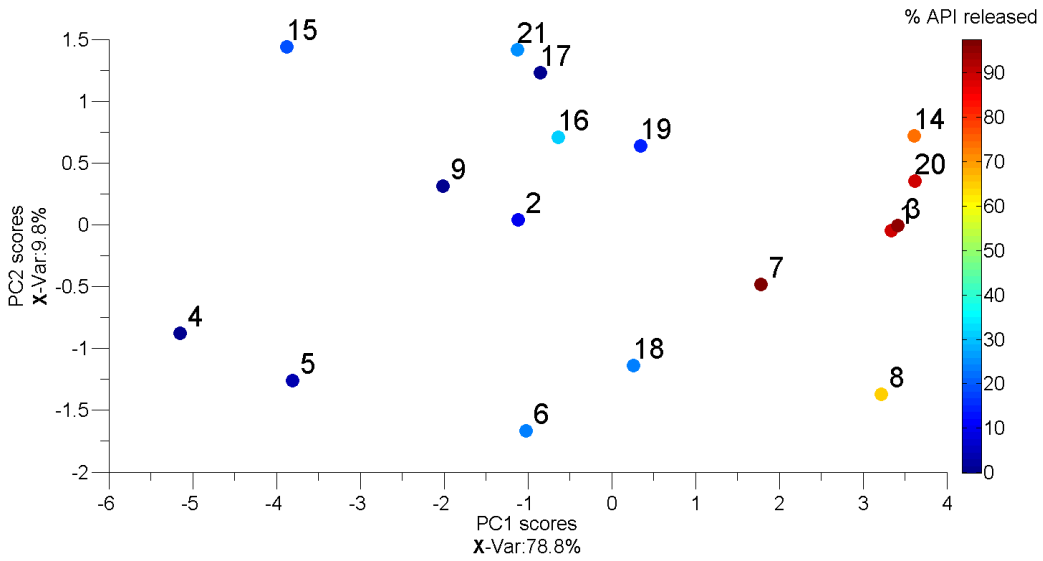

Figure 4.12 Score plot of the first two principal components of PCA for BWU Raman data. Color code: % API released after 120 min in dissolution medium at pH 6.2. The labels in the figure correspond to the batch identification number.

Comparing the score plot in Figure 4.13 (OWU – colored by standardized batch time) with the information provided in the score plot in Figure 4.12 (BWU – colored by percentage of API released at 120 min at pH 6.2), we see that batches with a high API release, such as batches 1, 3 and 16, have lower endpoint values in PC1 of Figure 4.13. Batches that have a lower percentage of API release, for example batches 4, 5 and 11, correspond to long runs (variation along PC1 of Figure 4.13). The authors would like to reinforce the idea that here the time is a standardize time and that not all (short or long) batches took the same time. This implies that a longer coating process leads to more coating being deposited and thus thicker coating and a lower percentage of API release after 120 min of dissolution testing.

The starting offset along component two remains unclear. However, the effect of spray rate in the acquired Raman signal is observable in inflections of the second principal component. When comparing the batch records to the trajectories' inflection points (present in PC2) of the different batches, they correspond to changes in spray rate. For example, batch 7, for which the spray rate was set to 5 g/min, had a sudden decrease in spray rate at 55% completion (1st inflection point) from 5 g/min to 0 g/min (due to a blockage in the spray line): the spray rate then went back to 5 g/min at 81%, which corresponds with the second inflection point in the image. Reader is advised to consult online version of this document for clarity. This demonstrates the ability of Raman (in-line PAT) to adequately monitor process performance and spot out-of-trend events.

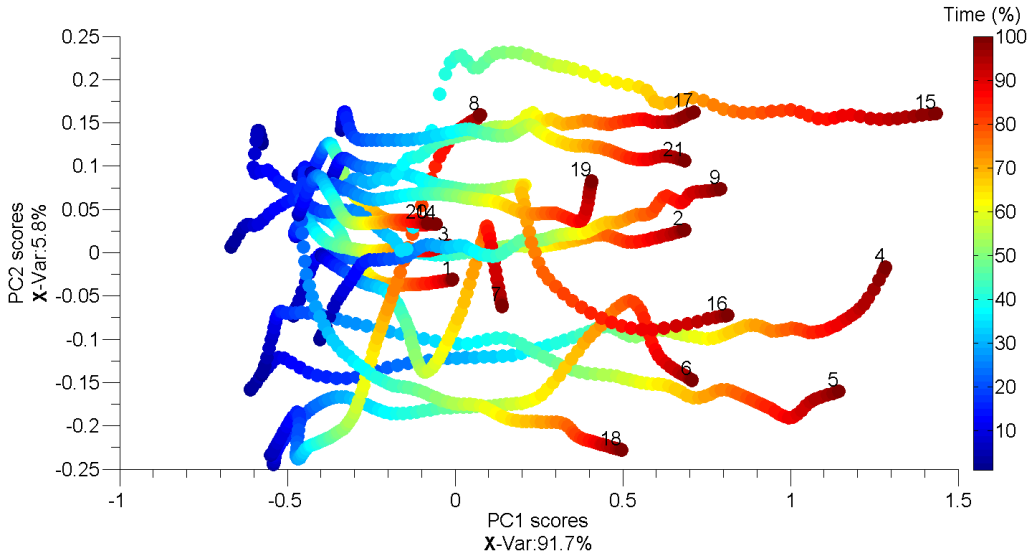

Figure 4.13 Score plot of the first two principal components of PCA for OWU Raman data. Color code: relative process time of each batch (0 to 100%). The labels in the figure correspond to the batch identification number.

4.5 Conclusion

In this work we investigated the potential benefits of using near-infrared (NIR), Raman, focused beam reflectance measurement (FBRM), process data and raw material properties to predicting API dissolution in simulated saliva being used as a surrogate for taste masking performance of reverse enteric polymer applied to melt-spray-congeal microspheres. Multiblock partial least squares (MBPLS) can provide a simple way to interpret one-to-one comparisons of different sources of information (or even combine them). It was possible to establish a lower threshold for the block importance for prediction that helped identify Raman as the tool best able to predict the taste masking performance and clearly illustrate that FBRM was not suitable for the task with the current setup and sampling strategy tested.

Strikingly, the partial least squares Raman model built proved to be as good as the MBPLS combining the useful blocks of information (NIR, Raman, Process and Raw Material). Raman can be used to monitor not only the endpoint coating thickness, but more importantly (for the intended application) the percentage of active pharmaceutical ingredients release at neutral pH.

Through observation-wise unfolding and batch-wise unfolding, it was possible to show that the variation in Raman correlates to the variations in product performance, showing that Raman can be used to monitor the coating process (beginning to end) and to identify process disruptions (such as spray rate changes). This work contributes to demonstrating the usefulness of MBPLS and how Raman could potentially be used in the future to establish a control strategy for fluid bed coating.

4.6 Acknowledgements

This project is financed by an NSERC-FQRNT (475318-191551) Industrial Innovation Scholarship and the Collaborative Research and Development Grants and Pfizer Inc. (449123-13). This work also benefited from important contributions made by Charles Bertrand from the Centre de caractérisation des matériaux, we kindly thank you for the sample preparation for thickness measurements. We would like to recognize the contributions of Marc Couture and Tobias Lundgren for the schematic representation of the Wurster fluid bed coater. We would also like to acknowledge the numerous colleagues from Pfizer who made many contributions to this work, such as Steve Hammond and the ones from Pfizer's Pediatric Network, such as Eddie Ebrahimi, Yangzhen Ciringh, and others such as Kevin Girard, Yong Zhou, Yang Angela Liu and Andrew Prpich. Finally, but not least, we would like to thank Philip Butler, from BASF, for supplying Kollicoat® Smartseal 30 D.

CHAPTER 5 CONCLUSION

5.1 Conclusion en français

Le masquage du goût est devenu un élément important du développement de formes médicamenteuses dans l'industrie pharmaceutique. Un procédé de fabrication plateforme qui permettrait de développer rapidement de nouvelles formulations pour la population pédiatrique devra reposer sur une approche efficace afin de masquer l'amertume des principes actifs (PA).

Du point de vue du QbD, la connaissance des produits et la compréhension des procédés sont essentielles pour la conception d'un procédé de fabrication pharmaceutique. En utilisant les outils du QbD, il a été possible d'évaluer la criticité des paramètres du procédé et de la formulation de la solution d'enrobage avec Kollicoat®Smartseal 30D, et de comprendre le rôle crucial de la microstructure du film d'enrobage pour le développement de microsphères dont le goût est masqué (chapitre 3).

Sept variables clefs du procédé d'enrobage avec Wurster ont été sélectionnées puis évaluées par un plan d'expérience D-optimal et une analyse de la variance. Le pourcentage de PA libéré à pH 6,2 a été utilisé comme méthode de substitution pour déterminer la performance au chapitre du masquage de goût du Kollicoat® Smartseal. Les sept variables étudiées été : la température du lit de produit, le débit d'air entrant, la pression d'air atomisé, le débit du spray (paramètres du procédé), le taux d'enrobage, le niveau de plastifiant, la présence de solides dans la suspension d'enrobage (caractéristique du matériel) et le durcissement. Les résultats montrent que le niveau d'enrobage et le niveau de plastifiant sont les paramètres critiques du procédé et renforcent l'importance du durcissement pour réduire la variabilité entre les lots en favorisant la formation d'un film complet. Le lien entre les caractéristiques du matériau, les paramètres du procédé et les attributs de qualité a permis une meilleure compréhension des paramètres qui affectent le profil de libération du PA à pH buccal (*in-vitro*). Il a été démontré que tant l'épaisseur que la morphologie de l'enrobage ont un impact sur la dissolution dans une salive simulée.

Les travaux futurs dans ce domaine devraient inclure une caractérisation quantitative de la porosité des films appliqués, ainsi qu'une évaluation de l'influence des principales variables de formulation et de procédé sur la porosité pour obtenir un meilleur contrôle de la performance de la dissolution à pH 6,2. De plus, une meilleure compréhension du mécanisme phénoménologique de la libération demeure nécessaire.

L’operation d’enrobage en lit fluidisé est un processus complexe de transfert de chaleur et de masse qui implique différents microprocessus, tels que la formation de gouttelettes, l'évaporation, le transfert de chaleur, l'impact des gouttelettes et le comportement des particules. Dans les travaux futurs, il serait important de comprendre les mécanismes fondamentaux à la fois du processus d’enrobage et de l'étape de durcissement afin de faciliter le choix de l'épaisseur du revêtement, la conception d'une stratégie de contrôle, la mise à l'échelle du processus et aussi pour faciliter le transfert du processus d’enrobage pour de microsphères avec d’autres PAs.

L’utilisation d’outils d’analyse des procédés et d’une stratégie d’analyse avancée des données a été essentielle pour : i) fournir un moyen simple de comparer les informations provenant de différentes sources (et comment les combiner), ii) améliorer les connaissances sur les paramètres du procédé qui influencent l’enrobage pour des films fins (chapitre 4).

Étonnamment, ces travaux ont montré que Raman est un outil utile pour suivre le procédé d’enrobage aussi performant que le MBPLS combinant les blocs d’information utiles (NIR, Raman, procédure et matière première), car Raman s’est révélé efficace pour suivre les trajectoires du procédé et analyser les attributs de qualité critiques définis (épaisseur et dissolution à pH 6,2). Du point de vue du QbD, la prochaine étape consistera à élaborer une stratégie de contrôle en utilisant les connaissances recueillies sur le procédé pour contrôler les paramètres critiques du procédé en vue d’obtenir des attributs de qualité critiques constants. Néanmoins, comme le montrent les résultats du chapitre 3, un outil capable de fournir des informations sur l’épaisseur du film et sur la structure des microsphères serait l’outil idéal pour recueillir des informations encore plus pertinentes pour le suivi du procédé d’enrobage avec un Wurster.

Afin de garantir le succès d’une plateforme utilisant des microsphères enrobées avec Kollicoat®Smartseal 30D, il faut d’assurer que le film de polymère est capable d’adhérer à la surface de la microsphère. Les deux grandes forces qui influencent l’adhésion sont : i) la tension interfaciale, qui dépend de la formulation de la microsphère, et ii) les contraintes internes du film. L’étude de la distribution du PA dans la microsphère sera la clef du succès de cette plateforme. Un second élément est la solubilité du PA lui-même, qui peut aussi avoir une incidence sur son taux de libération. Une étude où le système de classification biopharmaceutique (système qui classe les PA selon leur perméabilité et leur solubilité) est pris en considération, doit être réalisée pour s’assurer du succès de cette plateforme pédiatrique.

De manière générale, cette recherche a pour but de faciliter le développement de nouveaux produits pédiatriques conçus pour surmonter l'une des principales limites des médicaments pédiatriques actuels faible appétibilité). Bien que ce projet porte essentiellement sur les besoins pédiatriques, les résultats peuvent être appliqués à des patients gériatriques, car les microsphères peuvent être utilisées comme forme médicamenteuse pour les groupes de patients qui ont de la difficulté à avaler certaines formes pharmaceutiques telles que les comprimés ou les gélules.

5.2 Conclusion in English

Taste masking has become an important part of the dosage form development in the pharmaceutical industry because of increasing reports of noncompliance. A platform solution that would enable the rapid development of new formulations to pediatrics will need to have an effective approach to the bitter API taste problem.

From a QbD perspective product knowledge and process understanding are essential to design the pharmaceutical manufacturing process. Using QbD tools, it was possible to assess the criticality of both processing parameters and coating formulation of the Kollicoat®Smartseal 30D coating process and understand the crucial role of coating microstructure for the development of taste masked microspheres (Chapter 3).

A screening of seven key variables in a Wurster coating process was evaluated by D-optimal design and by analysis of variance. The percentage of API released at pH 6.2 was used as a surrogate method for taste masking performance evaluation of Kollicoat® Smartseal. The seven studied variables were: product bed temperature, inlet airflow, atomizing air pressure, spray rate (process parameters), coating level, plasticizer level, solids in coating suspension (material attributes) and curing. Results show that coating levels and plasticizer levels are the critical process parameters and reinforce the importance of curing to reduce the overall variability within the batch by promoting complete film formation. The links between material attributes, process parameters and quality attributes were demonstrated to allow a better understanding of the parameters that affect the API release profile at mouth pH (*in vitro*). It was demonstrated that not only thickness, but also coating morphology have an impact on the dissolution in 50 mM potassium phosphate buffer at pH 6.2.

Future work in this area should include quantitative characterization of the porosity of the coatings being applied, as well as the influence of key formulation and process variables on the porosity to gain a better control of the dissolution performance at pH 6.2. Further understanding of the phenomenological curing and release mechanism of Kollicoat®Smartseal 30D coating is still needed.

Fluid bed coating is a complex heat and mass transfer process that involves different microprocesses, such as droplet formation, evaporation, heat transfer, droplet impingement and particle behaviours. In future work, it would be important to understand the fundamental mechanisms behind both the coating process and the curing step in order to facilitate the choice of coating thickness, design of a control strategy, scale-up of the process and as well facilitate the transfer of coating process to micropsheres made with other APIs.

The use of PAT and advance data analysis strategy was key to (i) provide a simplistic way to compare different sources of information (and how to combine them) (ii) improve knowledge about process parameter influencing coating for thin coatings (Chapter 4).

Surprisingly, this work has shown that Raman is as efficient as combining the useful blocks of information (NIR, Raman, Process and Raw Material) by MBPLS to monitor the coating process. Raman spectroscopy has proven to be an efficient tool to monitor process trajectories and analyze the defined CQAs (thickness and dissolution at pH 6.2). From a QbD perspective the next step would be to develop a control strategy using the gathered process understanding to control CPPs so as to achieve consistent CQAs. Nevertheless, as per results shown in Chapter 3, a tool that is able to provide information regarding coating thickness and coating microstructure would be the prefered tool to gather even more relevant information for monitoring the Wurster coating process.

In order to guarantee the success of the platform approach using MSC microspheres coated with Kollicoat®Smartseal 30D one needs to ensure that the polymeric film is able to adhere to the MSC core surface. Two major forces that influence adhesion are: (i) the strength of the interfacial bonds, which are dependent on the core formulation, and (ii) the internal stresses within the film. Studying the API distribution within the MSC core will be key to the success of this platform. A second element to keep in mind is that the solubility of the API itself will also impact the release rate from the API. Conducting a study where the biopharmaceutics classification system (system that classifies APIs based on their permeability and solubility) is taken into account needs to be conducted to guarantee the success of this pediatric platform.

Overall, this research aims at facilitating the development of new pediatric products designed to overcome one of the major limitations with current pediatric medications (poor palatability). Although this project focuses on pediatric needs, results can also be transferred to geriatric patients as microspheres can be used as a platform approach for patient groups that have challenges with swallowing more typical tablet and capsule drug products.

ANNEXE I

Table I. 1 Coating conditions for each batch.

Batch number	Product Bed Temperature (°C)	Inlet Airflow (m^3/h)	Atomizing Air Pressure (bar)	Spray Rate (g/min)	Coating Level (% w/w)	Plasticizer Level (% $w/w_{dry\ polymer}$)	Solids in suspension (% w/w)
1	25.0	60	3	11	7.00	20	15.68
2	28.5	50	2	8	15.3	16	19.60
3	25.0	40	1	5	7.00	12	15.68
4	32.0	40	1	5	23.6	12	23.52
5	32.0	40	1	11	23.6	20	15.68
6	28.5	50	2	8	15.3	16	19.60
7	25.0	60	3	5	7.00	12	23.52
8	32.0	60	1	5	7.00	20	23.52
9	25.0	40	3	5	23.6	20	23.52
10	32.0	60	1	11	7.00	12	15.68
11	32.0	60	3	11	23.6	20	23.52
12	32.0	40	3	11	7.00	12	23.52
13	32.0	40	3	5	7.00	20	15.68
14	25.0	40	1	11	7.00	20	23.52
15	32.0	60	3	5	23.6	12	15.68
16	25.0	60	1	11	23.6	12	23.52
17	25.0	60	1	5	23.6	20	15.68
18	25.0	40	3	11	23.6	12	15.68
19	28.5	50	2	8	15.3	16	19.60
20	32.0	60	1	11	7.00	12	15.68
21	25.0	60	1	11	23.6	12	15.68

ANNEXE II

Table II. 1 ANOVA for main factor model for percentage of API release after 30 min of uncured coated microspheres

Source	Sum of Squares	Degrees of Freedom	Mean Square	F value	p-value
Block	1705.0	2	852.5		
Main factors					
Product Bed Temperature	140.9	1	140.9	1.5	0.2265
Inlet Airflow	6.9	1	6.9	0.1	0.7872
Atomizing Air Pressure	942.0	1	942.0	10.0	0.0026
Spray Rate	302.2	1	302.2	3.2	0.0789
Coating Level	18632.3	1	18632.3	197.9	< 0.0001
Plasticizer Level	8708.0	1	8708.0	92.5	< 0.0001
Solids in Suspension	27.9	1	27.9	0.3	0.5883
Residual	4989.4	53	94.1		
Total (corrected)	36423.8	62			

Table II. 2 ANOVA for main factor model for percentage of API release after 60 min of uncured coated microspheres

Source	Sum of Squares	Degrees of Freedom	Mean Square	F value	p-value
Block	1479.8	2	739.9		
Main factors					
Product Bed Temperature	225.7	1	225.7	3.0	0.0900
Inlet Airflow	53.6	1	53.6	0.7	0.4037
Atomizing Air Pressure	1038.2	1	1038.2	13.7	0.0005
Spray Rate	2.4	1	2.4	0.0	0.8591
Coating Level	13292.5	1	13292.5	175.7	< 0.0001
Plasticizer Level	4742.6	1	4742.6	62.7	< 0.0001
Solids in Suspension	2.2	1	2.2	0.0	0.8654
Residual	4009.2	53	75.6		
Total (corrected)	25033.6	62			

Table II. 3 ANOVA for main factor model for percentage of API release after 90 min of uncured coated microspheres

Source	Sum of Squares	Degrees of Freedom	Mean Square	F value	p-value
Block	1379.0	2	689.5		
Main factors					
Product Bed Temperature	176.8	1	176.8	2.4	0.1288
Inlet Airflow	39.0	1	39.0	0.5	0.4721
Atomizing Air Pressure	999.7	1	999.7	13.5	0.0006
Spray Rate	124.7	1	124.7	1.7	0.2007
Coating Level	10228.6	1	10228.6	137.7	< 0.0001
Plasticizer Level	2945.9	1	2945.9	39.6	< 0.0001
Solids in Suspension	8.4	1	8.4	0.1	0.7386
Residual	3937.7	53	74.3		
Total (corrected)	19842.1	62			

Table II. 4 ANOVA for main factor model for percentage of API release after 120 min of uncured coated microspheres

Source	Sum of Squares	Degrees of Freedom	Mean Square	F value	p-value
Block	1204.1	2	602.0		
Main factors					
Product Bed Temperature	196.5	1	196.5	3.2	0.0802
Inlet Airflow	10.3	1	10.3	0.2	0.6845
Atomizing Air Pressure	867.9	1	867.9	14.1	0.0004
Spray Rate	229.2	1	229.2	3.7	0.0594
Coating Level	7659.2	1	7659.2	124.0	< 0.0001
Plasticizer Level	1902.2	1	1902.2	30.8	< 0.0001
Solids in Suspension	3.9	1	3.9	0.1	0.8031
Residual	3273.4	53	61.8		
Total (corrected)	15317.2	62			

Table II. 5 ANOVA for main factor model for percentage of API release after 30 min of cured coated microspheres

Source	Sum of Squares	Degrees of Freedom	Mean Square	F value	p-value
Block	3558.8	2	1779.4		
Main factors					
Product Bed Temperature	560.0	1	560.0	2.5	0.1196
Inlet Airflow	121.2	1	121.2	0.5	0.4650
Atomizing Air Pressure	28.4	1	28.4	0.1	0.7230
Spray Rate	1186.4	1	1186.4	5.3	0.0253
Coating Level	31279.0	1	31279.0	139.8	< 0.0001
Plasticizer Level	5255.7	1	5255.7	23.5	< 0.0001
Solids in Suspension	95.0	1	95.0	0.4	0.5176
Residual	11860.7	53	223.8		
Total (corrected)	56877.1	62			

Table II. 6 ANOVA for main factor model for percentage of API release after 60 min of cured coated microspheres

Source	Sum of Squares	Degrees of Freedom	Mean Square	F value	p-value
Block	4372.2	2	2186.1		
Main factors					
Product Bed Temperature	686.9	1	686.9	3.0	0.0892
Inlet Airflow	102.6	1	102.6	0.4	0.5062
Atomizing Air Pressure	92.1	1	92.1	0.4	0.5289
Spray Rate	1706.0	1	1706.0	7.4	0.0086
Coating Level	48906.7	1	48906.7	213.5	< 0.0001
Plasticizer Level	6198.3	1	6198.3	27.1	< 0.0001
Solids in Suspension	4.1	1	4.1	0.0	0.8939
Residual	12141.5	53	229.1		
Total (corrected)	78333.4	62			

Table II. 7 ANOVA for main factor model for percentage of API release after 90 min of cured coated microspheres

Source	Sum of Squares	Degrees of Freedom	Mean Square	F value	p-value
Block	3487.1	2	1743.6		
Main factors					
Product Bed Temperature	963.1	1	963.1	5.0	0.0291
Inlet Airflow	112.5	1	112.5	0.6	0.4468
Atomizing Air Pressure	147.7	1	147.7	0.8	0.3837
Spray Rate	2151.4	1	2151.4	11.2	0.0015
Coating Level	55282.3	1	55282.3	288.7	< 0.0001
Plasticizer Level	6332.3	1	6332.3	33.1	< 0.0001
Solids in Suspension	47.8	1	47.8	0.2	0.6193
Residual	10147.4	53	191.5		
Total (corrected)	83293.0	62			

Table II. 8 ANOVA for main factor model for percentage of API release after 120 min of cured coated microspheres

Source	Sum of Squares	Degrees of Freedom	Mean Square	F value	p-value
Block	2711.7	2	1355.9		
Main factors					
Product Bed Temperature	928.8	1	928.8	6.4	0.0144
Inlet Airflow	103.4	1	103.4	0.7	0.4025
Atomizing Air Pressure	253.1	1	253.1	1.7	0.1924
Spray Rate	2096.6	1	2096.6	14.4	0.0004
Coating Level	59187.9	1	59187.9	407.7	< 0.0001
Plasticizer Level	5566.4	1	5566.4	38.3	< 0.0001
Solids in Suspension	120.7	1	120.7	0.8	0.3660
Residual	7694.7	53	145.2		
Total (corrected)	83214.4	62			

ANNEXE III

Principal Component Analysis (PCA)

```
function [T P Varex Eigenvalues] = fct_PCA(X,nbPC)
% PCA
X0 = X;
P = [];
T = [];
SSX = [];
error = realmax;

for i = 1:nbPC
    t_temp = ones(size(X,1),1);
    t = ones(size(X,1),1);

    while error > 1E-10

        p = X'*t / (t'*t);
        p = p / norm(p);
        t = X*p / (p'*p);

        % Check t convergence --------------------
        error = sum((t-t_temp).^2);
        t_temp = t;
        % ----------------------------------------
    end

    X = X - t*p';
    P = [P p];
    T = [T t];
        % Sum of squares -----------
    Xhat = t*p';
    ssX0 = sum(sum(X0 .* X0));
    ssX = sum(sum(Xhat .* Xhat));
    ssX = ssX / ssX0;
    SSX = [SSX; ssX];
    % -------------------------
    error = realmax;

end

% Varience explained by the model
Varex = SSX;
% Eigenvalues
Eigenvalues = var(T);
```

ANNEXE IV

Partial Least Squares (PLS)

```
function [T P W C U B SSX SSY] = fct_PLS(X,Y,nbPC)

E = X; % At iteration 0, there are no components and X = E
F = Y; % At iteration 0, there are no components and Y = F
% Create empty variables
T = [];
P = [];
W = [];
C = [];
U = [];
B = [];

u = randn(size(Y,1),1); % Create u seed variable

% In order to check convergence, we need dummy u and t variables
t_temp = ones(size(X,1),1);
u_temp = ones(size(X,1),1);
error_t = realmax;
error_u = realmax;

% Select number of components
size1 = size(X,1);
size2 = size(X,2);

% Sum of square variables for :
SSX = [];
SSY = [];

for i = 1:nbPC;

    while (error_t > 1E-20) && (error_u > 1E-20)

    w = (u'*E / (u'*u));
    w = w';
    w = w/norm(w);
    t = E*w / (w'*w);
    c = F'*t / (t'*t);
    c = c/norm(c);
    u = F*c / (c'*c);
     % Check t and u convergence --------------
    error_t = sum((t-t_temp).^2);
    t_temp = t;
    error_u = sum((u-u_temp).^2);
    u_temp = u;
    % ----------------------------------------
    end

p = E'*t / (t'*t);
```

```
% Scaling used by PLS Toolbox
% This makes it possible to have: nomr(W)=1
t = t*norm(p);
p = p/norm(p);

b = u'*t /(t'*t);

T(:,i) = t;
P(:,i) = p;
W(:,i) = w;
C(:,i) = c;
U(:,i) = u;
B(i,i) = b;


% Sum of squares -----------
Xhat = t*p';
ssX0 = sum(sum(X .* X));
ssX = sum(sum(Xhat .* Xhat));
ssX = ssX / ssX0;
SSX = [SSX; ssX];

Yhat = b*t*c';
ssY0 = sum(sum(Y .* Y));
ssY = sum(sum(Yhat .* Yhat));
ssY = ssY / ssY0;
SSY = [SSY; ssY];
% --------------------------

% Deflate variables
E = E - t*p';
F = F - b*t*c';

error_t = realmax;
error_u = realmax;

end

disp('Percent Variance Captured by Model X-Block')
Varex_X = sum(SSX);

%disp('Percent Variance Captured by Model Y-Block')
Varex_Y = sum(SSY);
```

ANNEXE V

Multiblock Partial Least Squares (MBPLS) (for one **y** block only)

```
function [Tscores Wloads Pt SS B Q] = fct_mbPLS_X_mod(nbPC, Y, Xa, Xb, Xc,
Xd, Xe, Xf, Xg, Xh, Xi, Xj, Xk, Xl)

% fct_mbPLS_X

% Check number of input arguments
% As nbPC and Y are mandatory, number of blocks is:
nb_blocks = nargin - 2;


% Create empty variables if nb_blocks is less than 12

if nb_blocks < 12
    Xl = [];
end
if nb_blocks < 11
    Xk = [];
end
if nb_blocks < 10
    Xj = [];
end
if nb_blocks < 9
    Xi = [];
end
if nb_blocks < 8
    Xh = [];
end
if nb_blocks < 7
    Xg = [];
end
if nb_blocks < 6
    Xf = [];
end
if nb_blocks < 5
    Xe = [];
end
if nb_blocks < 4
    Xd = [];
end
if nb_blocks < 3
    Xc = [];
end
if nb_blocks < 2
    Xb = [];
end

% Save copy of the original variables
Y0 = Y;
Xa0 = Xa;
```

```
Xb0 = Xb;
Xc0 = Xc;
Xd0 = Xd;
Xe0 = Xe;
Xf0 = Xf;
Xg0 = Xg;
Xh0 = Xh;
Xi0 = Xi;
Xj0 = Xj;
Xk0 = Xk;
Xl0 = Xl;

X = [Xa Xb Xc Xd Xe Xf Xg Xh Xi Xj Xk Xl];
X0 = X;
X2=X;

Pa = [];
Pb = [];
Pc = [];
Pd = [];
Pe = [];
Pf = [];
Pg = [];
Ph = [];
Pi = [];
Pj = [];
Pk = [];
Pl = [];

Pt=[];
Tt = [];

Ta = [];
Tb = [];
Tc = [];
Td = [];
Te = [];
Tf = [];
Tg = [];
Th = [];
Ti = [];
Tj = [];
Tk = [];
Tl = [];

ta = [];
tb = [];
tc = [];
td = [];
te = [];
tf = [];
tg = [];
th = [];
ti = [];
tj = [];
```

```
tk = [];
tl = [];

U = [];
W = [];
Q = [];

Wa = [];
Wb = [];
Wc = [];
Wd = [];
We = [];
Wf = [];
Wg = [];
Wh = [];
Wi = [];
Wj = [];
Wk = [];
Wl = [];

wa = [];
wb = [];
wc = [];
wd = [];
we = [];
wf = [];
wg = [];
wh = [];
wi = [];
wj = [];
wk= [];
wl= [];

SSXa = [];
SSXb = [];
SSXc = [];
SSXd = [];
SSXe = [];
SSXf = [];
SSXg = [];
SSXh = [];
SSXi = [];
SSXj = [];
SSXk= [];
SSXl= [];

ssXa = 0;
ssXb = 0;
ssXc = 0;
ssXd = 0;
ssXe = 0;
ssXf = 0;
ssXg = 0;
ssXh = 0;
ssXi = 0;
```

```
ssXj = 0;
ssXk=0;
ssXl=0;

SSX = [];
SSY = [];

error_t = realmax;
error_u = realmax;

for i = 1:nbPC
    tt_temp = ones(size(Xa,1),1);
    u_temp = ones(size(Xa,1),1);
    u = ones(size(Xa,1),1);

    while (error_t > 1E-20) && (error_u > 1E-20)

        if nb_blocks >= 1
            wa = Xa'*u / (u'*u);
            wa = wa / norm(wa);
            ta = Xa*wa;
        end
        if nb_blocks >= 2
            wb = Xb'*u / (u'*u);
            wb = wb / norm(wb);
            tb = Xb*wb;
        end
        if nb_blocks >= 3
            wc = Xc'*u / (u'*u);
            wc = wc / norm(wc);
            tc = Xc*wc;
        end
        if nb_blocks >= 4
            wd = Xd'*u / (u'*u);
            wd = wd / norm(wd);
            td = Xd*wd;
        end
        if nb_blocks >= 5
            we = Xe'*u / (u'*u);
            we = we / norm(we);
            te = Xe*we;
        end
        if nb_blocks >= 6
            wf = Xf'*u / (u'*u);
            wf = wf / norm(wf);
            tf = Xf*wf;
        end
        if nb_blocks >= 7
            wg = Xg'*u / (u'*u);
            wg = wg / norm(wg);
            tg = Xg*wg;
        end

        if nb_blocks >= 8
            wh = Xh'*u / (u'*u);
```

```
        wh = wh / norm(wh);
        th = Xh*wh;
    end

    if nb_blocks >= 9
        wi = Xi'*u / (u'*u);
        wi = wi / norm(wi);
        ti = Xi*wi;
    end

    if nb_blocks >= 10
        wj = Xj'*u / (u'*u);
        wj = wj / norm(wj);
        tj = Xj*wj;
    end

    if nb_blocks >= 11
        wk = Xk'*u / (u'*u);
        wk = wk / norm(wk);
        tk = Xk*wk;
    end

    if nb_blocks >= 12
        wl = Xl'*u / (u'*u);
        wl = wl / norm(wl);
        tl = Xl*wl;
    end

    T = [ta tb tc td te tf tg th ti tj tk tl];

    wt = T'*u / (u'*u);
    wt = wt / norm(wt);

    tt = T*wt / (wt'*wt);

    q = Y'*tt / (tt'*tt);
    u = Y*q / (q'*q);

% Check t and u convergence --------------
error_tt = sum((tt-tt_temp).^2);
tt_temp = tt;
error_u = sum((u-u_temp).^2);
u_temp = u;
% ----------------------------------------

end

    if nb_blocks >= 1
        pat = Xa'*tt / (tt'*tt);
        Xa = Xa - tt *pat';
    end
    if nb_blocks >= 2
        pbt = Xb'*tt / (tt'*tt);
        Xb = Xb - tt *pbt';
```

```
        end
        if nb_blocks >= 3
            pct = Xc'*tt / (tt'*tt);
            Xc = Xc - tt *pct';
        end
        if nb_blocks >= 4
            pdt = Xd'*tt / (tt'*tt);
            Xd = Xd - tt *pdt';
        end
        if nb_blocks >= 5
            pet = Xe'*tt / (tt'*tt);
            Xe = Xe - tt *pet';
        end
        if nb_blocks >= 6
            pft = Xf'*tt / (tt'*tt);
            Xf = Xf - tt *pft';
        end
        if nb_blocks >= 7
            pgt = Xg'*tt / (tt'*tt);
            Xg = Xg - tt *pgt';
        end
        if nb_blocks >= 8
            pht = Xh'*tt / (tt'*tt);
            Xh = Xh - tt *pht';
        end
        if nb_blocks >= 9
            pit = Xi'*tt / (tt'*tt);
            Xi = Xi - tt *pit';
        end
        if nb_blocks >= 10
            pjt = Xj'*tt / (tt'*tt);
            Xj = Xj - tt *pjt';
        end
        if nb_blocks >= 11
            pkt = Xk'*tt / (tt'*tt);
            Xk = Xk - tt *pkt';
        end
        if nb_blocks >= 12
            plt = Xl'*tt / (tt'*tt);
            Xl = Xl - tt *plt';
        end



X2=[Xa Xb Xc Xd Xe Xf Xg Xh Xi Xj Xk Xl];

    % Sum of squares -----------
if nb_blocks >= 1
    Xahat = tt*pat';
    ssXa0 = sum(sum(Xa0 .* Xa0));
    ssXa = sum(sum(Xahat .* Xahat));
    ssXa = ssXa / ssXa0;
    SSXa = [SSXa; ssXa];
end
if nb_blocks >= 2
```

```
    Xbhat = tt*pbt';
    ssXb0 = sum(sum(Xb0 .* Xb0));
    ssXb = sum(sum(Xbhat .* Xbhat));
    ssXb = ssXb / ssXb0;
    SSXb = [SSXb; ssXb];
end
if nb_blocks >= 3
    Xchat = tt*pct';
    ssXc0 = sum(sum(Xc0 .* Xc0));
    ssXc = sum(sum(Xchat .* Xchat));
    ssXc = ssXc / ssXc0;
    SSXc = [SSXc; ssXc];
end
if nb_blocks >= 4
    Xdhat = tt*pdt';
    ssXd0 = sum(sum(Xd0 .* Xd0));
    ssXd = sum(sum(Xdhat .* Xdhat));
    ssXd = ssXd / ssXd0;
    SSXd = [SSXd; ssXd];
end
if nb_blocks >= 5
    Xehat = tt*pet';
    ssXe0 = sum(sum(Xe0 .* Xe0));
    ssXe = sum(sum(Xehat .* Xehat));
    ssXe = ssXe / ssXe0;
    SSXe = [SSXe; ssXe];
end
if nb_blocks >= 6
    Xfhat = tt*pft';
    ssXf0 = sum(sum(Xf0 .* Xf0));
    ssXf = sum(sum(Xfhat .* Xfhat));
    ssXf = ssXf / ssXf0;
    SSXf = [SSXf; ssXf];
end
if nb_blocks >= 7
    Xghat = tt*pgt';
    ssXg0 = sum(sum(Xg0 .* Xg0));
    ssXg = sum(sum(Xghat .* Xghat));
    ssXg = ssXg / ssXg0;
    SSXg = [SSXg; ssXg];
end
if nb_blocks >= 8
    Xhhat = tt*pht';
    ssXh0 = sum(sum(Xh0 .* Xh0));
    ssXh = sum(sum(Xhhat .* Xhhat));
    ssXh = ssXh/ ssXh0;
    SSXh = [SSXh; ssXh];
end
if nb_blocks >= 9
    Xihat = tt*pit';
    ssXi0 = sum(sum(Xi0 .* Xi0));
    ssXi = sum(sum(Xihat .* Xihat));
    ssXi = ssXi / ssXi0;
    SSXi = [SSXi; ssXi];
end
if nb_blocks >= 10
```

```
    Xjhat = tt*pjt';
    ssXj0 = sum(sum(Xj0 .* Xj0));
    ssXj = sum(sum(Xjhat .* Xjhat));
    ssXj = ssXj / ssXj0;
    SSXj = [SSXj; ssXj];
end

if nb_blocks >= 11
    Xkhat = tt*pkt';
    ssXk0 = sum(sum(Xk0 .* Xk0));
    ssXk = sum(sum(Xkhat .* Xkhat));
    ssXk = ssXk / ssXk0;
    SSXk = [SSXk; ssXk];
end

if nb_blocks >= 12
    Xlhat = tt*plt';
    ssXl0 = sum(sum(Xl0 .* Xl0));
    ssXl = sum(sum(Xlhat .* Xlhat));
    ssXl = ssXl / ssXl0;
    SSXl = [SSXl; ssXl];
end
    ssX = (ssXa + ssXb + ssXc + ssXd + ssXe + ssXf + ssXg+ ssXh+ ssXi+
ssXj+ssXk+ssXl)/nb_blocks;
    SSX = [SSX; ssX];
    % ---------------------------

    pt = X'*tt / (tt'*tt);

    % Scaling
    tt = tt*norm(pt);
    wt = wt*norm(pt);
    pt = pt/norm(pt);

    Pt=[Pt pt];


    b = u'*tt /(tt'*tt);
    Y = Y - b*tt*q';

    Tt = [Tt tt];
    U = [U u];

    Ta = [Ta ta];
    Tb = [Tb tb];
    Tc = [Tc tc];
    Td = [Td td];
    Te = [Te te];
    Tf = [Tf tf];
    Tg = [Tg tg];
    Th = [Th th];
    Ti = [Ti ti];
    Tj = [Tj tj];
    Tk = [Tk tk];
```

```
    Tl = [Tl tl];

    W = [W wt];

    Wa = [Wa wa];
    Wb = [Wb wb];
    Wc = [Wc wc];
    Wd = [Wd wd];
    We = [We we];
    Wf = [Wf wf];
    Wg = [Wg wg];
    Wh = [Wh wh];
    Wi = [Wi wi];
    Wj = [Wj wj];
    Wk = [Wk wk];
    Wl = [Wl wl];

    Q(:,i) = q;
    B(i,i) = b;

    % Sum of squares -----------
    Yhat = b*tt*q';
    ssY0 = sum(sum(Y0 .* Y0));
    ssY = sum(sum(Yhat .* Yhat));
    ssY = ssY / ssY0;
    SSY = [SSY; ssY];
    % -------------------------

    error_t = realmax;
    error_u = realmax;

end

% Make output structures for output;
Tscores =
struct('Tt',Tt,'Ta',Ta,'Tb',Tb,'Tc',Tc,'Td',Td,'Te',Te,'Tf',Tf,'Tg',Tg,'Th'
,Th,'Ti',Ti,'Tj',Tj,'Tk',Tk,'Tl',Tl);
SS =
struct('SSX',SSX,'SSY',SSY,'SSXa',SSXa,'SSXb',SSXb,'SSXc',SSXc,'SSXd',SSXd,
'SSXe',SSXe,'SSXf',SSXf,'SSXg',SSXg,'SSXh',SSXh,'SSXi',SSXi,'SSXj',SSXj,'SS
Xk',SSXk,'SSXl',SSXl);
Wloads =
struct('W',W,'Wa',Wa,'Wb',Wb,'Wc',Wc,'Wd',Wd,'We',We,'Wf',Wf,'Wg',Wg,'Wh',W
h,'Wi',Wi,'Wj',Wj,'Wk',Wk,'Wl',Wl);
```

ANNEXE VI

```
function [BIP] = fct_BIP_mbPLS_superlevel(SSY,nbblocks,W)

BIP = [];

for i = 1:nbblocks
        wi = W(i,:);
        NUM = 0;
    for j = 1:size(W,2)

        wij = wi(j);

        num = wij.^2 * SSY(j);

        NUM = NUM + num;
    end

bip = (nbblocks*NUM/sum(SSY));

    BIP = [BIP; bip];
end
```

REFERENCES

[1] T. B. Ernest, D. P. Elder, L. G. Martini, M. Roberts, and J. L. Ford, "Developing paediatric medicines: identifying the needs and recognizing the challenges.," *J. Pharm. Pharmacol.*, vol. 59, pp. 1043–1055, 2007.

[2] World Health Organization (WHO), "Annex 5 Development of paediatric medicines: points to consider in formulation," *Forty-sixth Rep. WHO Expert Comm. Specif. Pharm. Prep.*, p. 235, 2012.

[3] S. Salunke, B. Brandys, G. Giacoia, and C. Tuleu, "The STEP (Safety and Toxicity of Excipients for Paediatrics) database: Part 2 - The pilot version," *Int. J. Pharm.*, vol. 457, pp. 310–322, 2013.

[4] C. P. Milne and J. B. Bruss, "The economics of pediatric formulation development for off-patent drugs," *Clin. Ther.*, vol. 30, no. 11, pp. 2133–2145, 2008.

[5] R. Sagraves, "Pediatric Dosing and Dosage Forms," pp. 2629–2650, 2007.

[6] E. Connor and P. Cure, "'Creating hope' and other incentives for drug development for children.," *Sci. Transl. Med.*, vol. 3, no. 66, p. 66cm1, 2011.

[7] D. B. Waisel, "Moral responsibility to attain thorough pediatric drug labeling," *Paediatr. Anaesth.*, vol. 19, no. 10, pp. 989–993, 2009.

[8] European Medicines Agency (EMA), "5-year Report to the European Commission," vol. 44, no. July, 2012.

[9] J. Breitkreutz, "European perspectives on pediatric formulations," *Clin. Ther.*, vol. 30, no. 11, pp. 2146–2154, 2008.

[10] D. Matsui, "Current issues in pediatric medication adherence.," *Paediatr. Drugs*, vol. 9, no. 5, pp. 283–288, 2007.

[11] M. R. DiMatteo, "Variations in patients' adherence to medical recommendations: a quantitative review of 50 years of research.," *Med. Care*, vol. 42, no. 3, pp. 200–209, 2004.

[12] S. Winnick, D. O. Lucas, A. L. Hartman, and D. Toll, "How do you improve compliance?," *Pediatrics*, vol. 115, pp. e718–e724, 2005.

[13] J. a. Mennella, A. C. Spector, D. R. Reed, and S. E. Coldwell, "The bad taste of medicines: Overview of basic research on bitter taste," *Clin. Ther.*, vol. 35, no. 8, pp. 1225–1246, 2013.

[14] A. Cram, J. a Bartlett, and J. Heimlich, "Oral Multiparticulates as a Flexible Solid Dosage Form Approach for Paediatric Use," *Biopharma Asia*, no. June, 2013.

[15] D. Douroumis, "Practical approaches of taste masking technologies in oral solid

forms.," *Expert Opin. Drug Deliv.*, vol. 4, pp. 417–426, 2007.

[16] N. S. Dey, S. Majumdar, and M. E. B. Rao, "Multiparticulate Drug Delivery Systems for Controlled Release," *Trop. J. Pharm. Res.*, vol. 7, no. September, pp. 1067–1075, 2008.

[17] V. Ivanovska, C. M. a Rademaker, L. van Dijk, and A. K. Mantel-Teeuwisse, "Pediatric Drug Formulations: A Review of Challenges and Progress.," *Pediatrics*, vol. 134, no. 2, pp. 361–372, 2014.

[18] D. Wright and S. Tomlin, "How to help if a patient can ' t swallow," vol. 286, no. March, pp. 271–274, 2011.

[19] T. Sam, T. B. Ernest, J. Walsh, and J. L. Williams, "A benefit/risk approach towards selecting appropriate pharmaceutical dosage forms - An application for paediatric dosage form selection," *Int. J. Pharm.*, vol. 435, no. 2, pp. 115–123, 2012.

[20] F. L. Lopez, T. B. Ernest, C. Tuleu, and M. O. Gul, "Formulation approaches to pediatric oral drug delivery: benefits and limitations of current platforms," *Expert Opin. Drug Deliv.*, vol. 12, no. 11, pp. 1727–1740, 2015.

[21] ICH Expert Working Group, "Pharmaceutical Development Q8," *ICH Harmon. Tripart. Guidel.*, vol. 8, no. August, pp. 1–28, 2009.

[22] A. S. Rathore, S. Mittal, M. Pathak, and A. Arora, "Guidance for performing multivariate data analysis of bioprocessing data: Pitfalls and recommendations," *Biotechnol. Prog.*, vol. 30, no. 4, pp. 967–973, 2014.

[23] J. Rantanen and J. Khinast, "The Future of Pharmaceutical Manufacturing Sciences," *J. Pharm. Sci.*, vol. 104, no. 11, pp. 3612–3638, 2015.

[24] Fda, "Guidance for Industry Guidance for Industry PAT — A Framework for Innovative Pharmaceutical," no. September, p. 19, 2004.

[25] L. A. Felton, "Use of polymers for taste-masking pediatric drug products," *Drug Dev. Ind. Pharm.*, vol. 0, no. 0, pp. 1–7, 2018.

[26] Z. Ayenew, V. Puri, L. Kumar, and A. K. Bansal, "Trends in pharmaceutical taste masking technologies: a patent review.," *Recent Pat. Drug Deliv. Formul.*, vol. 3, pp. 26–39, 2009.

[27] V. Vummaneni and D. Nagpal, "Taste Masking Technologies : An Overview and Recent Updates," *Int. J. Res. Pharm. Biomed. Sci.*, vol. 3, no. 2, pp. 510–524, 2012.

[28] BASF SE Care Chemicals Division Pharma Ingredients & Services, "Kollicoat(R) Smartseal 30D Technical information," no. June 2011. pp. 1–16, 2011.

[29] E. Shen, "Interview: Dr elizabeth shen, colorcon," *ONdrugDelivery*, vol. 2015, no. 59, pp. 20–22, 2015.

[30] U.S. Food and Drug Administration, “Drug Master Files (DMFs),” 2018. [Online]. Available: https://www.fda.gov/drugs/developmentapprovalprocess/formssubmissionrequirements/drugmasterfilesdmfs/default.htm. [Accessed: 06-Oct-2018].

[31] E. M. Agency, “Draft Guideline on Pharmaceutical Development of Medicines for Paediatric Use,” *Slides*, vol. 44, no. May, pp. 1–24, 2011.

[32] S. Joshi and H. U. Petereit, “Film coatings for taste masking and moisture protection,” *Int. J. Pharm.*, vol. 457, no. 2, pp. 395–406, 2013.

[33] H. Sohi, Y. Sultana, and R. K. Khar, “Taste masking technologies in oral pharmaceuticals: recent developments and approaches.,” *Drug Dev. Ind. Pharm.*, vol. 30, no. 5, pp. 429–448, 2004.

[34] K. Bhise, S. Shaikh, and D. Bora, “Taste mask, design and evaluation of an oral formulation using ion exchange resin as drug carrier.,” *AAPS PharmSciTech*, vol. 9, no. 2, pp. 557–562, 2008.

[35] V. Anand, R. Kandarapu, and S. Garg, “Ion-exchange resins: Carrying drug delivery forward,” *Drug Discov. Today*, vol. 6, no. 17, pp. 905–914, 2001.

[36] R. Pfeffer, R. N. Dave, D. Wei, and M. Ramlakhan, “Synthesis of engineered particulates with tailored properties using dry particle coating,” *Powder Technol.*, vol. 117, no. 1–2, pp. 40–67, 2001.

[37] M. Cerea, W. Zheng, C. R. Young, and J. W. McGinity, “A novel powder coating process for attaining taste masking and moisture protective films applied to tablets,” *Int. J. Pharm.*, vol. 279, no. 1–2, pp. 127–139, 2004.

[38] M. Qiao, L. Zhang, Y. Ma, J. Zhu, and K. Chow, “A novel electrostatic dry powder coating process for pharmaceutical dosage forms: Immediate release coatings for tablets,” *Eur. J. Pharm. Biopharm.*, vol. 76, no. 2, pp. 304–310, 2010.

[39] S. Obara, N. Maruyama, Y. Nishiyama, and H. Kokubo, “Dry coating: An innovative enteric coating method using a cellulose derivative,” *Eur. J. Pharm. Biopharm.*, vol. 47, no. 1, pp. 51–59, 1999.

[40] N. Pearnchob and R. Bodmeier, “Dry polymer powder coating and comparison with conventional liquid-based coatings for Eudragit(R) RS, ethylcellulose and shellac,” *Eur. J. Pharm. Biopharm.*, vol. 56, no. 3, pp. 363–369, 2003.

[41] N. Pearnchob and R. Bodmeier, “Dry Powder Coating of Pellets with Micronized Eudragit(R) RS for Extended Drug Release,” *Pharm. Res.*, vol. 20, no. 12, pp. 1970–1976, 2003.

[42] S. Kucera, J. Li, S. Engels, and B. Jensen, “Utilization of a Novel Rotor- Granulator Powder Layering Technique to Taste Mask Acetaminophen Pellets with Utilization of a Novel Rotor-Granulator Powder Layering Technique to Taste Mask Acetaminophen

Pellets with EUDRAGIT ® E PO."

[43] S. Kucera, J. Li, S. Engels, and B. Jensen, "Novel Rotor-Granulator Powder Layering Process to Obtain Sustained Release Pellets with EUDRAGIT ® RS PO Novel Novel Powder Powder Layering Layering Process Process to to Obtain Obtain Sustained Sustained Release Release Pellets Pellets with with EUDRAGIT," 2010.

[44] M. Capece, J. Barrows, and R. N. Davé, "Controlled Release from Drug Microparticles via Solventless Dry-Polymer Coating," *J. Pharm. Sci.*, vol. 104, no. 4, pp. 1340–1351, 2015.

[45] B. Guignon, E. Regalado, A. Duquenoy, and E. Dumoulin, "Helping to choose operating parameters for a coating fluid bed process," *Powder Technol.*, vol. 130, pp. 193–198, 2003.

[46] D. Jones, "Fluidized Bed Equipment Types," vol. 20, no. 20, 1994.

[47] E. Teunou and D. Poncelet, "Batch and continuous fluid bed coating - Review and state of the art," *J. Food Eng.*, vol. 53, pp. 325–340, 2002.

[48] R. Dixit and S. Puthli, "Fluidization Technologies: Aerodynamic Principles and Process Engineering RAHUL," *J. Pharm. Sci.*, vol. 98, no. 11, pp. 3933–3960, 2009.

[49] S. Srivastava and G. Mishra, "Fluid Bed Technology : Overview and Parameters for Process Selection," *Int. J. Pharm. Sci. Drug Res.*, vol. 2, no. 4, pp. 236–246, 2010.

[50] E. S. K. Tang, L. W. Chan, and P. W. S. Heng, "Coating of multiparticulates for sustained release," *Am. J. Drug Deliv.*, vol. 3, no. 1, pp. 17–28, 2005.

[51] C. S. Gautam and L. Saha, "Fixed dose drug combinations (FDCs): Rational or irrational: A view point," *Br. J. Clin. Pharmacol.*, vol. 65, no. 5, pp. 795–796, 2008.

[52] S. L. Patwekar and M. K. Baramade, "Controlled release approach to novel multiparticulate drug delivery system," *Int. J. Pharm. Pharm. Sci.*, vol. 4, no. 3, pp. 757–763, 2012.

[53] P. Chandrasekaran and R. Kandasamy, "Solid oral flexible formulations for paediatric and geriatric patients: Age-appropriate formulation platforms," *Indian J. Pharm. Sci.*, vol. 80, no. 1, pp. 14–25, 2018.

[54] N. Al-Hashimi, N. Begg, R. Alany, H. Hassanin, and A. Elshaer, "Oral Modified Release Multiple-Unit Particulate Systems: Compressed Pellets, Microparticles and Nanoparticles," *Pharmaceutics*, vol. 10, no. 4, p. 176, 2018.

[55] D. P. Processes, "Comparing Drug Layering and Direct Pelletisation Processes," no. March, 2014.

[56] C. M. Oh, Q. Guo, P. Wan Sia Heng, and L. W. Chan, "Spray-congealed microparticles for drug delivery – an overview of factors influencing their production and characteristics," *Expert Opin. Drug Deliv.*, vol. 11, no. 7, pp. 1047–1060, 2014.

[57] J. B. Lo, L. E. Appel, S. M. Herbig, S. B. McCray, and A. G. Thombre, “Formulation design and pharmaceutical development of a novel controlled release form of azithromycin for single-dose therapy,” *Drug Dev. Ind. Pharm.*, vol. 35, no. 12, pp. 1522–1529, 2009.

[58] L. W. Chan, E. S. K. Tang, and P. W. S. Heng, “Comparative study of the fluid dynamics of bottom spray fluid bed coaters.,” *AAPS PharmSciTech*, vol. 7, no. 2, p. E37, 2006.

[59] E. Kleinbach and T. Riede, “Coating of solids,” *Chem. Eng. Process. Process Intensif.*, vol. 34, pp. 329–337, 1995.

[60] S. C. Porter and L. a Felton, “Techniques to assess film coatings and evaluate film-coated products.,” *Drug Dev. Ind. Pharm.*, vol. 36, no. 2, pp. 128–142, 2010.

[61] R. J. Campbell and G. L. Sackett, “Film Coating Theory,” in *Pharmaceutical Unit Operations:Coating*, K. E. Avis, A. Shukla, and R.-K. Chang, Eds. Buffalo Grove: Interpharm Press, Inc., 1999, pp. 55–176.

[62] S. R. L. Werner, J. R. Jones, A. H. J. Paterson, R. H. Archer, and D. L. Pearce, “Air-suspension particle coating in the food industry: Part I - state of the art,” *Powder Technol.*, vol. 171, pp. 25–33, 2007.

[63] L. A. Felton and S. C. Porter, “An update on pharmaceutical film coating for drug delivery,” *Expert Opin. Drug Deliv.*, vol. 10, no. 4, pp. 421–435, 2013.

[64] S. Baliga, S. Muglikar, and R. Kale, “Salivary pH: A diagnostic biomarker,” *J. Indian Soc. Periodontol.*, vol. 17, no. 4, pp. 461–465, Oct. 2013.

[65] A. Amelian and K. Winnicka, “Polymers in pharmaceutical taste masking applications,” *Polimery/Polymers*, vol. 62, no. 6, pp. 419–427, 2017.

[66] G. Van Savage and C. T. Rhodes, “The sustained release coating of solid dosage forms: A historical review,” *Drug Dev. Ind. Pharm.*, vol. 21, no. 1, pp. 93–118, 1995.

[67] K. Saleh, R. Cherif, and M. Hemati, “An experimental study of fluidized-bed coating: influence of operating conditions on growth rate and mechanism,” *Adv. Powder Technol.*, vol. 10, no. 3, pp. 255–277, 1999.

[68] S. T. Yang, G. Van Savage, J. Weiss, and I. Ghebre-Sellassie, “The effect of spray mode and chamber geometry of fluid-bed coating equipment and other parameters on an aqueous-based ethylcellulose coating,” *Int. J. Pharm.*, vol. 86, pp. 247–257, 1992.

[69] S. El Mafaldi, M. Hayert, and D. Poncelet, “Fluidization Control in the Wurster Coating Process,” *Chem. Ind.*, vol. 57, no. 12, pp. 641–644, 2003.

[70] S. R. L. Werner, J. R. Jones, A. H. J. Paterson, R. H. Archer, and D. L. Pearce, “Air-suspension coating in the food industry: Part II - micro-level process approach,” *Powder Technol.*, vol. 171, no. 1, pp. 34–45, 2007.

[71] S. C. Porter, “Scale-Up of Film Coating,” in *Pharmaceutical Process Scale Up*, M. Levin, Ed. Basel, New York: Marcel Dekker, Inc., 2002, pp. 259–310.

[72] D. Geldart and M. J. Rhodes, “From minimum fluidization to pneumatic transport - a critical review of the hydrodynamics,” in *Circulating Fluidized Bed Technology I*, P. Basu, Ed. Elsevier, 1986, p. 21.

[73] F. N. Christensen and P. Bertelsen, “Qualitative Description of the Wurster-Based Fluid-Bed Coating Process,” *Drug Dev. Ind. Pharm.*, vol. 23, no. 5, pp. 451–463, 1997.

[74] M. Rhodes, *Introduction to particle technology*, 1st ed. John Wiley & Sons Inc., 1998.

[75] D. Kunii and O. Levenspiel, “Fluidization and Mapping of Regimes,” *Fluid. Eng.*, no. 2, pp. 61–94, 1991.

[76] L. a. Felton, “Mechanisms of polymeric film formation,” *Int. J. Pharm.*, vol. 457, no. 2, pp. 423–427, 2013.

[77] P. D. Hede, P. Bach, and A. D. Jensen, “Two-fluid spray atomisation and pneumatic nozzles for fluid bed coating/agglomeration purposes: A review,” *Chem. Eng. Sci.*, vol. 63, pp. 3821–3842, 2008.

[78] R. P. Singh and D. R. Heldman, *Food Engineering*, 4th ed. Academic Press, 2009.

[79] T. Kourti, *Quality by Design in the Pharmaceutical Industry: Process Modelling, Monitoring and Control using Latent Variable Methods*, vol. 42, no. 11. IFAC, 2009.

[80] L. X. Yu *et al.*, “Understanding Pharmaceutical Quality by Design,” *AAPS J.*, vol. 16, no. 4, pp. 771–783, 2014.

[81] a. S. Rathore, R. Bhambure, and V. Ghare, “Process analytical technology (PAT) for biopharmaceutical products,” *Anal. Bioanal. Chem.*, vol. 398, no. 1, pp. 137–154, 2010.

[82] U. S. Food and Drug Administration/Center for Biologics Evaluation and Research, “Guidance for Industry. Q9 Quality Risk Management,” *Food Drug Adm.*, no. June, pp. 1–72, 2006.

[83] D. C. Montgomery, *Design and Analysis of Experiments*, 8th ed. John Wiley & Sons Inc., 2012.

[84] S. N. Politis, P. Colombo, G. Colombo, and D. M. Rekkas, “Design of experiments (DoE) in pharmaceutical development,” *Drug Dev. Ind. Pharm.*, vol. 43, no. 6, pp. 889–901, 2017.

[85] A. S. El-Hagrasy, F. D’Amico, and J. K. Drennen, “A process analytical technology approach to near-infrared process control of pharmaceutical powder blending. Part I: D-optimal design for characterization of powder mixing and preliminary spectral data evaluation,” *J. Pharm. Sci.*, vol. 95, no. 2, pp. 392–406, 2006.

[86] F. Triefenbach, “Design of experiments: the D-optimal approach and its implementation

as a computer algorithm," *Bachelor's Thesis Inf. Commun. …*, no. January, 2008.

[87] D. L. Massart, B. G. M. Vandeginste, L. M. C. Buydens, S. De Jong, P. J. Lewi, and J. Smeyers-Verbeke, *Handbook of Chemometrics and Qualimetrics: Part A*. Elsevier, 1997.

[88] B. M. Wise, N. B. Gallagher, and W. Windig, *Chemometrics Tutorial for PLS _ Toolbox and Solo*. 2006.

[89] S. Wold, M. Sjöström, and L. Eriksson, "PLS-regression: A basic tool of chemometrics," *Chemom. Intell. Lab. Syst.*, vol. 58, no. 2, pp. 109–130, 2001.

[90] J. a Westerhuis, T. Kourti, and J. F. MacGregor, "Analysis of multiblock and hierarchical PCA and PLS models," *J. Chemom.*, vol. 12, no. 5, pp. 301–321, 1998.

[91] S. García-Muñoz, T. Kourti, J. F. MacGregor, A. G. Mateos, and G. Murphy, "Troubleshooting of an Industrial Batch Process Using Multivariate Methods," *Ind. Eng. Chem. Res.*, vol. 42, no. 15, pp. 3592–3601, 2003.

[92] J. a. Lopes, J. C. Menezes, J. a. Westerhuis, and a. K. Smilde, "Multiblock PLS analysis of an industrial pharmaceutical process," *Biotechnol. Bioeng.*, vol. 80, no. 4, pp. 419–427, 2002.

[93] M. Vivien and R. Sabatier, "Generalized orthogonal multiple co-inertia analysis(-PLS): New multiblock component and regression methods," *J. Chemom.*, vol. 17, no. 5, pp. 287–301, 2003.

[94] L. E. Wangen and B. R. Kowalski, "A multiblock partial least squares algorithm for investigating complex chemical systems," *J. Chemom.*, vol. 3, no. 1, pp. 3–20, 1989.

[95] J. F. MacGregor, C. Jaeckle, C. Kiparissides, and M. Koutoudi, "Process monitoring and diagnosis by multiblock PLS methods," *AIChE J.*, vol. 40, no. 5, pp. 826–838, 1994.

[96] M. a Nemeth, "Multi- and Megavariate Data Analysis," *Technometrics*, vol. 45, no. 4, pp. 362–362, 2003.

[97] E. Schirm, H. Tobi, T. W. De Vries, I. Choonara, and L. T. W. De Jong-Van Den Berg, "Lack of appropriate formulations of medicines for children in the community," *Acta Paediatr. Int. J. Paediatr.*, vol. 92, no. 12, pp. 1486–1489, 2003.

[98] B. K. Park, J. S. Lee, and K. D. Kihm, "Comparative study of twin-fluid atomization using sonic or supersonic gas jets," *At. Sprays*, vol. 6, pp. 285–304, 1996.

[99] P. Sriamornsak, S. Puttipipatkhachorn, and S. Prakongpan, "Calcium pectinate gel coated pellets as an alternative carrier to calcium pectinate beads," *Int. J. Pharm.*, vol. 156, no. 2, pp. 189–194, 1997.

[100] S. Wieland-Berghausen, U. Schote, M. Frey, and F. Schmidt, "Comparison of microencapsulation techniques for the water-soluble drugs nitenpyram and

clomipramine HC1," *J. Control. Release*, vol. 85, no. 1–3, pp. 35–43, 2002.

[101] A. Prasad, Y. Lan, and N. Langley, "Taste Masking of Ibuprofen Granules Using a Novel Reverse Enteric Film Coating," in *CRS 2011 Annual Meeting*, 2016, no. August 2011, pp. 3–5.

[102] M. Xu, P. W. S. Heng, and C. V Liew, "Evaluation of coat uniformity and taste-masking efficiency of irregular-shaped drug particles coated in a modified tangential spray fluidized bed processor," *Expert Opin Drug Deliv*, vol. 12, no. 10, pp. 1597–1606, 2015.

[103] A. Chivate, V. Sargar, P. Nalawade, and V. Tawde, "Formulation and development of oral dry suspension using taste masked Ornidazole particles prepared using Kollicoat® Smartseal 30 D," *Drug Dev. Ind. Pharm.*, vol. 39, no. 7, pp. 1091–1097, 2013.

[104] D. Hörter and J. B. Dressman, "Influence of physicochemical properties on dissolution of drugs in the gastrointestinal tract," *Adv. Drug Deliv. Rev.*, vol. 25, no. 1, pp. 3–14, 1997.

[105] Q. W. Yang *et al.*, "Curing of aqueous polymeric film coatings: Importance of the coating level and type of plasticizer," *Eur. J. Pharm. Biopharm.*, vol. 74, no. 2, pp. 362–370, 2010.

[106] M. Irfan, A. R. Ahmed, K. Kolter, R. Bodmeier, and A. Dashevskiy, "Curing mechanism of flexible aqueous polymeric coatings," *Eur. J. Pharm. Biopharm.*, vol. 115, pp. 186–196, 2017.

[107] S. Gittings, N. Turnbull, C. J. Roberts, and P. Gershkovich, "Dissolution methodology for taste masked oral dosage forms," *J. Control. Release*, vol. 173, no. 1, pp. 32–42, 2014.

[108] E. A. Johannessen, L. Wang, C. Wyse, D. R. S. Cumming, and J. M. Cooper, "Biocompatibility of a lab-on-a-pill sensor in artificial gastrointestinal environments," *IEEE Trans. Biomed. Eng.*, vol. 53, no. 11, pp. 2333–2340, 2006.

[109] W. Curatolo, "Interdisciplinary Science and the design of a single-dose antibiotic therapy," *Pharm. Res.*, vol. 28, no. 9, pp. 2059–2071, 2011.

[110] B. Y. Shekunov, P. Chattopadhyay, H. H. Y. Tong, and A. H. L. Chow, "Particle size analysis in pharmaceutics: Principles, methods and applications," *Pharm. Res.*, vol. 24, no. 2, pp. 203–227, 2007.

[111] D. C. Montgomery, *D esign and Analysis of Experiments Eighth Edition*. .

[112] E. P. Barrett, L. G. Joyner, and P. P. Halenda, "The Determination of Pore Volume and Area Distributions in Porous Substances. I. Computations from Nitrogen Isotherms," *J. Am. Chem. Soc.*, vol. 73, no. 1, pp. 373–380, 1951.

[113] R. O. Williams and J. Liu, "Influence of processing and curing conditions on beads

coated with an aqueous dispersion of cellulose acetate phthalate," *Eur. J. Pharm. Biopharm.*, vol. 49, no. 3, pp. 243–252, 2000.

[114] P. K. Gaur, S. Mishra, R. Gautam, A. P. Singh, and M. Yasir, "Film Coating Technology: Past, Present and Future," *J. Pharm. Sci. Pharmacol.*, vol. 1, no. 1, pp. 57–67, 2014.

[115] K. I. Dragnevski, A. F. Routh, M. W. Murray, and A. M. Donald, "Cracking of drying latex films: An ESEM experiment," *Langmuir*, vol. 26, no. 11, pp. 7747–7751, 2010.

[116] F. Siepmann, J. Siepmann, M. Walther, R. MacRae, and R. Bodmeier, "Aqueous HPMCAS coatings: Effects of formulation and processing parameters on drug release and mass transport mechanisms," *Eur. J. Pharm. Biopharm.*, vol. 63, no. 3, pp. 262–269, 2006.

[117] S. a. Kucera, L. a. Felton, and J. W. McGinity, "Physical aging in pharmaceutical polymers and the effect on solid oral dosage form stability," *Int. J. Pharm.*, vol. 457, no. 2, pp. 428–436, 2013.

[118] "Über die Auflösungsgeschwindigkeit fester Körper ," *Zeitschrift für Physikalische Chemie* , vol. 35U. p. 283, 1900.

[119] T. Nakano and H. Yuasa, "Suppression of agglomeration in fluidized bed coating. IV. Effects of sodium citrate concentration on the suppression of particle agglomeration and the physical properties of HPMC film," *Int. J. Pharm.*, vol. 215, no. 1–2, pp. 3–12, 2001.

[120] K. Christoph Link and E.-U. Schlünder, "Fluidized bed spray granulation," *Chem. Eng. Process. Process Intensif.*, vol. 36, pp. 443–457, 1997.

[121] I. Ghebre-Sellassie, *Pharmaceutical Pelletization Technology*. New York: Marcel Dekker Inc, 1989.

[122] T. Yoshida, T. C. Lai, G. S. Kwon, and K. Sako, "pH- and ion-sensitive polymers for drug delivery," *Expert Opin. Drug Deliv.*, vol. 10, no. 11, pp. 1497–1513, Nov. 2013.

[123] P. Avalle *et al.*, "Development of Process Analytical Technology (PAT) methods for controlled release pellet coating," *Eur. J. Pharm. Biopharm.*, vol. 87, no. 2, pp. 244–251, 2014.

[124] T. Peng *et al.*, "Study progression in application of process analytical technologies on film coating," *Asian J. Pharm. Sci.*, no. 2014, pp. 1–10, 2015.

[125] K. Knop and P. Kleinebudde, "PAT-tools for process control in pharmaceutical film coating applications," *Int. J. Pharm.*, vol. 457, no. 2, pp. 527–536, 2013.

[126] K. Korasa and F. Vrečer, "Overview of PAT process analysers applicable in monitoring of film coating unit operations for manufacturing of solid oral dosage forms," *Eur. J. Pharm. Sci.*, vol. 111, no. October 2017, pp. 278–292, 2018.

[127] A. Bogomolov, M. Engler, M. Melichar, and A. Wigmore, “In-line analysis of a fluid bed pellet coating process using a combination of near infrared and Raman spectroscopy,” *J. Chemom.*, vol. 24, no. 7–8, pp. 544–557, 2010.

[128] M. Blanco and I. Villarroya, “NIR spectroscopy: A rapid-response analytical tool,” *TrAC - Trends Anal. Chem.*, vol. 21, no. 4, pp. 240–250, 2002.

[129] M. Andersson, S. Folestad, J. Gottfries, M. O. Johansson, M. Josefson, and K. G. Wahlund, “Quantitative analysis of film coating in a fluidized bed process by in-line NIR spectrometry and multivariate batch calibration.,” *Anal. Chem.*, vol. 72, no. 9, pp. 2099–2108, 2000.

[130] P. Atkins and J. De Paula, *Atkins’ Physical Chemestry*, 8th ed. W.H. Freeman and Company, 2006.

[131] J. Hisazumi and P. Kleinebudde, “In-line monitoring of multi-layered film-coating on pellets using Raman spectroscopy by MCR and PLS analyses,” *Eur. J. Pharm. Biopharm.*, vol. 114, pp. 194–201, 2017.

[132] A. F. T. Silva *et al.*, “Particle sizing measurements in pharmaceutical applications: Comparison of in-process methods versus off-line methods,” *Eur. J. Pharm. Biopharm.*, vol. 85, no. 3 PART B, pp. 1006–1018, 2013.

[133] F. Alshihabi, T. Vandamme, and G. Betz, “Focused beam reflectance method as an innovative (PAT) tool to monitor in-line granulation process in fluidized bed,” *Pharm. Dev. Technol.*, vol. 18, no. 1, pp. 73–84, 2013.

[134] F. Folttmann, K. Knop, P. Kleinebudde, and M. Pein, “In-line spatial filtering velocimetry for particle size and film thickness determination in fluidized-bed pellet coating processes,” *Eur. J. Pharm. Biopharm.*, vol. 88, no. 3, pp. 931–938, 2014.

[135] S. Kukec, G. Hudovornik, R. Dreu, and F. Vrečer, “Study of granule growth kinetics during in situ fluid bed melt granulation using in-line FBRM and SFT probes Study of granule growth kinetics during in situ fluid bed melt granulation using in-line FBRM and SFT probes,” vol. 9045, no. May 2013, 2014.

[136] Å. Rinnan, F. van den Berg, and S. B. Engelsen, “Review of the most common pre-processing techniques for near-infrared spectra,” *TrAC - Trends Anal. Chem.*, vol. 28, no. 10, pp. 1201–1222, 2009.

[137] P. Nomikos and J. F. Macgregor, “Multivariate SPC Charts for Batch Monitoring Processes,” *Technometrics*, vol. 37, no. 1, pp. 41–59, 1995.

[138] S. Wold, N. Kettaneh, H. Fridén, and A. Holmberg, “Modelling and diagnostics of batch processes and analogous kinetic experiments,” *Chemom. Intell. Lab. Syst.*, vol. 44, no. 1–2, pp. 331–340, 1998.

[139] R. Turton, “Challenges in the modeling and prediction of coating of pharmaceutical dosage forms,” *Powder Technol.*, vol. 181, no. 2, pp. 186–194, 2008.

[140] D. Markl *et al.*, “Calibration-free in-line monitoring of pellet coating processes via optical coherence tomography,” *Chem. Eng. Sci.*, pp. 1–9, 2014.

[141] C. V. Liew, L. I. K. U. N. Wang, P. Wan, and S. I. A. Heng, “Development of a Visiometric Process Analyzer for Real-Time Monitoring of Bottom Spray Fluid-Bed Coating,” *J. Pharm. Sci.*, vol. 99, no. 1, pp. 346–356, 2010.

[142] A. P. Ferreira and M. Tobyn, “Multivariate analysis in the pharmaceutical industry: Enabling process understanding and improvement in the PAT and QbD era,” *Pharm. Dev. Technol.*, vol. 20, no. 5, pp. 513–527, 2015.